

Editor-in-Chief B.E.Paton

EDITORIAL BOARD

Yu.S. Borisov,
B.V. Khitrovskaya (*exec. secretary*),
V.F. Khorunov, V.V. Knysh, I.V. Krivtsun,
S.I. Kuchuk-Yatsenko (*vice-chief editor*),
Yu.N. Lankin, V.N. Lipodaev (*vice-chief editor*),
L.M. Lobanov, A.A. Mazur,
I.K. Pokhodnya, V.D. Poznyakov, I.A. Ryabtsev,
K.A. Yushchenko,
A.T. Zelnichenko (*exec. director*)
(*Editorial Board Includes PWI Scientists*)

**INTERNATIONAL EDITORIAL
COUNCIL**

N.P. Alyoshin
N.E. Bauman MSTU, Moscow, Russia
V.G. Fartushny
Welding Society of Ukraine, Kiev, Ukraine
Guan Qiao
Beijing Aeronautical Institute, China
V.I. Lysak
Volgograd State Technical University, Russia
B.E. Paton
PWI, Kiev, Ukraine
Ya. Pilarczyk
Weiding Institute, Gliwice, Poland
U. Reisgen
Welding and Joining Institute, Aachen, Germany
O.I. Steklov
Welding Society, Moscow, Russia
G.A. Turichin
St.-Petersburg State Polytechn. Univ., Russia
M. Zinigrad
College of Judea & Samaria, Ariel, Israel
A.S. Zubchenko
OKB «Gidropress», Podolsk, Russia

Founders

E.O. Paton Electric Welding Institute
of the NAS of Ukraine
International Association «Welding»

Publisher

International Association «Welding»

Translators

A.A. Fomin, O.S. Kurochko,
I.N. Kutianova
Editor
N.A. Dmitrieva
Electron galley
D.I. Sereda, T.Yu. Snegiryova

Address

E.O. Paton Electric Welding Institute,
International Association «Welding»
11, Bozhenko Str., 03680, Kyiv, Ukraine
Tel.: (38044) 200 60 16, 200 82 77
Fax: (38044) 200 82 77, 200 81 45
E-mail: journal@paton.kiev.ua
www.patonpublishinghouse.com

State Registration Certificate
KV 4790 of 09.01.2001
ISSN 0957-798X

Subscriptions

\$348, 12 issues per year,
air postage and packaging included.
Back issues available.
All rights reserved.

This publication and each of the articles contained
herein are protected by copyright.
Permission to reproduce material contained in this
journal must be obtained in writing from the
Publisher.

CONTENTS

SCIENTIFIC AND TECHNICAL

- Kuchuk-Yatsenko S.I., Shvets Yu.V. and Shvets V.I.*
Influence of non-metallic inclusions in pipe steels of
strength class X65–X80 on values of impact toughness
of flash-butt welded joints 2
- Osin V.V.* Tribotechnical properties of deposited metal
of 50Kh9S3G type with increased sulphur content 8
- Demidenko L.Yu., Onatskaya N.A. and Polovinka V.D.*
Effect of temperature of thermomechanical treatment
on quality of dissimilar metal joints 11
- Borisov Yu.S., Vojnarovich S.G., Kislitsa A.N. and
Kalyuzhny S.N.* Investigation of spraying spot and
metallization pattern under conditions of microplasma
spraying of coatings of titanium dioxide 15
- Korzhik V.N., Borisova A.L., Popov V.V., Kolomytsev
M.V., Chajka A.A., Tkachuk V.I. and Vigilyanskaya N.V.*
Cermets coatings of chromium carbide–nichrome
system produced by supersonic plasma gas air
spraying 19

INDUSTRIAL

- Zyakhor I.V., Zavertanny M.S. and Chernobaj S.V.*
Linear friction welding of metallic materials (Review) 25
- Chvertko P.N., Semyonov L.A. and Gushchin K.V.*
Flash-butt welding of thin-walled profiles of
heat-hardened aluminium alloys 32
- Zhudra A.P., Krivchikov S.Yu. and Dzykovich V.I.*
Application of complex-alloyed powders produced by
thermocentrifugal sputtering in flux-cored wires 36
- Pereplyotchikov E.F., Ryabtsev I.A., Lankin Yu.N.,
Semikin V.F. and Osechkov P.P.* Modernization of
control system of A1756 machine for plasma-powder
surfacing 41

INFORMATION

- Training of specialists-welders of Kazakhstan in Ukraine 45
- Index of articles for TPWJ'2014, Nos. 1–12 46
- List of authors 50



INFLUENCE OF NON-METALLIC INCLUSIONS IN PIPE STEELS OF STRENGTH CLASS X65–X80 ON VALUES OF IMPACT TOUGHNESS OF FLASH-BUTT WELDED JOINTS

S.I. KUCHUK-YATSENKO, Yu.V. SHVETS and V.I. SHVETS

E.O. Paton Electric Welding Institute, NASU

11 Bozhenko Str., 03680, Kiev, Ukraine. E-mail: office@paton.kiev.ua

The comprehensive mechanical tests of high-strength steel pipe joints produced using flash-butt welding were carried out. The quality of joints completely meets the requirements of the international standard API STANDARD 1104. During tests on impact bending the single dropouts of KCV_{-40} values lower than the level required by standards DNV-OS-F101 and STO Gazprom 2-3.7-380–2009 were observed. The decrease in KCV_{-40} was predetermined by formation of zones of $1-2 \text{ mm}^2$ area in the plane of a joint differed by structural heterogeneity, which is characteristic also for base metal and revealed in a sharply distinct anisotropy of its ductile properties. It is shown that the areas with structural heterogeneity do not form colonies, therefore they do not decrease the general serviceability of the welded joint. The sizes of such areas do not exceed the admissible values accepted by the standards for defects of welds made by arc welding. The presence of single local dropouts of KCV_{-40} values observed during tests of welded joints produced using FBW should not be considered as a sign of rejection. 8 Ref., 1 Table, 11 Figures.

Keywords: flash-butt welding, high-strength steel, impact toughness of welded joints, heat treatment of welds

The many-year works in flash-butt welding (FBW) of large-diameters pipes [1] at the E.O. Paton Electric Welding Institute have found the further development over the recent years. The technology of FBW of thick-walled pipes of 1219–1420 mm diameter of high strength steels used in construction of modern pipelines of high efficiency was developed. The technology of welding and heat treatment provides the joints with high values of mechanical properties, which meet the requirements of international standards [2–4]. Basing on this technology CJSC «Pskov-elektrosvar» (Russia) jointly with the E.O. Paton Electric Welding Institute developed a new generation of equipment for FBW of pipes of 1219–1420 mm diameter. At the present time the comprehensive tests of this equipment and weld-

ing technology and its adaptation to standard requirements specified for the quality of welded joints during construction of off-shore and on-shore pipelines including under conditions of the Extreme North are carried out.

For such pipelines the International standards [3, 4] specified the standard values of impact toughness of welded joints of circumferential welds of not less than 37.5 J/cm^2 at the test temperature, which should be $20 \text{ }^\circ\text{C}$ lower than the design temperature of pipeline service.

The aim of the present article is determination of factors, which influence the value and stability of values of impact toughness of high-strength steel pipe joints produced by FBW.

The development of welding technology was carried out on the sectors of pipes of 1219 mm diameter with the wall thickness of 27 mm, which are manufactured of sheet steel 10G2FB of X70 strength class, produced by controllable rolling

Mechanical properties of metal of pipes and welded joints

Investigation area	Yield strength, MPa	Tensile strength, MPa	Impact toughness, J/cm ² , at T, °C			
			+20	-20	-30	-40
Base metal	$\frac{484.4-493.5}{490.0}$	$\frac{546.7-556.8}{553.0}$	$\frac{334.7-336.6}{335.8}$	–	–	$\frac{333.0-336.6}{334.9}$
Welded joint after heat treatment	–	$\frac{550.6-561.4}{554.6}$	$\frac{147.9-219.5}{173.2}$	$\frac{86.8-171.1}{137.9}$	$\frac{84.5-167.5}{115.5}$	$\frac{19.1-129.1}{98.6}$

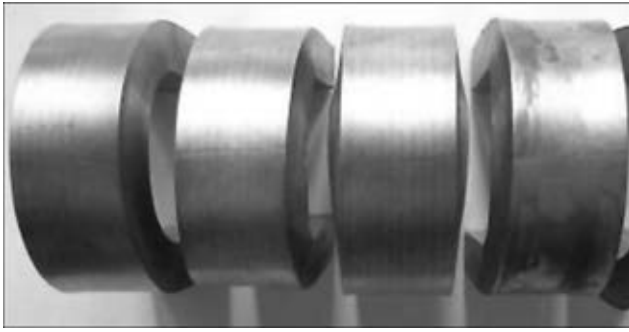


Figure 1. Specimens of welded joint tested on static bending after heat treatment

with thermal mechanical strengthening, of the following chemical composition, wt.%: 0.06 C; 0.21 Si; 1.42 Mn; 0.12 Ni; 0.07 Mo; 0.04 V; 0.04 Al; 0.02 Ti; 0.05 Cr; 0.02 Nb; 0.004 S; 0.012 P. The mechanical properties of base metal and also of welded joints after heat treatment are given in the Table. The modes of welding and heat treatment are presented in [5, 6]. All the welded joints were subjected to non-destructive testing (radiographic, ultrasonic) of a high resolution capacity.

The mechanical tests of welded butts were carried out at the PWI laboratory according to the requirements stated in work [3]. This laboratory is certified according to the International standards. Metallographic examinations were carried out in the light microscope «Neophot-32», analyses of fracture surfaces and microstructure of joints were made in the JEOL Auger-microprobe JAMP 9500F (Japan) in the laboratory of metallographic investigations.

In the specimens, tested for static bending after heat treatment and presented in Figure 1, the cracks and fractures were not detected.

As is seen from the Table and Figures 1, 2 the values of impact toughness in heat-treated welded joints meet the requirements in the temperature range of +20– –30 °C [3, 4], specified for the off-shore pipelines. With the reduction of testing temperature T_{test} of specimens for bending tests the values of KCV are reduced and scattering of their values increases (see Fi-

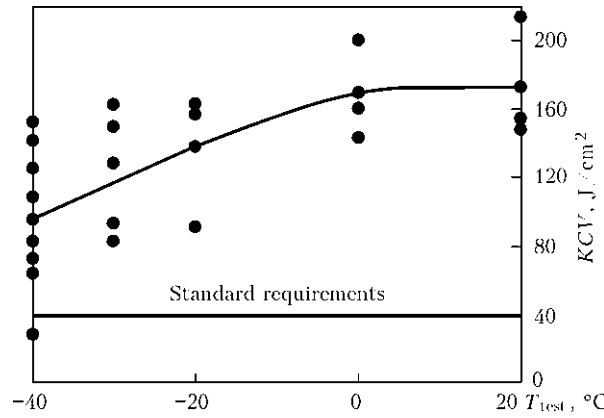


Figure 2. Temperature dependence of impact toughness of welded joints

gure 2). Nevertheless at $T_{test} = -30$ °C they remain at a sufficiently high level of 84.5–167.5 J/cm² and at $T_{test} = -40$ °C, which is envisaged for continental pipelines under the conditions of the Extreme North, scattering of values increases and single dropouts below the level of 37.5 J/cm² are observed, regulated by the standard DNV-OS-F101. The number of such specimens tested at the mentioned temperature does not exceed 10–15 %. Here, the average value of KCV remains sufficiently high – 98.6 J/cm³.

The testing of welded joints of all the specimens using non-destructive methods did not detect any imperfections of metal structure in the plane of the joint, which could be classified as defective ones, even at setting up the devices to increased sensibility.

Macro- and microstructure of the pipe joint, produced at the optimal mode with the further heat treatment, are given in Figure 3. The total HAZ width after welding and heat treatment amounts to about 60 mm. The base of microstructure of HAZ metal, as well as base metal is ferrite. Along the joint line the microstructure is featured by somewhat large size of ferrite grain (10–15 μm) as compared to HAZ microstructure and presence of partially decayed residual austenite with formation of grain bainite.

In the course of comparison of weld microstructure of specimens, which showed minimum

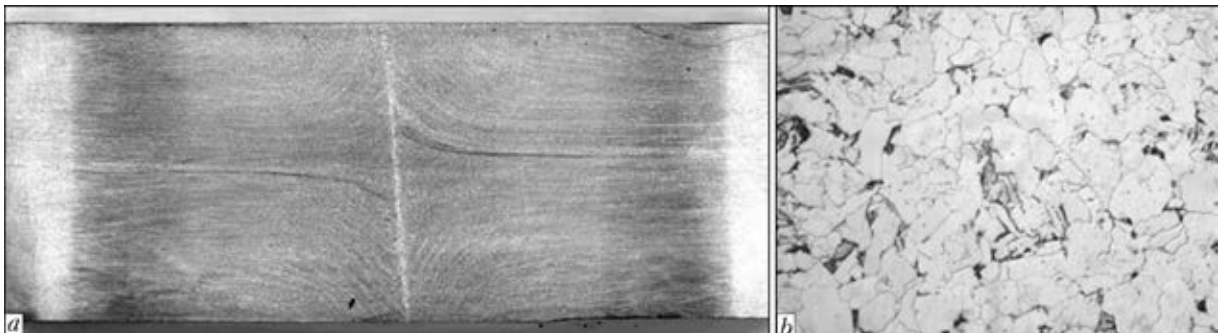


Figure 3. Macro- (a) and microstructure (b – ×1000) of joints of pipe steel at the area of joint line

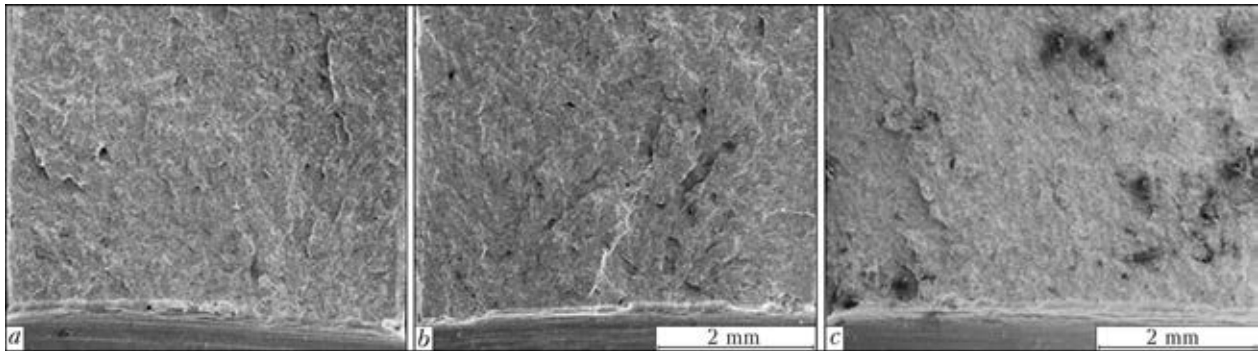


Figure 4. Macrostructure of fractures of welded specimens after impact bending tests: *a* – $KCV_{-40} = 110$; *b* – 29.1; *c* – 19.1 J/cm²

and maximum values of KCV_{-40} during tests, no differences were revealed.

The analysis of structure of fractures of welded specimens after tests on impact bending was performed. The investigations showed that fractures of specimens are crystalline in all the cases (Figure 4). The developed relief in some cases is connected with presence of coarse non-metallic inclusions (NMI) in metal.

Microstructure of fracture surfaces of all the specimens is morphologically the same (Figure 5). The facets of chips with the structure elements typical of cleavage fracture, such as steps of river pattern and lugs, are combined with tear ridges, i.e. the elements of tough fracture. The presence of secondary cracks along the interfaces are characteristic.

The impact toughness of specimens with such microstructure at almost absent NMI corresponded to standard requirements (see Figure 4, *a*).

In the specimens with a low impact toughness the cluster of NMI was revealed at the fracture surface (see Figure 4, *c*). X-ray spectral microanalysis of chemical composition allowed distinguishing the following types. These are the complex oxides of silicon, calcium, aluminium of up to 50 µm size (Figure 6, spectra 1, 2),

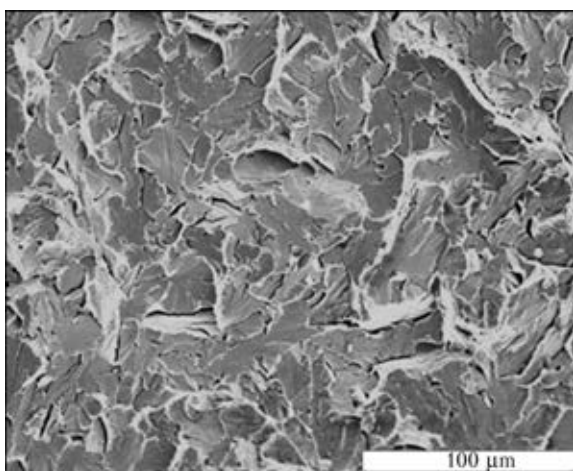
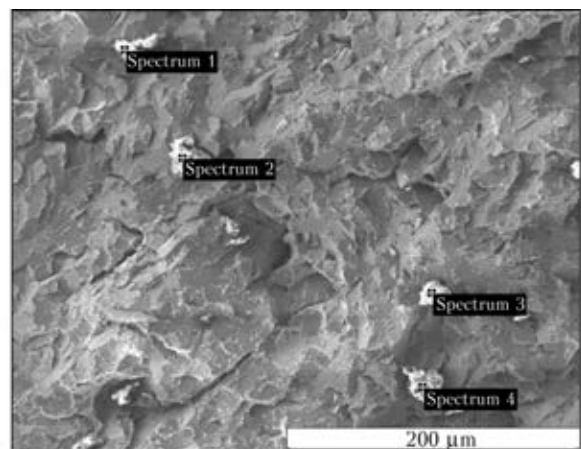


Figure 5. Microstructure of fracture surface of welded specimens after impact bending tests

particles on the base of silicon (Figure 6, spectra 3, 4). These inclusions are refractory products of metallurgical reactions, which transfer to the weld almost without suffering the changes under the thermodeformational conditions of welding. Impurity and alloying elements such as sulfur, niobium and titanium also can be included to their composition.

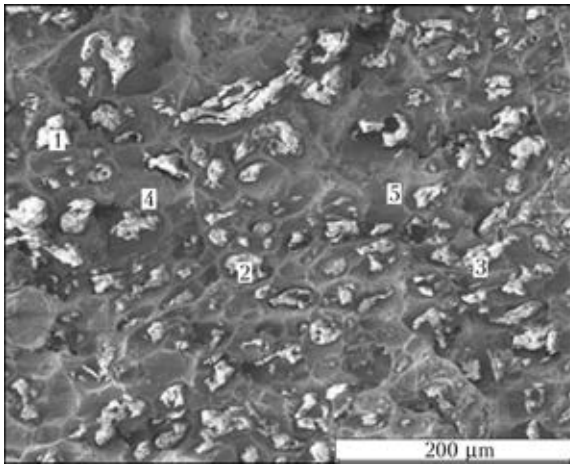
Another type of the observed inclusions, forming clusters, are silicates. The areas with the particles of silicates, which could be observed, occupied the area up to several square millimeters. The fused appearance and multitude of particles give grounds to suppose that they represent the fragments of a liquid film crushed in a butt (Figure 7).

To evaluate the effect of NMI in steel on structure and composition of inclusions in welds, the metallographic examinations of base metal were carried out.



Spectrum	C	O	Al	Si	S	Fe
1	37.48	26.42	14.67	3.23	0.88	17.32
2	66.53	19.90	–	0.25	–	13.30
3	22.66	0.72	–	72.67	–	3.94
4	39.47	2.23	–	46.02	–	12.27

Figure 6. Refractory NMI at the fracture surface of welded joint, and results of their X-ray spectral microanalysis (here and after – at.%)



Spectrum	C	O	Al	Si	S	Ca	Ti	Cr	Mn	Fe
1	5.89	60.91	2.19	11.83	0	0.17	0.82	0	16.63	1.57
2	11.50	56.43	6.40	12.94	0.41	0.70	1.02	0	9.28	1.33
3	1.02	55.44	2.39	16.09	0.10	0.11	0.50	0.02	22.84	1.50
4	4.81	1.39	0.04	0.58	0.08	0	0.24	0.19	1.92	90.76
5	3.64	0.82	0	0.29	0.11	0.19	0	0	1.86	93.08

Figure 7. Manganese aluminosilicates on the fracture surface of pipe joints

Microstructure of base metal represents a ferrite matrix with negligible amount of pearlite colonies (Figure 8, *a*). The size of grains of ferrite amounts by estimation to the limits from several to 10 μm (11–12 according to ASTM), here the coarse grains of ferrite are elongated along the direction of rolling. The characteristic is the considerable level of foliation of microstructure, which is observed due to stringer-type location of products of the eutectoid transformation.

NMI which are mainly represented by complex oxides and sulfides of aluminium, silicon, calcium, manganese, iron (Figure 8, *b*), in microstructure are distributed non-homogeneously and are often concentrated in the strips of rolling.

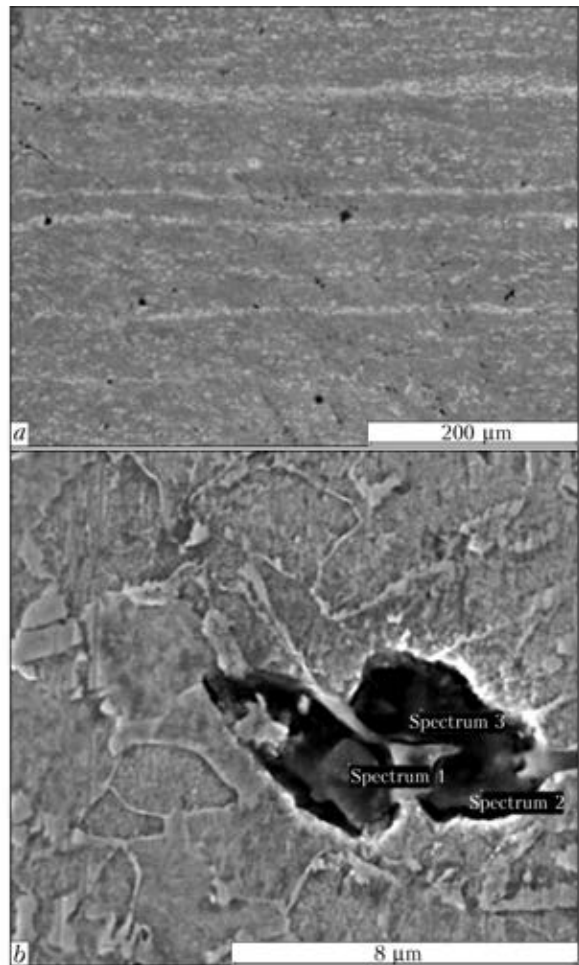
To determine the influence of structural heterogeneity of the pipe base metal on impact toughness the tests of specimens, cut out from base metal at different position of notch in Charpy specimens relatively to the strips of rolling, were carried out. Thus, in case of notch on the surface of pipe across the direction of rolling at $T_{test} = -40\text{ }^{\circ}\text{C}$, $KCV = (333.0-336.2)/334.9$, and with notch in the middle of the surface of the pipe end along the central line of rolling, $KCV = (9.8-236.5)/53.5\text{ J/cm}^2$.

The impact toughness tests of specimens of base metal with notch along the central line of rolling showed that the results do not meet the requirements [4, 5]. The characteristic fractures of specimens are shown in Figure 9.

The values of tests of specimens with notch along the strips of rolling differ sharply by the expressed instability. Among nine specimens with notch along the central line of rolling, six ones had the results lower than the required 37.5 J/cm^2 (at minimum value of 9.8 J/cm^2). As is seen, in the limits of strip on single areas the impact toughness is high. Local decrease of plastic properties was caused by structure heterogeneity of rolling strips. However, it can not

weaken the metal even in the limits of area com measurable with the sheet thickness.

On the fracture of base metal, opened along the rolling strip, the numerous inclusions are observed (Figure 10). As to their nature they are



Spectrum	O	Al	Si	S	Ca	Mn	Fe
1	59.87	0.74	24.29	9.53	0.23	2.52	2.82
2	36.10	1.73	1.36	0	0.98	0	59.83
3	46.09	1.31	6.84	0.53	5.14	2.53	37.56

Figure 8. Microstructure of base metal (*a*), and NMI in base metal (*b*)

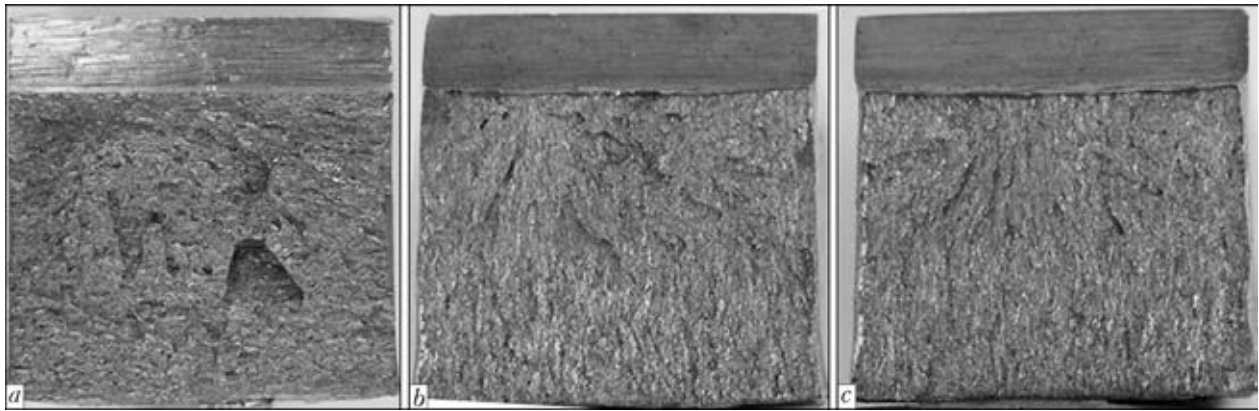


Figure 9. Fracture surface of Charpy impact specimens with notch along the central rolling line: *a* – $KCV = 9.84$; *b* – 22.2 ; *c* – 30.8 J/cm^2

very close to those observed in the base metal. Their base is oxide structures of silicon, aluminium, manganese, iron oxides and sulfides.

The most obviously that transfer of NMI from the rolling strips to the plane of joint occurs through the melt, being formed on the surface of flashing during welding. The thickness of melt layer during flashing of low-alloyed steels is changed in the limits of 0.1–0.6 mm.

It is shown in work [7] that at the presence of holes, filled with oxides of iron or any metal fillers, in the part edges being flashed the zone, enriched with filler, is formed in the melt at the places of their escape to the edges being flashed. During upsetting this zone of melt is deformed and its area is many times increased.

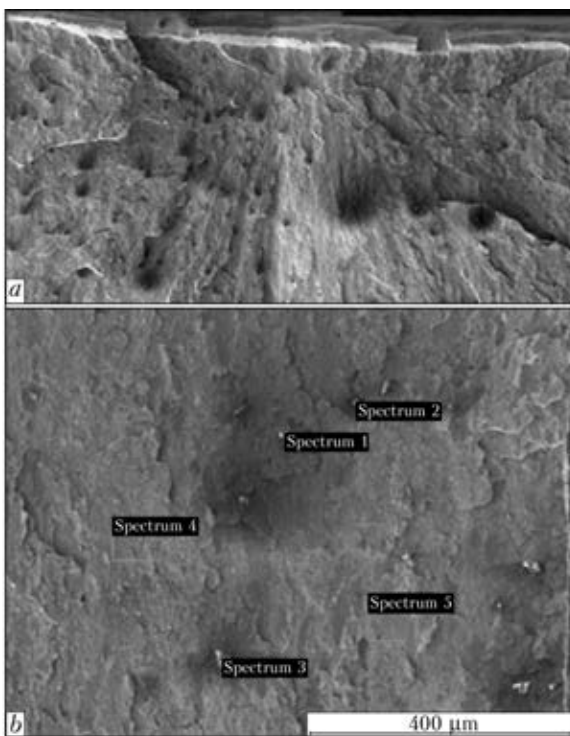
In the studied case of formation of structural homogeneity in the plane, the role of filler is played by the content of liquation strip in the place of its escape to the flashing surface.

During evaluation of mechanical properties of welded joints of large-diameter pipes according to the standards [3, 4] the values of tests of standard specimens, cut out of sectors of 300 mm width symmetrically on four regions of pipe perimeter, are considered. Here, the results of mechanical tests and values of non-destructive testing are compared. Basing on the analysis of these data on each sector the conclusion about admission of dropouts of values of mechanical properties and detection of defects is made.

During tests of welded joints of pipes, produced using FBW at the optimal modes, no dropouts from standard requirements on tensile strength and also during tests on static bending were revealed.

To evaluate the distribution of areas with low properties of KCV in the full-scale specimen the coordinate binding of position of impact specimens in the investigated sector of pipe of 300 mm width was made. Figure 11 shows results of KCV_{-40} along the perimeter and across the thickness of welded butt.

As is seen, the impact specimens with the values lower than the required ones, do not form the colonies, but distributed stochastically in the section of welded joint. Consequently, welded joint will not have the weakened areas noticeably extended from the point of view of values of toughness.



Spectrum	O	Al	Si	S	Ca	Mn	Fe
1	63.20	0.04	19.42	0.51	4.65	2.48	9.70
2	29.10	0.15	0.40	8.43	3.82	2.12	55.98
3	6.88	1.98	0.27	2.41	0.32	0.13	88.01
4	8.27	0.62	0.49	1.21	1.75	1.56	86.10
5	11.15	0.47	1.66	4.62	0.23	1.86	80.01

Figure 10. Macro- (*a*) and microstructure (*b*) of base metal fracture, opened along the rolling strip, and results of X-ray spectral microanalysis

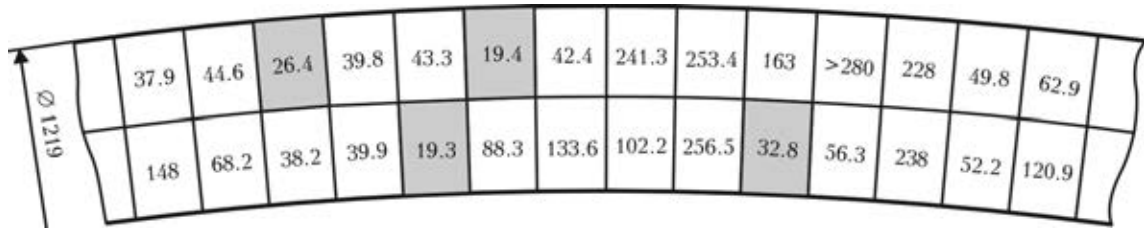


Figure 11. Test results of specimens along the perimeter and across the thickness of welded butt on impact bending at $T_{\text{test}} = -40\text{ }^{\circ}\text{C}$

All the given data give grounds to suppose that the presence of areas of structural heterogeneity in welded joints and, correspondingly, local decrease in values of impact toughness at the tested zone of welded joint area should not be considered as the rejection mark during evaluation of the quality of joints produced using FBW.

Using standards [4, 8] for electric arc welding the sizes of admissible defects and their total extension at any area of weld of 300 mm at non-destructive testing are determined. The maximum total length of such areas is 50 mm, and width is up to 1.5 mm as-applied to the defects of the «lack of penetration» type. Even if one accepts that the areas with structural heterogeneity in FBW are close to lack of penetrations in arc welding, then the mentioned dropouts of values of impact toughness in the butt welds are in the admissible ranges according to the standard. Actually, the mechanical properties of areas with structural heterogeneity are much higher and do not contain discontinuities, where metallic bond is absent at all.

Therefore the presence of single dropouts of values of impact toughness at low test temperatures should not be referred to rejection signs.

Conclusions

1. The comprehensive mechanical tests of high-strength steel pipe joints produced by FBW were carried out. The quality of joints completely meets the requirements of the International standard API STANDARD 1104. It was found that in impact bending tests the separate dropouts of KCV_{-40} values lower than the level required by standards DNV-OS-F101 and STO Gazprom 2-3.7-380-2009 were observed.

2. Using means of non-destructive testing methods of welded joints, none of welding de-

fects was revealed in the joints with low values of KCV_{-40} . It was established that decrease in values of KCV_{-40} is predetermined by formation of zones of 1–2 mm² area in the plane of joint characterized by structural heterogeneity, typical also of the base metal, which is revealed in a sharply distinct anisotropy of its ductile properties.

3. It is shown that the areas with structural heterogeneity do not form colonies but are distributed stochastically in the section of welded joint, therefore, they do not decrease the general serviceability of welded joint. The sizes of such areas do not exceed the admissible values accepted by the standards for defects of welds produced in arc welding.

4. The presence of separate local dropouts of KCV_{-40} values, observed during tests of welded joints produced using FBW, should not be considered as a rejecting sign.

1. Kuchuk-Yatsenko, S.I. (1986) *Resistance butt welding of pipelines*. Kiev: Naukova Dumka.
2. *API STANDARD 1104*: Welding of pipelines and related facilities. 21st ed.
3. *DNV-OS-F101*: Offshore standard. Submarine pipelines systems. Jan. 2000.
4. *STO Gazprom 2-3.7-380-2009*: Instruction on technology of welding of marine pipelines. Moscow.
5. Kuchuk-Yatsenko, S.I., Shvets, Yu.V., Zagadarchuk, V.F. et al. (2012) Flash-butt welding of thick-walled pipes from high-strength steels of K56 strength class. *The Paton Welding J.*, **5**, 2–7.
6. Kuchuk-Yatsenko, S.I., Shvets, Yu.V., Zagadarchuk, V.F. et al. (2013) Technology of heat treatment of pipe joints from steel of K56 grade produced by flash-butt welding. *Ibid.*, **2**, 2–7.
7. Kuchuk-Yatsenko, S.I., Kazymov, B.I., Zagadarchuk, V.F. et al. (1984) Formation of «dead spots» in joint produced by resistance welding. *Avtomatich. Svarka*, **11**, 23–26.
8. *STO Gazprom 22.4-359-2009*: Instruction on non-destructive testing of welded joints in construction of land and underwater gas pipelines from steels X-80, X-100. Moscow.

Received 29.10.2014



TRIBOTECHNICAL PROPERTIES OF DEPOSITED METAL OF 50Kh9S3G TYPE WITH INCREASED SULPHUR CONTENT

V.V. OSIN

E.O. Paton Electric Welding Institute, NASU
11 Bozhenko Str., 03680, Kiev, Ukraine. E-mail: office@paton.kiev.ua

Steels alloyed with sulphur (for instance, silchrome) are widely applied in manufacture of tools for cold rolling of metal. Their reconditioning repair requires materials ensuring deposited metal composition close to that of base metal. The work is a study of sulphur influence on tribotechnical properties of deposited metal of 50Kh9S3G type. Sulphur content in the deposited metal was varied in the range of 0.02 to 1.70 %. Investigations revealed that sulphur forms complex sulphides, which prevent seizure of interacting metal surfaces, thus increasing deposited sample wear resistance. To ensure optimum tribotechnical properties of deposited metal, volume content of complex sulphides of the main alloying elements should be within 1.5 to 2.0 %, and their dimensions should be ≤ 0.02 mm. This condition is ensured at total content of sulphur of 0.5–0.8 % in the deposited metal. At lower sulphur content the quantity of forming sulphides is insufficient to make an essential influence on deposited metal properties. At higher sulphur content the forming coarse sulphide inclusions are less strongly retained by deposited metal matrix and during testing they crumble and are removed from the wearing zone. This adversely affects wear resistance of deposited metal and contacting part. 10 Ref., 2 Tables, 3 Figures.

Keywords: *deposition, deposited metal, sulphur alloying, sulphides, tribotechnical properties*

Steel 50Kh9S3G, known as «silchrome» trade mark, is quite widely applied for manufacturing metal cold working tools, in particular, for deep cold drawing dies, as well as heavy-duty parts of some friction pairs. These parts operation process is characterized by significant mechanical loads and they fail most often as a result of seizure wear. For reconditioning cladding of cold drawing dies PWI developed flux-cored wire PP-Np-50Kh9S3G, providing deposited metal similar to base metal as to its composition [1]. Increase of seizure resistance of deposited metal of this type remains to be an urgent problem.

From scientific-technical publications [2–8] and earlier wear resistance studies at different kinds of wear of 23Kh5M3FS deposited metal [9] alloyed with sulphur, it is known that inclusions of complex sulphides prevent seizure wear, lower the friction coefficient, and improve the quality of deposited metal wearing surfaces. An objective was set to improve the tribotechnical characteristics of deposited metal of 50Kh9S3G type due to sulphur alloying.

Considering the experience of earlier studies [9], sulphur content in deposited metal of this type was varied within 0.02–1.30 % (Table 1).

Wear resistance and friction coefficient of deposited metal were assessed using an all-purpose component of friction machine, designed for laboratory-experimental evaluation of tribotechnical properties of friction pairs at room and elevated temperatures [10]. Wetting was assessed by the presence or absence of increase of counterbody or sample mass. Testing was conducted by hole abrasion method by «shaft-plane» schematic without additional lubricant feeding into friction zone. Samples for tribotechnical studies, cut out of deposited metal third-fourth layer, had the dimensions of $3 \times 17 \times 25$ mm. Wearing surface was 3×25 mm. Counterbody in the form of a ring of 40 mm diameter and 12 mm width was made from quenched steel 45 with hardness HRC 42.

Table 1. Composition and hardness of metal deposited with test flux-cored wires

Flux-cored wire designation	Weight fraction of elements, %					HRC hardness
	C	Mn	Si	Cr	S	
PP-Np-50Kh9S3G-Op-1	0.55	0.52	2.65	9.23	0.02	56
PP-Np-50Kh9S3G-Op-2	0.50	0.81	2.80	9.04	0.27	58
PP-Np-50Kh9S3G-Op-3	0.64	0.55	2.65	9.25	0.70	58
PP-Np-50Kh9S3G-Op-4	0.62	0.52	2.80	8.65	1.05	55
PP-Np-50Kh9S3G-Op-5	0.67	0.58	2.65	8.80	1.30	56

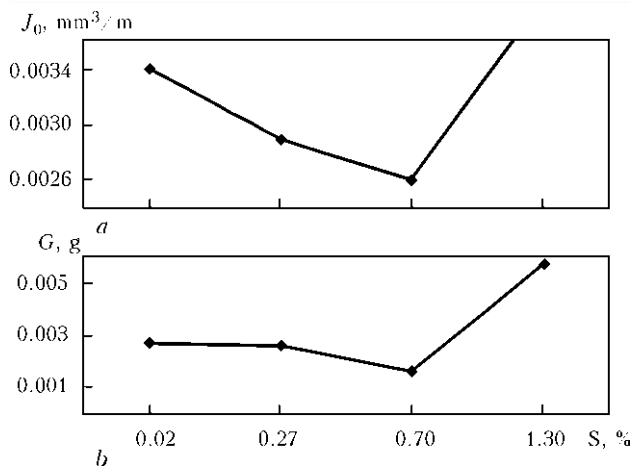


Figure 1. Wear of samples of 50Kh9S3G deposited metal with different content of sulphur (a) and counterbodies tested in pair with them (b)

The following test mode was selected by the results of pre-testing: sliding velocity of 0.06 m/s, 30 N load, test duration of 60 min after run-in and sliding distance of about 227 m. This mode ensured stabilization in time of tribotechnical characteristics of all the studied materials. At testing sample wear was determined by the volume of abrasion hole, and counterbody wear — by the difference in its mass before and after testing.

Wearing characteristics of deposited samples and counterbodies at metal-over-metal friction at room temperature are shown in Figure 1. As is seen from the given data, wear of deposited metal of 50Kh9S3G type at metal-over-metal friction at room temperature first decreases with increase of sulphur content to 0.7 %, and then, at increase of its content to 1.3 %, wear is intensified again. Counterbody wear is similar to wear of deposited metal samples. No seizure wear was detected as shown by test results. In sample-counterbody friction pair the best wear resistance was provided at sulphur content within 0.5–0.8 %. At increase of sulphur content in the sample up to 1.3 % counterbody wear was also somewhat increased.

Sulphur influence on friction coefficient of 50Kh9S3G deposited metal was studied (Figure 2). Deposited metal friction coefficient decreases up to sulphur content of 0.7 % and then, with increase of sulphur content to 1.3 %, it remains at approximately the same level. As in the case of wear, sulphur content of 0.5 to 0.8 % should be regarded as the optimum one.

A similar dependence of sample wear on sulphur content was observed also in [9]. Apparently, sample wear resistance and, consequently counterbody wear resistance, is associated with morphology and quantity of sulphide inclusions.

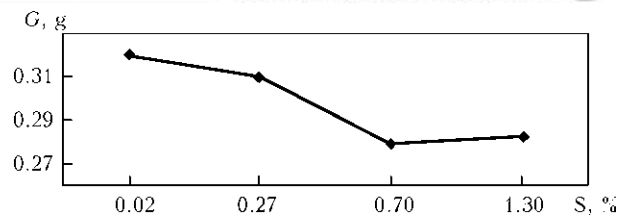


Figure 2. Sulphur influence on friction coefficient of 50Kh9S3G deposited metal

Investigation of microstructure of 50Kh9S3G deposited metal with different sulphur content was performed. Microstructure of 50Kh9S3G deposited metal without sulphur consists of martensite and residual austenite with a small amount of nonmetallic inclusions — silicates and oxides (Figure 3, a).

With addition of 0.27 % S, sulphide and oxysulphide inclusions appear in deposited metal microstructure (Figure 3, b). With further increase of sulphur content up to 0.7 %, deposited metal microstructure is refined, quantity and size of sulphide and oxysulphide inclusions increasing (Figure 3, c). In samples with sulphur content of 1.3 %, a multitude of individual sulphides of globular and elongated shape, as well as fine sulphide clusters are observed (Figure 3, d). Scarce very coarse sulphides and oxysulphides are also revealed, whereas practically no silicates are observed.

Sulphur content influence on nonmetallic inclusion volume fraction in unetched polished sections was studied in quantitative analyzer «Omnimet» at 600 magnification when scanning through 100 fields of view. At 0.7 % S content in the deposited metal, volume fraction of sul-

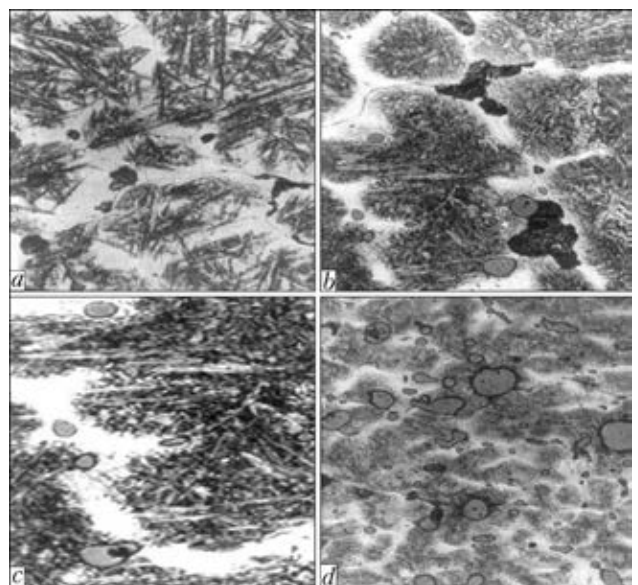


Figure 3. Microstructure ($\times 1000$) of 50Kh9S3G deposited metal with different sulphur content, %: a — 0.02; b — 0.27; c — 0.70; d — 1.30

**Table 2.** Composition of sulphide phase of 50Kh9S3G deposited metal with 0.7 % S

Deposited metal type	Analyzed section	Weight fraction of elements, %				
		S	Si	Mn	Cr	Fe
50Kh9S3G	Sulphide	12.53	1.22	28.81	13.15	44.28
	Matrix	0.03	3.40	0.59	9.27	86.26

phides in upper deposited layers reaches 1.99 % (by volume), and at 1.3 % S content it is ≤ 3.21 %.

Dimensions of sulphide inclusions are greater than those of silicate ones, and sulphide inclusions become coarser with increase of sulphur content. At sulphur content of 0.7 %, sulphide inclusions size is from 0.007 to 0.02 mm, and at sulphur content of 1.3 % it is from 0.025 to 0.05 mm, and single inclusions of 0.075 mm size were also found.

Microhardness of nonmetallic inclusions was determined in the LECO hardness meter M-400 at 10 g load. Sulphides have essentially lower microhardness than silicates, average microhardness of sulphides is 2835 MPa, and that of silicates is 9130 MPa. Results of X-ray microprobe analysis show that manganese and chromium actively react with sulphur, making up almost half of sulphide phase volume (Table 2). Fraction of iron sulphides is also high, while silicon is mostly present in the composition of complex sulphides.

Comparing the results of studying the microstructure of 50Kh9S3G deposited metal with the results of its wear resistance studies, leads to the conclusion that in order to ensure optimum tribotechnical properties of 50Kh9S3G deposited metal, volume fraction of complex sulphides of the main alloying elements in its structure should be within the ranges of 1.5 to 2.0 %, and their dimensions should be ≤ 0.02 mm. In order to satisfy these conditions, it is necessary for sulphur content in the deposited metal to be equal to 0.5 to 0.8 %.

At lower content of sulphur the quantity of forming sulphides is insufficient for them to make a significant influence on properties of 50Kh9S3G deposited metal. At greater sulphur content, the forming coarse sulphide inclusions are weakly retained by deposited metal matrix, and during testing they are crushed and removed from the wearing zone. This impairs the wear resistance of deposited metal and mating part. Moreover, sulphide crushing out can be promoted by the combination of low microhardness and

large volume fraction of sulphide inclusions, that may lead to inability to resist high contact pressures in the friction zone.

Conclusions

1. It is established that at sulphur alloying of 50Kh9S3G deposited metal, sulphides of the main alloying elements prevent seizure of wearing surfaces under the conditions of dry metal-over-metal friction.

2. To ensure optimum tribotechnical properties of 50Kh9S3G deposited metal, volume fraction of complex sulphides in its structure should be equal to 1.5–2.0 %, and their dimensions should be ≤ 0.02 mm. To satisfy this condition, sulphur content in the deposited metal should be within 0.5–0.8 %. At lower sulphur content sulphides cannot have any essential influence on deposited metal tribotechnical properties. At higher sulphur content the forming coarse sulphides are weakly retained by deposited metal matrix and crush out during wear and are removed from the wearing zone that impairs the wear resistance.

1. Ryabtsev, I.A., Kondratiev, I.A. (1999) *Mechanised electric arc surfacing of metallurgical equipment parts*. Kiev: Ekotekhnologiya.
2. Fedorchenko, I.M., Pugina, L.I., Slys, I.G. et al. (1973) Bearing sulphurised metal-ceramic materials on the base of stainless steels. In: *Friction and wear at high temperatures*, 115–120. Moscow: Nauka.
3. Vinogradov, Yu.M. (1965) Sulphidizing, selenizing and tellurizing of steels, cast iron and alloys. *Metalovedenie i Termich. Obrab. Metallov*, **10**, 36–41.
4. Kovalchenko, M.S., Sychev, V.V., Tkachenko, Yu.G. et al. (1973) Influence of temperature on friction characteristics of some sulphides, selenides and tellurides of refractory metals. In: *Friction and wear at high temperatures*, 133–138. Moscow: Nauka.
5. Artamonov, A.Ya., Barsegyan, Sh.E., Repkin, Yu.D. (1968) Examination of lubricating properties of molybdenum and tungsten disulphides. *Poroshk. Metallurgiya*, **12**, 53–58.
6. Samsonov, G.V., Barsegyan, Sh.E., Tkachenko, Yu.G. (1973) On mechanism of lubricating action of sulphides and selenides of refractory metals. *Fiz.-Khimich. Mekhanika Materialov*, **9(1)**, 58–61.
7. Lunev, V.V., Averin, V.V. (1988) *Sulphur and phosphorus in steel*. Moscow: Metallurgiya.
8. Osin, V.V., Ryabtsev, I.A. (2004) Effect of sulphur on properties of iron-base alloys and prospects of its application in surfacing materials. *The Paton Welding J.*, **10**, 18–21.
9. Osin, V.V., Ryabtsev, I.A., Kondratiev, I.A. (2006) Study of sulfur effect on properties of deposited metal of Kh5MFS type. *Ibid.*, **12**, 12–15.
10. Ryabtsev, I.I., Chernyak, Ya.P., Osin, V.V. (2004) Block-module unit for testing of deposited metal. *Svarshchik*, **1**, 18–20.

Received 20.10.2014



EFFECT OF TEMPERATURE OF THERMOMECHANICAL TREATMENT ON QUALITY OF DISSIMILAR METAL JOINTS

L.Yu. DEMIDENKO, N.A. ONATSKAYA and V.D. POLOVINKA

Institute of Pulse Processes and Technologies, NASU
43a Oktyabrsky Ave., 54018, Nikolaev, Ukraine. E-mail: iipt@iipt.com.ua

At present time, pressure welding methods acquire more and more distribution for quality joining of dissimilar metals. The Institute of Pulse Processes and Technologies of the NAS of Ukraine has developed a new method of welding of materials in solid state using current pulses. In essence, it lies in the fact that metals being welded at ambient temperature are pressure contracted and specific amount of current pulses of amplitude density not less than $1.2 \cdot 10^9$ A/m² and duration not less than $2 \cdot 10^{-4}$ s are passed through deformation zone for intensification of plastic deformation at stage of physical contact formation. At that mutual deformation of surface projection provides for sufficiently tight contact of surfaces being welded and allows for their isolating from ambient environment. A welded joint is formed at further heating by type of diffusion one without application of special shield of the surfaces from oxidation. Aim of present work is an investigation of effect of temperature of thermomechanical treatment on quality of joints in welding of dissimilar metals in solid state using current pulses of large density. Such research methods as mechanical shearing tests, optical metallography and micro X-ray spectral analysis were used at that. It was determined as the result of experiments that 800 °C temperature is the most favorable for providing a quality steel 20 plus copper M1 welded joint, since at that no discontinuities are present in joint zone and clearly expressed initial structure is preserved in metal itself. 9 Ref., 3 Tables, 5 Figures.

Keywords: *welded joints of dissimilar metals, temperature of thermomechanical treatment, current pulses of large density, self-sealing of inter-contact zone, metallographic investigations, mechanical shearing tests*

Application of metals and alloys dissimilar on their properties is typical for manufacture of welded joints in current commercial production [1, 2]. This allows for using specific properties of each of them in full extent, reducing consumption of expensive and rare metals, producing of parts with high service properties and reducing their weight. In this connection, development of new, efficient and low-power consuming technological processes for producing of quality welded joints from dissimilar metals is relevant.

The Institute of Pulse Processes and Technologies (IPPT) of the NAS of Ukraine developed a new method of welding of metals in solid state using current pulses [3]. It is a variant of pressure welding with preheating.

In essence, it lies in the fact that metals being welded at ambient temperature are pressure contracted and specific amount of current pulses of amplitude density not less than $1.2 \cdot 10^9$ A/m² and duration not less than $2 \cdot 10^{-4}$ s are passed through deformation zone for intensification of plastic deformation at stage of physical contact formation. At that mutual deformation of surface projection provides for sufficiently tight contact of surfaces being welded and allows their isolating

from ambient environment. A welded joint is formed at further heating without application of special shield of the surfaces from oxidation [4].

Steel 20 and copper M1 were selected for welding of dissimilar metals using proposed method. First of all, they are widely used in manufacture of technical parts in electrical technologies, transport, machine building and, secondly, they have significant differences in their physical-mechanical properties and crystallographic characteristics. Mutual solubility of these metals is relatively small and depends on temperature [5], therefore it was relevant to investigate their effect on quality of produced welded joints.

Aim of present work is an investigation of effect of temperature of thermomechanical treatment (TMT) on quality of joints in welding of dissimilar metals in solid state using current pulses of large density.

Materials and experiment procedure. Rectangular plates of 170 mm length, 12 mm width and 2.5 mm thickness were used as mock-up specimens for welding of dissimilar metals using current pulses of large density, at that zone of welding with length $l \approx 22$ mm were taken in the middle of specimen (Figure 1).

Mechanical preparation of plate surfaces was carried out immediately before welding. It lied in their grinding up to combs height (microirregularities) $H_0 = 5-6$ μm. Then, the plate surfaces were degreased by acetone. Plastic defor-

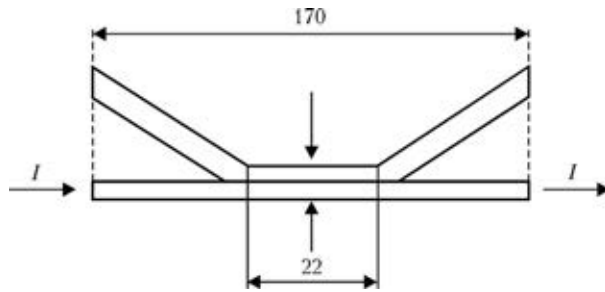


Figure 1. Scheme of contraction of specimens for treatment by current pulses

mation of microprojections over contact surfaces was carried out by pressing of the specimens at ambient (room) temperature in special device at calculation nominal pressure equal 50 MPa. Pulse current treatment of contact zone of pressed plates was performed by means of current passing along one steel plate. Parameters of pulse current was the same as in work [4], namely, amplitude of current density $J = 1.85 \cdot 10^9 \text{ A/m}^2$, pulse duration (attenuating sine wave) $\tau \approx 3 \cdot 10^{-4} \text{ s}$, number of pulses $N = 90$ and pulse sequence frequency 0.5 Hz.

Pulse-treated specimens together with device were set in a chamber electric furnace for further heating.

Welded joints in order to determine the effect of TMT temperature on their quality were heated in the furnace to welding temperature, which according to [6] was selected in 0.5–0.7 range from melting temperature, i.e. at 750, 800 and 850 °C and holding at indicated temperature during 20 min. At least three specimens are necessary for each temperature level.

Quality of the welded joints were estimated using the results of metallographic investigations and mechanical tests of templates, cut out from contact zone of welded specimens (see Figure 1). At that, each template was cut along the cross section. One part of the templates was used for metallographic investigations and another one for mechanical tests.

The microsections for metallographic investigations were taken normal to contact plane. Preparation of sections to investigations lied in

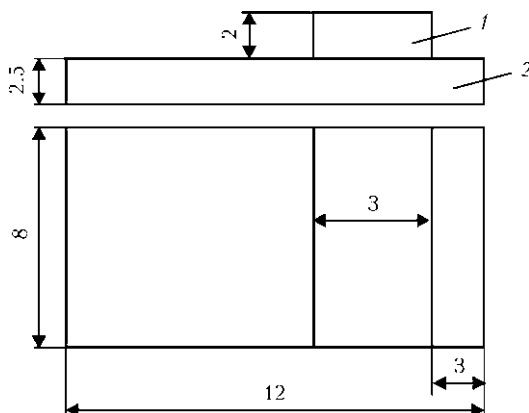


Figure 2. Scheme of specimen for shearing tests: 1 – copper plate section; 2 – steel plate

mechanical grinding and further etching in 4 % alcoholic nital [7].

Welded joint quality was preliminary estimated by condition of boundary along the joint line (by discontinuities presence). At that, estimation of boundary condition was carried out along its width, which is determined using metallographic microscope «Microtech» of MMO-1600 model at 400-fold magnification. If discontinuities along the joint line are present, their measurement is performed at 1000-fold magnification in 100 points homogeneously distributed along the joint line. Fraction (in percent expression) of that or other values of boundary width along the joint line was calculated based on their results.

Distribution (diffusion) of elements was examined using a method of micro X-ray spectrum analysis in the cross section from base metal to joint line as well as along the joint line from copper side.

Mechanical strength tests (shearing tests) were carried out in accordance to GOST 10885–85 for determination of stresses, promoting shearing deformation with fracture of welded joint along welding line. For this purpose, the specimens for investigations were produced from part of the templates (Figure 2).

The tests were carried out at laboratory bench, designed for investigation of static characteristics of materials and developed at IPPT using the device, scheme of which is given in Figure 3. This device allows for providing pure shearing stress in tested section of the specimen when applying tensile stresses F_s to guide plates. Loading of the specimens was carried out gradually with holding at each step during 3 min.

Strength of the joints was estimated on shearing stresses $\tau_{sh} = F_{sh}/S_{sh}$, where F_{sh} is the shearing force of tested section, kN; S_{sh} is the area of the section to be sheared, mm^2 .

Results of experiments and their discussion.

Earlier the investigations were carried on study of change of surface projection under effect of pulse current using the scheme of current passing indicated above with the help of the Philips scanning electron microscope SEM 515 (Holland). Their results showed that treatment of preliminary compressed metal plates of steel 20 + copper M1 by current pulses of large density promotes for significant deformation of their surface projection, as a consequence of which area of physical contact covering 60 to 80 % of general contact area is formed [4]. Mutual deformation of surface projection if applicable to investigated welding method provides for sufficiently tight contact of surfaces being welded, that allows for their isolating from environment and creates the possibility of producing of welded joint without application of shielding medium at further heating. This fact was verified experimentally in the same work.



Table 1. Results of mechanical shearing tests of templates of steel 20 + copper M1 welded joints

Heat treatment temperature T , °C	Shearing stress τ_{sh} , MPa	Relative shearing stress $\bar{\tau}_{sh}$
750	176.0 ± 6.2	0.96
800	180.7 ± 3.5	0.98
850	174.2 ± 5.1	0.95

Rise of temperature at stage of volumetric interaction is necessary for artificial increase of ductility of welded metals and acceleration of diffusion processes. Besides, the heat treatment intensifies diffusible solution of hydrogen from near-surface metal in metal depth. As the result oxidized layer is diffused and does not play a role of barrier for emergence of dislocations in the joint zone. Rates of activation and setting of contact surfaces are increased at that, and development of interaction of metals being joined takes place in contact plane with formation of strong metallic bonds as well as in volume of contact zone.

Table 1 gives the averaged results of measurement of shearing stresses of welded joints produced at different temperatures.

Comparison of strength of welded joints and base metal was carried out. For that, base metal specimen (copper in given case), which is similar to welded one (see Figure 2), was subjected to thermo-deformation impact, simulating welding conditions, and tested using the same procedure. Thus, relative shearing stress $\bar{\tau}_{sh}$ was determined for all investigated welding temperatures as

$$\bar{\tau}_{sh}(T) = \tau_{sh}(T) / \tau(T),$$

where $\tau_{sh}(T)$ is the shearing stress, received at welding temperature, MPa; $\tau(T)$ is the shearing strength of base metal after heat treatment on welding mode, MPa.

Table 1 provides for calculation values of relative value of shearing stress.

The results of mechanical tests determined that shearing strength of produced welded joints is changed in a narrow range from 174.2 to 180.7 MPa at variation of welding temperature from 750 to 850 °C, that corresponds to copper strength 0.95–0.98.

Figure 4 shows the microstructures of zones of produced welded joints, and Table 2 gives the results of change of boundary width and its portion along the joint line. It can be seen from the Table that rise of TMT results in reduction of boundary width as well as increase of number of points along the joint line, in which its minimum width was registered. Thus, 8 % of joint line examined length have defects of 0.5–1.0 μm size at 750 °C THT temperature. The rest 92 % have boundary width less than 0.5 μm . Defects of pore type and discontinuities in the joint zone are already absent at higher temperatures (800 and

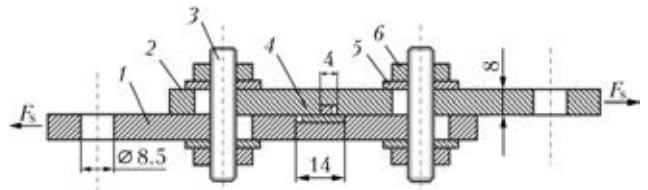


Figure 3. Scheme of device for shearing testing of specimens: 1, 2 – upper and lower guide plates, respectively; 3 – pin; 4 – welded specimen; 5 – washer; 6 – nut

850 °C), and joint zone itself represents a grain boundary oriented in plate of initial contact (Figure 4, b, c).

However, comparison of microstructures of produced welded joints shows that rise of TMT temperature to 850 °C results in grain growth in steel 20 in the joint zone as well as base metal (see Figure 4, c). This is undesirable moment, since it can promote reduction of welded joint strength characteristics.

It can be concluded based on the results of metallographic examinations that TMT temperature of 800 °C is the most preferable for providing of quality welded joint from steel 20 + copper M1. At that, no discontinuities are present in the joint zone, clearly expressed initial structure is preserved in the metal itself, and joint zone represents a grain boundary oriented in plane of initial contact.

Micro X-ray spectral analysis of nature of distribution of main elements in the cross section of central part of welded specimen, received after TMT at 800 °C during 20 min, indicate that the composition is changed from 100 % Fe (or Cu) to 100 % Cu (or Fe) (Figure 5) in near-contact zone of the joint. At that, penetration depth of copper (concentration up to 1 %) in steel 20 metal is around 15 μm from joint line, and that for iron in copper makes approximately 13 μm . The results obtained can be completely agreed with current understanding that appearance of diffusion zones at joint boundary is typical for metals with limited mutual solubility [8]. Their formation is related with the fact that some amount of copper atoms penetrates (diffuse) in iron through interface as a result of specific solubility. Similarly, some amount of iron atoms diffuses in copper (Table 3).

The results, presented in Table 3 and Figure 5, show formation of solid solutions along the joint line and in cross section from the side of steel 20 as well

Table 2. Width of boundary and its percent content along joint line at different TMT temperatures

Heat treatment temperature T , °C	Boundary width, μm		
	1.0	<0.5	<0.5
750	7	1	92
800	–	–	100
850	–	–	100

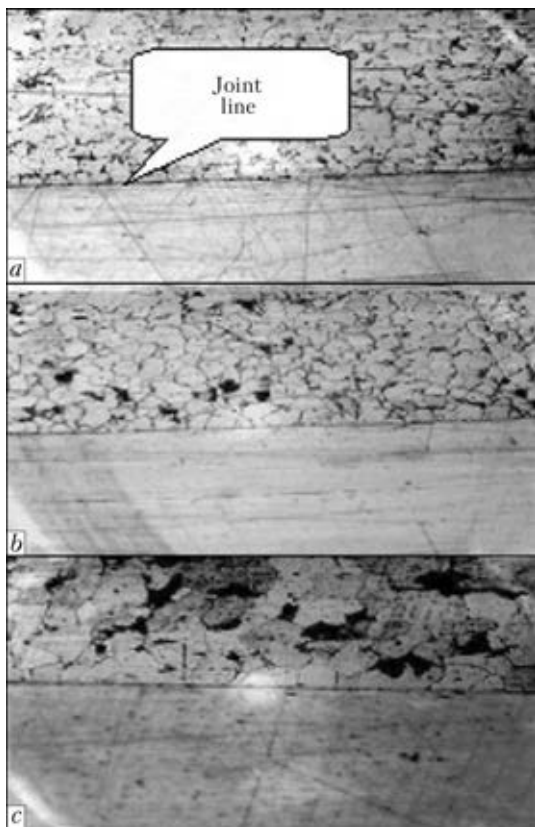


Figure 4. Microstructure (x400) of zone of steel 20 + copper M1 welded joints at $T = 750$ (a), 800 (b) and 850 (c) °C

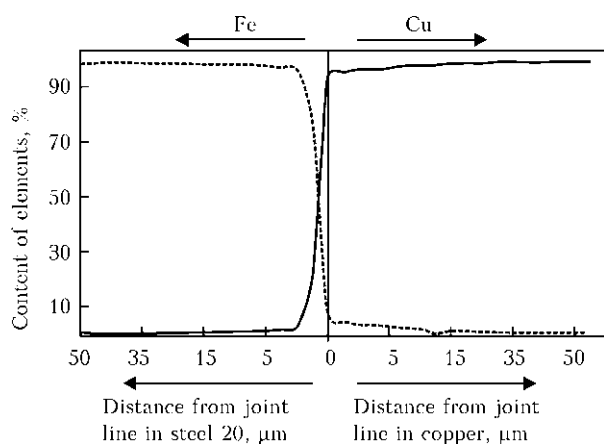


Figure 5. Nature of distribution of main elements in cross section of central part of steel 20 + copper M1 welded joint after TMT at $T = 800$ °C

as copper M1. This is an indication of processes of interatomic interaction of contact surfaces. At that, no phase formations, capable to result in welded joint embrittlement, were found.

Thus, welding method under investigation allows for producing of quality joints of steel 20 + copper M1 at lower parameters of thermal deformation than in traditional diffusion welding. Besides, it can be done without application of special shield of surfaces being welded from oxidation, for example, vacuum processing or using controlled inert gas atmosphere. Isolation of welding zone from ambient media in welding using current pulses is provided as a result of self-sealing of

Table 3. Distribution of elements along joint line from copper side (in %) at depth around 10 μm

Point No.	Cu	Fe	Cr	Mn	Ni
1	99.60	0.38	–	–	0.02
2	97.82	2.12	0.06	–	–
3	96.84	2.74	–	0.11	0.32
4	96.82	3.14	–	0.03	0.02
5	97.22	2.45	–	0.13	0.20
6	96.40	3.27	0.12	0.02	0.22
7	96.85	3.09	–	–	0.07
8	96.56	3.13	0.02	0.05	0.25

inter-contact zone due to current-stimulated intensive plastic deformation of surface layers of metals being joined. Further heating of sealed space promotes formation of autovacuum, providing self-cleaning of surfaces from oxide films [9] and production of welded joint.

Conclusions

1. TMT temperature of 800 °C is the most favorable for welding of steel 20 and copper M1 dissimilar materials in solid state using current pulses, since no defects of discontinuity type are present in the joint zone, and clearly expressed initial structure is preserved in the metal itself.

2. It is shown that zones of solid solutions are formed in cross section along the joint line from the side of steel 20 as well as copper M1. At that, no phase formations, capable to result in welded joint embrittlement, were found in these zones.

3. The results of mechanical tests indicate that produced welded joints have sufficiently high shearing strength comparable with base metal strength.

- Middeldorf, K., von Hofe, D. (2008) Trends in joining technology. *The Paton Welding J.*, **11**, 33–39.
- Reisgen, U., Stein, L., Steiners, M. (2010) Stahl-Aluminium-Mischverbindungen: Schweißen oder Loeten? Die Kombination zweier etablierter Fügeverfahren macht Unmögliches möglich. *Schweißen und Schneiden*, **62**(5), 278–284.
- Polovinka, V.D., Yurchenko, E.S., Vovchenko, O.I. *Method of diffusion welding of metals*. Pat. 79181 Ukraine. Int. Cl. B23K 31/02. Publ. 25.05.07.
- Vovchenko, A.I., Demidenko, L.Yu., Onatskaya, N.A. (2011) Intensification of plastic deformation of metal surfaces under action of current pulses in pressure welding. *Naukovi Notatky: Mizhvuz. Zbirnyk*, **32**, 63–68.
- Kurt, A., Uygur, E., Mutlu, E. (2006) The effect of allotropic transformation temperature in diffusion-welded low-carbon steel and copper. *Metallofiz. Nov. Tekhnol.*, **28**(1), 39–52.
- Kazakov, N.F. (1976) *Diffusion welding of materials*. Moscow: Mashinostroenie.
- Kovalenko, V.S. (1973) *Metallographic reagents*. Moscow: Metallurgiya.
- Karakozov, E.S. (1976) *Joining of metals in solid phase*. Moscow: Metallurgiya.
- Paton, B.E., Medovar, B.I., Saenko, V.Ya. (1980) Spontaneous cleaning of metals from oxide films. *Doklady AN SSSR*, **159**(1), 1117–1118.

Received 05.05.2014



INVESTIGATION OF SPRAYING SPOT AND METALLIZATION PATTERN UNDER CONDITIONS OF MICROPLASMA SPRAYING OF COATINGS OF TITANIUM DIOXIDE

Yu.S. BORISOV, S.G. VOJNAROVICH, A.N. KISLITSA and S.N. KALYUZHNY

E.O. Paton Electric Welding Institute, NASU

11 Bozhenko Str., 03680, Kiev, Ukraine. E-mail: office@paton.kiev.ua

Analyzed is the gained experience in application of gas-thermal technologies in producing of electroconductive, dielectric and resistive coatings for machine building, instrument-making industry and other industry branches. It is shown that the most challenging method for formation of resistive coatings in manufacture of heating elements is a method of the plasma-arc spraying. It was found that during the process of manufacture of the resistive heating elements of small sizes (for example, for radio electronics) by using the method of traditional plasma-arc spraying the losses of material being sprayed, caused by a geometric factor, are increased. In this connection, to increase the degree of applying of sprayed materials, the technology of microplasma spraying is the mostly challenging. The work is aimed at the study of formation of a spraying spot and a metallization pattern under the conditions of microplasma spraying of the titanium dioxide coating. It was found during investigations that the spraying spot of TiO_2 has a form of ellipse with 6.0–9.2 mm sizes of axes, where the smaller axis is directed along the horizontal line, and the larger one – along the vertical line. Ratio of axes is 1.01–1.47 and depends on the spraying mode parameters. Determined are the losses of material being sprayed due to a geometric factor, which were 53 % in spraying of path of 1 mm width and less than 1 % in spraying the path of 5 mm width. 19 Ref., 1 Table, 5 Figures.

Keywords: *microplasma spraying, titanium dioxide, resistive heating element, metallization pattern*

Today, a large experience has been gained in producing of different types of coatings, such as electroconductive, dielectric and resistive ones using the methods of gas thermal spraying (GTS), which are designed for different industry branches (machine building, electrical engineering, instrument-making etc.) [1–3].

The resistive coatings, produced by the GTS methods, represent a great practical interest. Analysis of literature about carried out investigations on application of GTS methods for formation of resistive coatings in electrical engineering confirms many times the challenging future of these technologies [4, 5]. With the development and improvement of the GTS technology during the recent years a method of plasma-arc technology finds the more and more wide application in the production of the resistive coatings [6–9]. In particular, this method was perfect in manufacture of resistive heating elements (RHE) [10–12].

The RHE, manufactured by the method of plasma-arc spraying, are characterized by a significant decrease in temperature in current-carrying layers and increase in service life [13–15].

However, during the process of manufacture of RHE of small sizes for radio electronics using the traditional plasma-arc spraying the additional costs appear, caused by increase in losses of material being sprayed, which are characterized as losses connected with a geometric factor. These losses are predetermined by the fact that the spot diameter of spraying for the traditional plasma-arc spraying is 20–25 mm, that exceeds the path width (2–5 mm) of the RHE.

To increase the degree of application of the material being sprayed it is rational to apply the technology of a microplasma spraying (MPS) [16, 17]. This technology will allow producing coatings from different types of materials, reducing greatly the losses of material being sprayed due to a small diameter of a spraying spot (3–5 mm), having in this case the minimum thermal effect on the substrate, thus allowing coatings to be sprayed on thin-walled parts without their distortion.

In the present work the formation of the spraying spot and metallization pattern was studied under the conditions of microplasma deposition of titanium dioxide coatings, the losses of material being sprayed, caused by a geometric factor

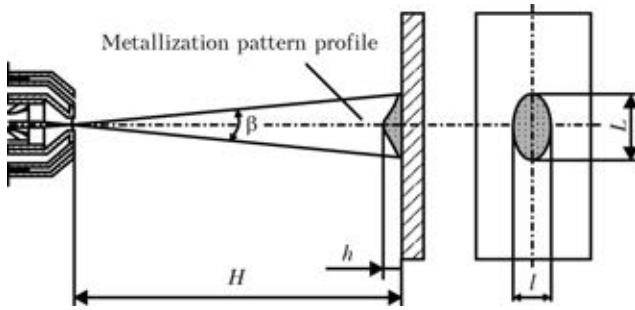


Figure 1. Scheme of metallization pattern investigation

depending on width of path being sprayed, were determined.

To analyze the material losses, connected with a geometric factor, a number of experiments was carried out for determination of parameters of the metallization pattern, which describes the distribution of the coating material mass in the spraying spot. The metallization patterns were obtained during the process of spraying at a fixed plasmatron into a spot on flat specimens of 20 mm size during 10 s, and then the measurements of vertical (large) L and horizontal (small) axes l of spraying spot, as well as maximum height of the deposited hill h were made (Figure 1).

Using a digital camera the macrofilming of profiles of the metallization pattern was made in the directions normal to its axes (Figure 2).

Then, the processing of image was made for determination of coordinates of the pattern profile. Using MathCad program the metallization pattern was designed according to these coordinates and its describing function was determined, from which the pattern area for larger and smaller axes was calculated. Having data about the sizes of metallization pattern, it is possible to determine such a parameter as an angle of opening of the plasma jet:

$$\beta = 0.5 \arctg \frac{L}{2H}, \quad (1)$$

where L is the bead width; H is the distance of spraying.

Losses of material, connected with geometric factor, were determined as

$$L_{g.f} = (1 - S_{x-x}/S_{tot}) \cdot 100, \% \quad (2)$$

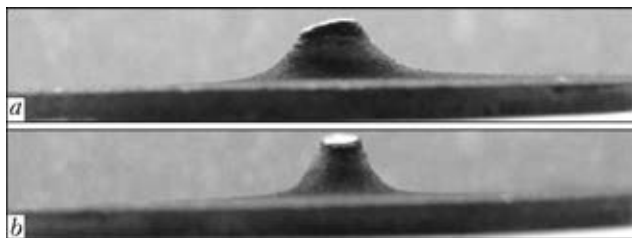


Figure 2. Metallization pattern profiles of TiO_2 material: a – large axis; b – small axis

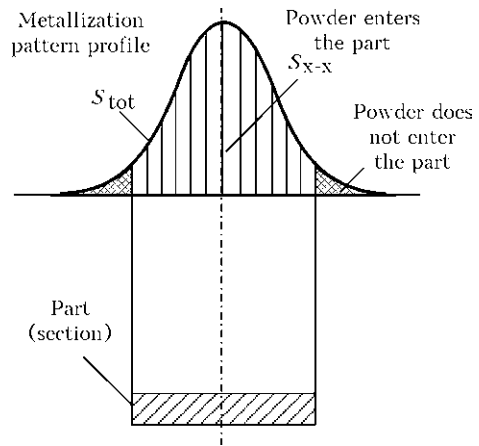


Figure 3. Losses of material due to geometric factor

where S_{x-x} is the area of metallization pattern confined by part size; S_{tot} is the total area of metallization pattern (Figure 3).

The spraying was performed in MPN-004 type installation for MPS. «Metachim» powder of titanium dioxide (TiO_2) with different sizes of powder of 15–40 μm was used as a material for spraying.

The intervals of varying, values of mode parameters being studied and results of the experiment for measurement of geometric parameters of the spraying spot are given in the Table.

It was found during investigations that the spraying spot of TiO_2 powder has a form of an ellipse with 6.0–9.2 mm size of axes, where the smaller axis is directed along the horizontal line and the larger one – along the vertical line. Ratio of axes is 1.01–1.47 and depends on parameters of the spraying mode. Probably, this shape of the spraying spot is caused by the fact that during the powder feeding from batcher MD-004 a gravity force, directed normal to the jet axis, has an effect on its particles. As the powder particles are differed by the size and,

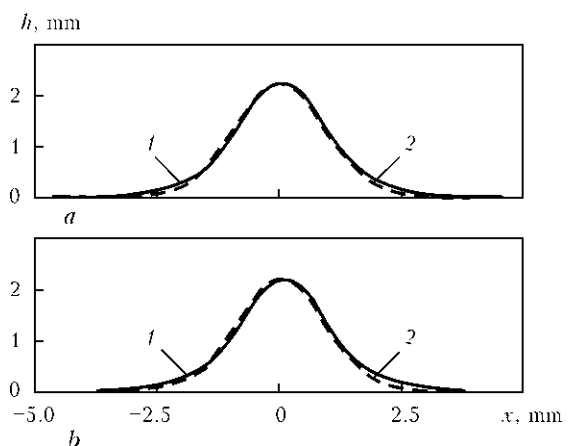


Figure 4. Transverse section of metallization patterns in axes of spraying spot: a – section along large axis $y = 2.21 \cdot e^{-0.56x^2}$; b – section along small axis $y = 2.21 \cdot e^{-0.6x^2}$; 1 – diagram of Gauss distribution (calculated); 2 – real metallization pattern profile

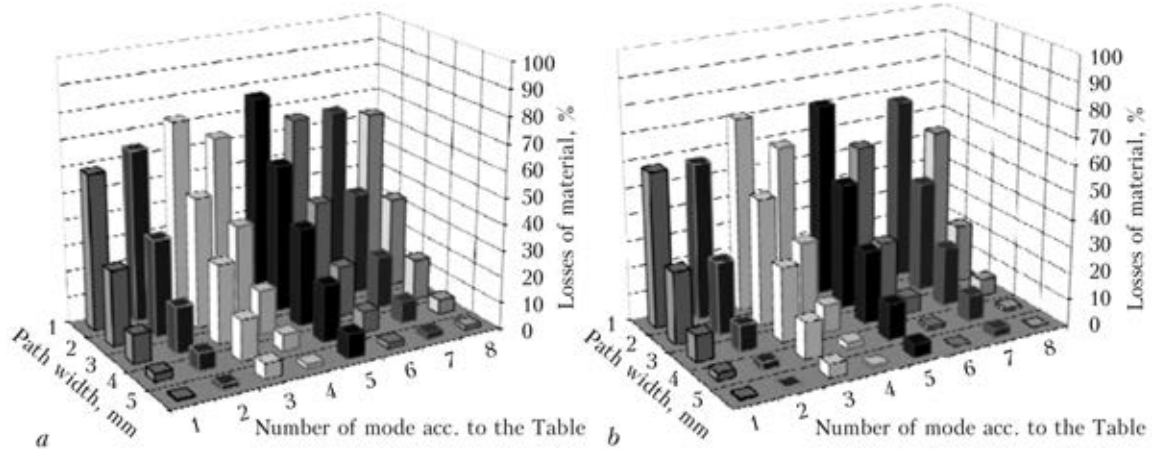


Figure 5. Losses of spraying material connected with geometric factor depending on size of the resistive path: *a* – for large diagonal; *b* – for smaller diagonal

Parameters of metallization pattern depending on mode of TiO₂ spraying

Mode number	<i>I</i> , A	<i>G</i> _{pl} , l/min	<i>H</i> , mm	<i>P</i> _{p.c.} g/min	Height of metallization pattern, mm	Large axis, mm	Smaller axis, mm
1	45	120	200	1.8	2.21	9.2	7.5
2	45	120	100	0.6	1.04	6.3	4.7
3	45	60	200	0.6	0.53	8.2	7.4
4	45	60	100	1.8	2.31	7.2	5.6
5	35	20	200	0.6	0.35	8.8	6.2
6	35	120	100	1.8	2.27	8.6	6.6
7	35	60	200	1.8	0.81	7.2	7.0
8	35	60	100	0.6	1.34	7.6	5.4

consequently, the mass and aerodynamic resistance, they will penetrate into the jet for different depth under the gravity force action. Under these conditions the produced spraying spot will have a shape of ellipse, the larger axis of which is located in the vertical plane, i.e. it coincides with the direction of the gravity force action (see Figure 1). The analysis of nature of the curves showed that the geometry of the metallization pattern at MPS is described rather reliably by the Gauss function [18]:

$$y = y_0 e^{-kx^2}, \tag{3}$$

where *y*₀ is the thickness of coating at the bead axis; *k* is the coefficient of coating material concentration in the spraying spot.

Using experimental data, obtained as a result of measurements the metallization pattern profiles (measurements were made in large *L* and small *l* axes, see Figure 1) were plotted, which coincided with Gauss curves, for different modes of spraying (Figure 4). Coefficient of correlation *K* was 0.9849–0.9992. Value of *k* varied in the range of 0.12–0.97.

As a result of the carried out calculations according to formula (1) it was found that the

angle of opening of the microplasma jet is within the ranges of 2–5.2°. The obtained results correlate with values given in literature for laminar plasma jets [19].

Calculations of losses of material being sprayed, caused by a geometric factor, depending on size of the resistive path, were made for each experiment and are given in the form of histograms (Figure 5).

The analysis of histogram can state that the least losses are provided in applying of the mode 6 (see the Table). This mode is characterized by a minimum value of current and high consumption of plasma gas, that reduces the temperature of the plasma jet, thus decreasing the spraying distance to substrate without risk of its overheating. Decrease in the distance leads in turn to minimizing of the spraying spot. In this case the losses were 53 % in spraying of path of 1 mm width and less than 1 % in spraying of path of 5 mm.

Conclusions

1. It was established as a result of study of the process of titanium dioxide coating formation under the MPS conditions that the geometric sizes of the spraying spot depend on the spraying proc-



ess parameters. The spraying spot has a form of ellipse with 6.0–9.2 mm sizes of axes at 1.01–1.47 ratio of axes, and metallization pattern is described by the Gauss distribution.

2. It was shown that it is possible to control the material losses, caused by geometric factor, by selection of MPS modes of resistive paths of TiO₂ material. Minimum losses are attained on the conditions of plasmatron operation at the mode 6, which is characterized by minimum current value and high consumption of plasma gas that reduces the plasma jet temperature and, thus, decreasing the spraying distance to substrate without risk of its overheating with decrease of the spraying spot. This allows providing the minimum losses of material being sprayed to path from 1 up to 5 mm width that equal to 53 % in spraying of path of 1 mm width and less than 1 % in spraying of path of 5 mm width.

1. Vashkevich, F.F., Spalnik, A.Ya., Pluzhko, I.A. (2009) Electrothermal insulation of inductors for internal heating of tube shells. In: *Building, materials science, machine building*. Dnepropetrovsk: PGSA.
2. Borisov, Yu.S., Kislitsa, A.N. (2002) Microplasma spraying using wire materials. *The Paton Welding J.*, **3**, 50–51.
3. Kovalenko, G.D., Zombzhitsky, A.P. (1980) Specifics of plasma spraying of electric heating coatings with dielectric filler. *Fizika i Khimiya Obrab. Materialov*, **4**, 86–89.
4. Lyasnikov, V.N., Perov, V.V., Lavrova, V.N. (1977) Application of plasma-arc spraying of alundum in manufacturing of cathode-heating assembly-unit. In: *Electronic engineering*, Series Microwave electronics, Issue 4, 85–87.
5. Baklanov, D.I., Belyajkov, I.N., Virnik, A.M. et al. *Method of manufacturing of resistive heating element*. Pat. 2066514 RF. Int. Cl. H 05 B 3/12. Publ. 10.09.96.
6. Scheitz, S., Toma, L., Berger, L.-M. et al. (2011) Thermisch gespritzte keramische Schichttheizelemente. *Thermal Spray Bull.*, **4**, 88–92.
7. Lyasnikov, V.K., Bogatyrev, G.F. (1978) Plasma spraying of powder materials on parts of electronic devices. In: *Review on electronic engineering*, Series Technology, industrial engineering and equipment, Issue 4, 62.
8. Robson, G.J. (1976) Applications of plasma spraying in hard facing. In: *Proc. of Public Session and Metals Technology Conf. (Sydney)*, 6.5.1–6.5.12.
9. Hasui, A. (1975) *Procedure of spraying*. Moscow: Mashinostroenie.
10. Dostanko, A.P., Vityaz, P.A. (2001) *Plasma processes in production of products of electronic engineering*, Vol. 3. Minsk: FU AIN FORM.
11. Baranovsky, N.D., Sharonov, E.A., Vannovsky, V.V. (1991) Electrical properties of plasma coatings of plane heating elements. In: *Proc. of Conf. on Thermal Spraying in Industry of USSR and Abroad* (Leningrad, 27–29 May 1991), 60–61.
12. Griffen, L.A., Dyadchko, A.G. et al. (1990) Heating elements for fittings, produced by thermal spraying method of powders. *Poroshk. Metallurgiya*, **5**, 102–104.
13. Ershov, A.A., Urbakh, E.K., Faleev, V.A. et al. (1995) Plasma deposition of resistive layers of strip electrical heater. In: *Proc. of Conf. on Physics of Low Temperature Plasma* (Petrozavodsk), Pt 3, 409–411.
14. Anshakov, A.S., Kazanov, A.M., Urbakh, E.K. (1998) Creation of low temperature heater by method of plasma spraying. *Fizika i Khimiya Obrab. Materialov*, **3**, 56–61.
15. Smyth, R.T. (1973) Thermal spraying of fine powders. In: *Proc. of 7th Int. Metal Spraying Conf.* (London, 1973), 89–95.
16. Borisov, Yu.S., Pereverzev, Yu.N., Bobrik, V.G. et al. (1999) Deposition of narrow-band coatings by method of microplasma spraying. *Avtomatich. Svarka*, **6**, 53–55.
17. Kislitsa, A.N., Kuzmich-Yanchuk, E.K., Kislitsa, N.Yu. (2009) Producing of narrow bands by microplasma spraying method from Ni–Cr wire. In: *Abstr. of All-Ukr. Sci.-Techn. Conf. of Young Scientists and Specialists on Welding and Related Technologies* (Kiev, 27–29 May, 2009), 94.
18. Vojnarovich, S.G. (2012) Investigation of shape and size of spraying spot and pattern of metallization under conditions of microplasma spraying of coatings from hydroxyapatite. *Vestnik NUK*, **3**, 81–84.
19. Antsiferov, V.N., Bobrov, G.V., Druzhinin, L.K. (1987) *Powder metallurgy and spraying of coatings*. Ed. by B.S. Mitin. Moscow: Metallurgiya.

Received 21.10.2014



CERMET COATINGS OF CHROMIUM CARBIDE–NICHROME SYSTEM PRODUCED BY SUPERSONIC PLASMA GAS AIR SPRAYING

V.N. KORZHIK, A.L. BORISOVA, V.V. POPOV, M.V. KOLOMYTSEV, A.A. CHAJKA,
V.I. TKACHUK and N.V. VIGILYANSKAYA

E.O. Paton Electric Welding Institute, NASU
11 Bozhenko Str., 03680, Kiev, Ukraine. E-mail: office@paton.kiev.ua

It is a well-known fact that application of supersonic methods of thermal spray deposition results in significant increase of service properties of parts. However, up to moment no trails were made on producing of carbide or cermet coatings with the help of supersonic methods of plasma spraying. Present work is dedicated to production of cermet coatings from chromium carbide–nichrome compositions using a method of supersonic plasma gas air spraying (SPGAS). SPGAS technology has series of advantages in comparison with well-known technology of HVOF spraying. First of all, it concerns efficiency, economy and characteristics (temperature, speed) of gas jet. Structure and phase composition of produced coatings were investigated. It is shown that spraying using supersonic gas jets promotes for increase of content of Cr_7C_3 carbide and reduction of NiCr in the coatings as a result of oxidation and formation of oxides. Coating from composite powder differs by higher level of density and homogeneity, has layered fine-laminated structure with inclusions of fine carbides, contains lower amount of oxide phase, but larger quantity of chromium carbide Cr_3C_2 in comparison with coating from mechanical mixture $\text{Cr}_3\text{C}_2 + \text{NiCr}$. These coatings can be recommended for application as wear-resistant at increased temperatures. 6 Ref., 6 Tables, 7 Figures.

Keywords: *supersonic plasma gas air spraying, cermet coatings, chromium carbide, powders, microstructure, phase composition, microhardness*

Plasma coatings based on chromium carbides are characterized by combination of such properties as resistance to wear by abrasive particles and hard surfaces at high temperatures (540–840 °C), high resistance under conditions of fretting-corrosion and aggressive media (for example, in liquid sodium at 200–625 °C), heat resistance at temperatures to 980 °C, radiation resistance [1].

Cr_3C_2 mechanical mixtures (rarely its mixture with Cr_7C_3 or Cr_{23}C_6 carbide) with such metals as Ni, Co, Ni+Cr, NiCr at different combination of component content (amount of metallic binder can be from 6–8 to 45 wt.%) are used for spray deposition of cermet coatings with chromium carbide.

Main methods, which are used for spray deposition of coatings with chromium carbides, are plasma, detonation and HVOF spraying [1–3].

It is a well known fact that application of supersonic methods of thermal coating deposition results in significant increase of their service properties. However, up to moment no trails were made on producing of carbide or cermet coatings with the help of supersonic methods of plasma spraying.

Present work is dedicated to production of cermet coatings from chromium carbide–nichrome compositions using a method of supersonic plasma gas air spraying (SPGAS), examination of structure and phase composition of produced coatings.

SPGAS technology has series of advantages in comparison with well-known technology of

Table 1. Comparative characteristics of HVOF and SPGAS technologies

Technology	Gas consumption, m ³ /h				Powder consumption, kg/h		Coefficient of material use, %	Jet characteristics	
	Propane	O ₂	N ₂	Air	Metallic alloys	Oxides		Speed, m/s	Temperature, °C
HVOF	3–4	15–21	1	–	Up to 23	–	40–75	1400–2700	2800
SPGAS	0.3–40	–	–	10–40	Up to 50	Up to 20	60–80	3000	3200–6300



Table 2. Composition of powders

Powder grade	Content of elements, wt.%						
	Cr	Ni	C	Mn	Fe	Si	Rest
PP-53	71.10	17.10	9.49	0.036	1.75	0.065	0.41
PP-53B	Base	20	9.40	Not indicated			

Table 3. Composition of particles of initial powders based on XSM results

Powder particle	Content of elements, wt.%				
	Cr	Ni	C	O*	Additives
Carbide (1 in Figure 1, a, c)	70.10–79.70	1.50–5.60	18.9–21	–	Fe – 0.73
Metallic (2 in Figure 1, a, c)	52–71.10	24.23–24.39	–	–	W – 0.71; Fe – 1.45
Cermet (3 in Figure 1, b, d)	30.77–68.10	10.55–49.81	9.17–13.60	6.2–7.7	Mg – 0.48–1.24; Al – 0.6; Fe – 0.55; W – 1.13–1.45

* Found in separate particles.

HVOF spraying. First of all, it concerns efficiency, economy (cost of gases) and characteristics of gas jet (temperature, speed) (Table 1).

Coating spray deposition in present work was carried out on «Kiev-S» installation, developed by Gas Institute and PWI of the NAS of Ukraine. Air mixture with addition of propane (around 4 vol.%) was used as plasma gas at following technological parameters: $I = 260$ A, $U = 360$ V,

180 mm distance, air pressure made 4 atm and consumption $20 \text{ m}^3/\text{h}$.

Powders of two types, namely PP-53 $\text{Cr}_3\text{C}_2\text{25}(\text{Ni}20\text{Cr})$ and PP-53B $\text{Cr}_3\text{C}_2(\text{Ni}20\text{Cr})$ (Table 2) from «Bay State Surface Technologies, Inc.» (USA) were used as materials for coating spray deposition.

Powders of particle size 15–44 μm were applied for coating spray deposition.

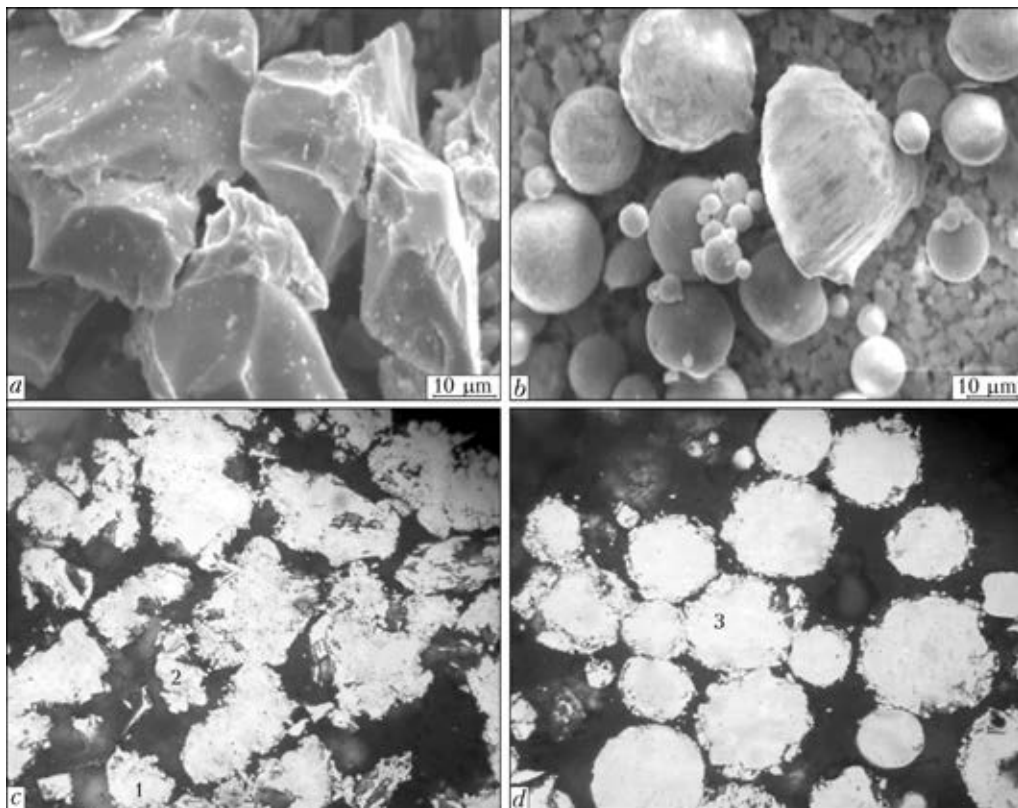


Figure 1. Appearance (a, c) and microstructure ($\times 800$) of particles (b, d) of PP-53 (a, c) and PP-53B (b, d) powders: 1 – carbide; 2 – metallic; 3 – cermet particles

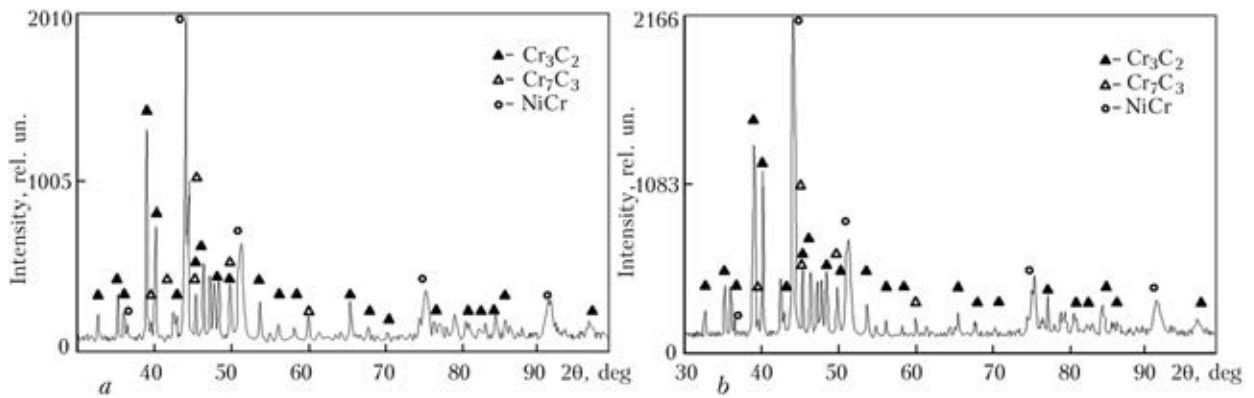


Figure 2. X-ray patterns of particles of $\text{Cr}_3\text{C}_2 + \text{NiCr}$ powder: *a* – PP-53; *b* – PP-53B

Examinations of initial powders showed that they differ by appearance, microstructure, microhardness and phase composition. Thus, PP-53 powder consists of faceted particles (Figure 1 *a, c*) and being a mechanical mixture of carbide and metallic particles, which vary vastly on microhardness (13300 ± 1500 and 1980 ± 600 MPa, respectively).

Powder PP-53B consists of spherical particles (Figure 1, *b, d*), and each particle, taking into account structure and microhardness, includes metallic as well as carbide phases (microhardness of particles is varied in 5000–10500 MPa range).

Examination of composition of powder particles using X-ray spectral microanalysis (XSMA) (Table 3) showed that nickel or carbon are virtually absent in PP-53 powder. According to

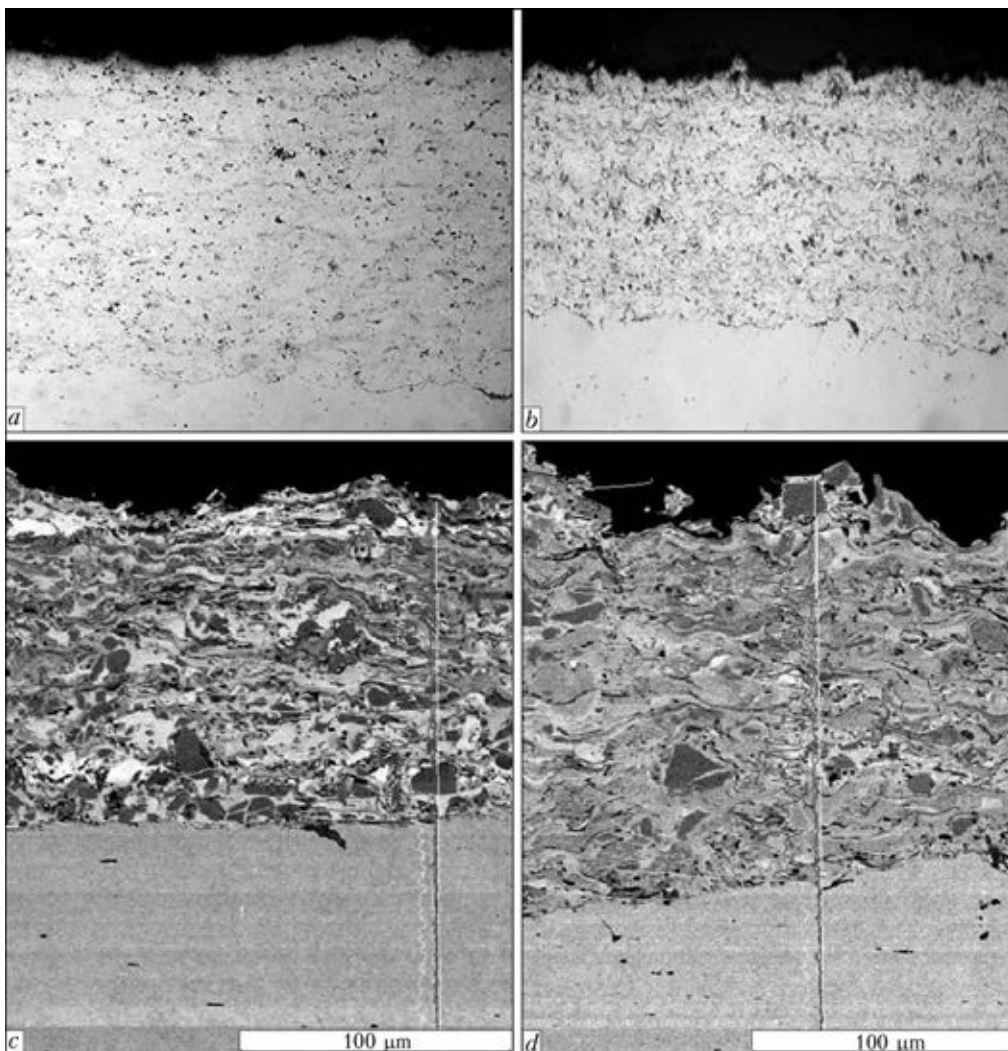


Figure 3. Microstructure of coatings from PP-53 (*a, c*) and PP-53B (*b, d*) powder (*a, b* – Neophot microscope, $\times 400$; *c, d* – CamScan electron-probe analysis)



Table 4. Characteristic of sprayed coatings

Powder grade	Microhardness, MPa		Phase composition, wt.%
	Average	Most probable	
PP-53	8420 ± 1550	9000; 11500	Cr ₇ C ₃ – 26; Cr ₃ C ₂ – 11; NiCr – 48; NiCr ₂ O ₄ – 15
PP-53B	9960 ± 1400	10500	Cr ₇ C ₃ – 21; Cr ₃ C ₂ – 15; NiCr – 53; NiCrO ₃ – 11

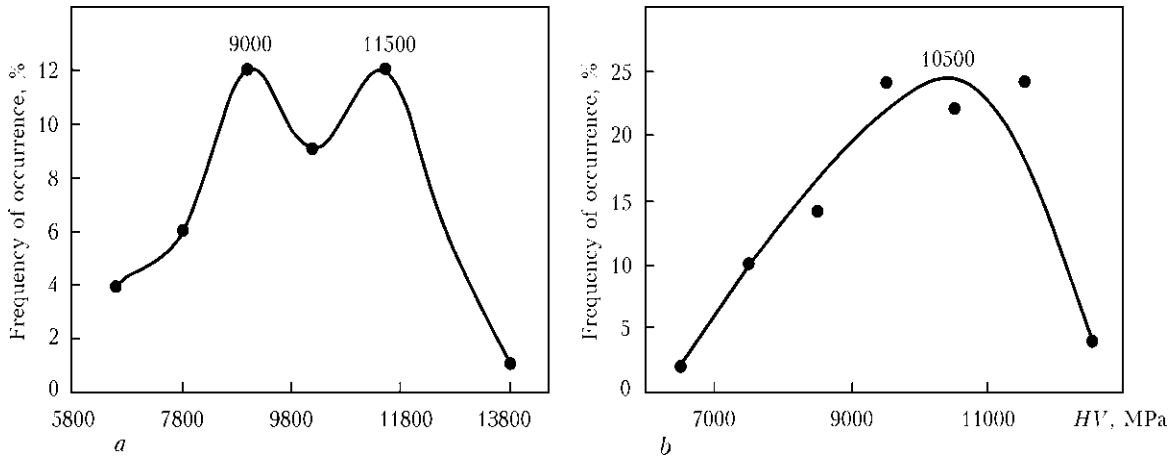


Figure 4. Microhardness variation curves of plasma coatings from PP-53 (a) and PP-53B (b) powders

carbon amount in the carbide particles (19–21 wt.%), they are close to Cr₃C₂ (19.34 vol. %) carbide on composition. Moreover, Cr₇C₃ carbide (9.01 wt.% C) (Figure 2, a) was found in powder using X-ray phase structural analysis (XPSA) method.

Particles of PP-53B powder contain all three elements (Cr, Ni and C) as well as additives of these elements such as small amount of Mg, Al,

W, Fe and Ca (see Table 3). Some particles have areas enriched by oxygen at the level of 6–7 wt.%.

At the same time, results of XPSA of PP-53B particles indicate that they do not differ from PP-53 powder (Figure 2, b) on qualitative content, and since each particle contains metallic as well as carbide phases, the powder can be considered as composite one, consisting from cermet particles.

Metallographic examination of sprayed coatings determined no fundamental differences in their structure depending on powder type (Figure 3). The only thing that can be noted is higher level of homogeneity of coatings from composite powder (PP-53B) in comparison with coatings from mechanical mixture (PP-53). Besides, some difference is observed in values of average microhardness of coatings and nature of microhardness variation curves (Table 4, Figure 4).

Thus, two most probable values of microhardness can be marked on microhardness variation curve of the coating, produced from PP-53 powder (mechanical mixture Cr₃C₂ and NiCr). This can be an evidence of presence in the structure, as in initial powder, of zones with harder carbide phases (HV = 11500 MPa) and metal enriched zones (HV = 9000 MPa). Microhardness variation curve of the coating from composite powder PP-53B has only one probable value of microhardness 10500 MPa, i.e. average between two indicated above.

XPSA of phase composition of sprayed coatings showed (Figure 5) that they contain chro-

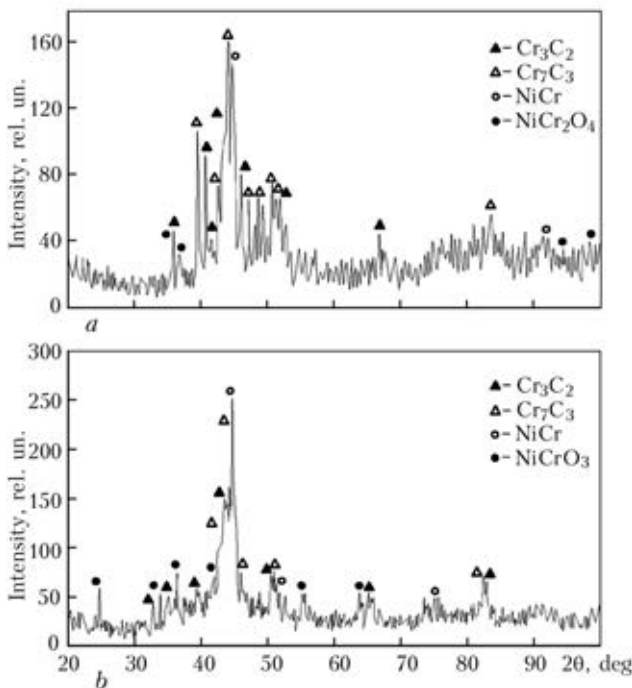


Figure 5. X-ray patterns of sprayed coatings: a – PP-53; b – PP-53B powder



Table 5. Content of elements, determined by XSMA method, in structural zones of coatings from PP-53 and PP-53B powders (acc. to Figure 6, *a* and *b*, respectively)

Spectrum to be analyzed	Content of elements, wt.%					Supposed phase
	Cr	Ni	C	O	Fe	
1 (<i>a</i>)	13.33	81.57	–	–	4.30	NiCr
2 (<i>a</i>)	81.82	1.45	16.72	–	–	Cr ₇ C ₃
3 (<i>a</i>)	89.40	–	10.60	–	–	Cr ₃ C ₂
4 (<i>a</i>)	56.41	18.50	4.87	20.22	–	Oxide
1 (<i>b</i>)	61.13	25.89	11.66	–	–	Zones of cermets (metal + carbide)
2 (<i>b</i>)	13.99	75.11	8.71	–	0.93	
3 (<i>b</i>)	26.50	61.97	8.89	–	0.79	
4 (<i>b</i>)	28.93	59.57	–	9.44	0.49	Oxide

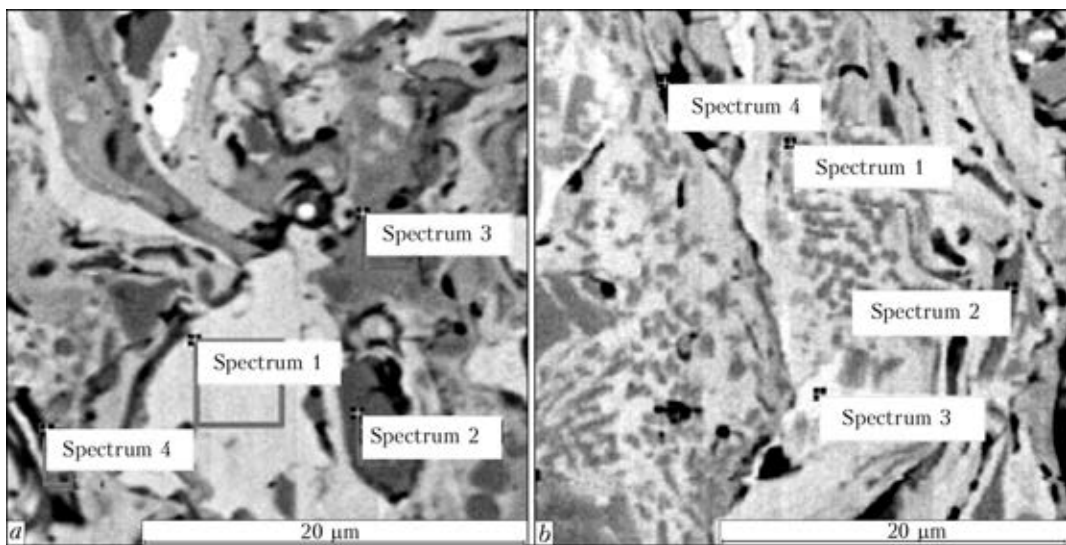


Figure 6. Zones of coatings from PP-53 (*a*) and PP-53B (*b*) powders examined by XSMA method

mium carbide Cr₃C₂, Cr₇C₃, nichrome (Ni₈₀Cr₂₀) and oxides NiCr₂O₄ (for coating from mechanical mixture) or NiCrO₃ (for coating from composite powder), the latter were not found in initial powders. Presence of indicated phased in the sprayed coatings conforms the results of local XSMA (Table 5) of separate structural elements of the sprayed coatings (Figure 6).

It can be noted when comparing intensity of X-ray reflections of separate phases in initial

powders (see Figure 2) and in sprayed coatings (see Figure 5) that spraying promotes increase of content of Cr₇C₃ carbide in the coating in comparison with Cr₃C₂ and NiCr content reduces as a result of oxidation and oxide formation. X-ray spectrum microanalysis of the sprayed coat-

Table 6. Results of XSMA of sprayed coating from PP-53B powder (acc. to Figure 7)

Spectrum to be analyzed	Composition, wt.%					
	C	O	Cr	Fe	Ni	W
2	1.91	–	–	97.66	–	–
3	9.10	6.10	52.61	2.62	29.58	–
4	9.72	5.32	49.80	3.93	30.39	0.83
5	8.56	6.55	55.21	2.23	26.75	0.68
6	8.38	7.15	55.76	2.59	25.38	0.73

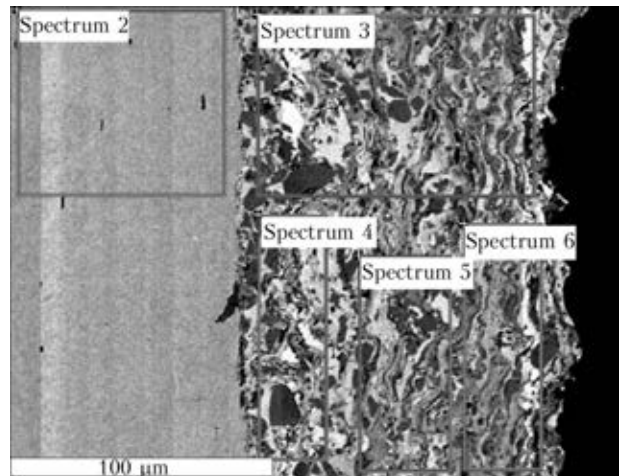


Figure 7. Coating from PP-53B powder examined by XSMA method



ings (Figure 7, Table 6) showed that averaged composition (spectrum 3) and content of separate zones on depth (spectra 4–6) are somewhat differ from values of the initial powder (see Table 1). This takes place as a result of appearance of oxide phases in the coatings. At that, amount of oxygen in the case of PP-53B powder coating somewhat increases in direction from base interface to outer surface of the coating, while carbon content is reduced to the contrary.

The similar dependence is observed for PP-53 powder coating. This fact is related with rise of temperature of coating being sprayed in proportion to build-up of coating layer. Comparison of characteristics of sprayed coatings from PP-53 and PP-53B powders allows for noting that coating from composite powder differs by higher level of density and homogeneity, has layered fine-lamellar structure with inclusions of fine carbides, contains lower amount of oxide phase, but larger quantity of chromium carbide Cr_3C_2 in comparison with coating from mechanical mixture $\text{Cr}_3\text{C}_2 + \text{NiCr}$.

It is a well-known fact that refractory properties, stability and hardness of chromium carbides are reduced with decrease of carbon amount in them [4, 5]. Therefore, carbon loss is undesirable in the processes of thermal spraying of cermet chromium carbide based coatings. Review paper [6] dedicated to effect of thermal spraying methods (HVOF, air plasma spraying (APS), vacuum plasma spraying (VPS) and detonation

spraying) on properties of the coatings from mechanical mixture $\text{Cr}_3\text{C}_2 + \text{NiCr}$ indicates that hardness, abrasive wear resistance and thermal resistance of the coatings depend on carbon loss in spraying. Thus, for example, VPS coatings have higher hardness and abrasive wear resistance, but lower thermal resistance among others, and APS coatings with argon-helium plasma gas are superior on their properties to the coatings using argon-hydrogen mixture etc.

The results of present work allows for concluding that quality of $\text{Cr}_3\text{C}_2 + \text{NiCr}$ composition coating can also be increased with the help of composite powder of the same compositions instead of mechanical mixture.

1. Borisov, Yu.S., Kharlamov, Yu.A., Sidorenko, S.L. et al. (1987) *Thermal coatings from powder materials*: Refer. Book. Kiev: Naukova Dumka.
2. Guilemagy, M., Nutting, I., Llorca-Isern, N. (1996) Microstructural examination of HVOF chromium carbide coatings for high temperature applications. *J. Thermal Spray Techn.*, 5(4), 483–489.
3. Guilemagy, J.M., Espallargas, N., Suegama, P.H. et al. (2006) Comparative study of Cr_3C_2 -NiCr coating. *Corrosion Sci.*, 48, 2998–3013.
4. Kiffer, R., Benezovsky, F. (1968) *Solid materials*. Moscow: Metallurgiya.
5. (1986) *Properties, production and application of refractory joints*. Ed. by T.Ya. Kosolapova. Moscow: Metallurgiya.
6. Takenchi, J., Nakahira-Kobe, A., Takara, G. (1993) Barbezat-Wohlen Plasma-Technik. $\text{Cr}_3\text{C}_2 + \text{NiCr}$ cermet coatings. In: *Proc. of Thermal Spray Conf.* (Aachen, 1993), 1–14.

Received 17.09.2014

LINEAR FRICTION WELDING OF METALLIC MATERIALS (Review)

I.V. ZYAKHOR, M.S. ZAVERTANNY and S.V. CHERNOBAJ

E.O. Paton Electric Welding Institute, NASU

11 Bozhenko Str., 03680, Kiev, Ukraine. E-mail: office@paton.kiev.ua

Capabilities and prospects for application of linear friction welding for joining various metallic materials, namely steels, titanium alloys, high-temperature nickel alloys and composite materials are considered. Parameters of the mode of linear friction welding for different material combinations and their mechanical properties are given. Structure of joints in linear friction welding is similar to that for other friction welding variants. Width of characteristic joint sections (zones of dynamic recrystallization, thermomechanical and thermal impact) depends on mode parameters – welding time, axial force, vibration amplitude and frequency. Modern tendencies in modelling of heat evolution and deformation in linear friction welding are analyzed. Cost reduction and improvement of reliability of equipment for realization of this process remain an urgent problem. At present the field of industrial application of this process is limited to aerospace companies, where components of gas turbine engines from titanium alloys are joined, and in the future application of high-temperature and nickel alloy and composite materials is possible. 35 Ref., 5 Figures.

Keywords: *linear friction welding, process stages, joint structure, modelling, titanium alloys, high-temperature nickel alloys, composite materials*

Over an almost 60 year period of research and industrial application of friction welding (FW) in the world, an extensive volume of information has been accumulated on joining various structural materials. About 20 variants of technological processes using frictional heating to produce permanent joints, surfacing, forming, welding up holes, producing riveted joints have been proposed and implemented in practice [1]. Rotational FW, which was invented back in 1956, became the most widely applied in different industries.

Method of vibrational FW was described practically in time with the start of FW commercial application. This method uses relative reciprocating displacement for surfacing and joining parts with rectangular cross-section [2, 3]. In 1969 the mechanism of reciprocating motion for low-carbon steel welding has been patented [4].

Method of vibrofrictional welding, which was later called linear friction welding (LFW), was widely applied for joining thermoplastic products [5], whereas its application for welding metallic materials was restrained by complexity and considerable cost of development of reliable equipment. At the end of 1980s, the requirements of leading enterprises in aerospace industry necessitated development of technologies and equipment for LFW of various alloys for creation of welded rotors of aircraft gas turbine engines (GTE).

In 1990 the Welding Institute put into operation the first specialized machine with electro-mechanical drive for LFW of metals. Successful welding of rectangular samples of 25×6 mm section from carbon and stainless austenitic steels, aluminium alloy 5154, titanium alloy Ti-6Al-4V [6–8] was the starting point for such companies as Rolls Royce, MTU Aero Engines and Pratt & Whitney showing active interest in LFW technologies. LinFic® concept of LFW equipment based on application of high-precision computerized hydraulic force drives was developed and implemented through combined efforts of a group of eight European companies. Since that time leading research centers and enterprises of various countries started intensively working on development of equipment, studying LFW process, and its industrial application.

The objective of this review is analysis of technological capabilities and features of formation of metallic material joints in linear friction welding.

General characteristic of LFW process. LFW process schematic is shown in Figure 1, diagram of mode parameter variation in time – in Figure 2.

Mechanism of welded joint formation at LFW is similar to that at rotational FW [9]. Welded joint forms in the following sequence:

- initial rubbing-in of friction surfaces. Relative displacement of surfaces results in breaking up of oxide and grease films on contacting microprotrusions with opening of juvenile sections, with formation and immediate breaking up of adhesion bridges;
- avalanche-like increase of the number of interacting microprotrusions, as well as actual contact area and fast increase of temperature in the butt;

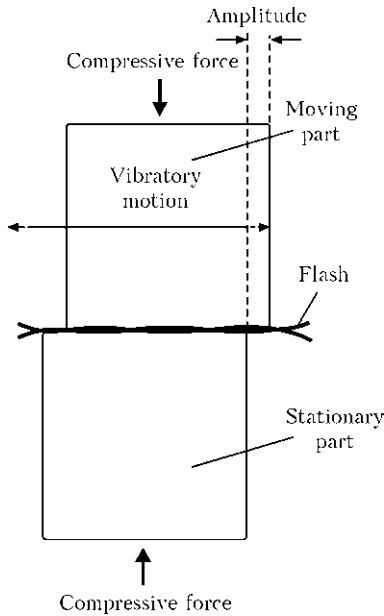


Figure 1. Schematic of LFW process

- upsetting start (driving plasticized metal out of the butt), increase of butt temperature up to a certain value;
- quasistationary (equilibrium) state of the friction process. Heat evolution power, temperature in the butt, and upsetting speed are at a certain set level;
- deceleration, i.e. controllable lowering of the speed of relative displacement to zero, during which the welded joint is formed;
- forging. Formed joint is subjected to compressive deformation by an axial force, which, as a rule, does not exceed the force applied at heating.

Unlike FW, at LFW the joint form is characterized by unusual flash (Figure 3). An essentially larger amount of flash forms on the faces in the direction of reciprocal displacement that is due to displacement of plasticized metal predominantly in the direction of vibrations.

LFW advantages. This method allows producing sound joints from various materials, such

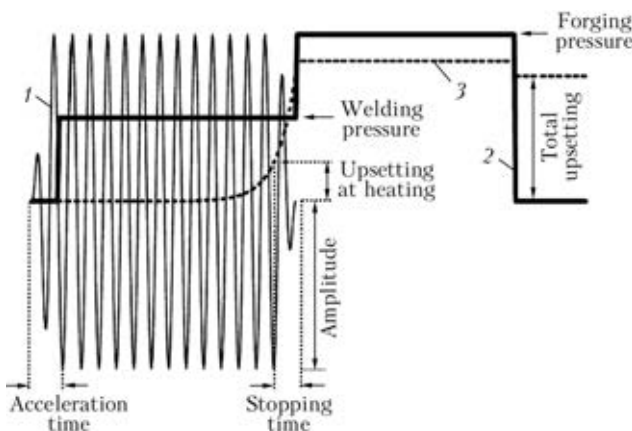


Figure 2. Diagram of variation of LFW parameters in time: 1 – amplitude; 2 – compressive force; 3 – upsetting



Figure 3. Welded joint of titanium alloy at LFW

as titanium and nickel alloys, different steels, aluminium and its alloys, composite materials (CM), etc. The main difference of LFW from rotational FW is the possibility of solid-phase welding of products with rectangular cross-section. LFW has several advantages, also inherent to other FW variants [6–9]:

- capability of joining parts from difficult-to-weld materials both in similar and in dissimilar combinations;
- high efficiency;
- high and stable quality of the joints;
- hygienic value – absence of evolutions of harmful gases, ultraviolet and electromagnetic radiation;
- no need for application of filler materials, fluxes and shielding gases;
- joint forms in the solid phase, structural changes in the base metal proceed to a small depth;
- low energy consumption.

Main disadvantages of LFW are the high cost and complexity of equipment manufacturing, due to the need for application of high-rigidity high-precision force drives and sophisticated computerized control systems [7–9].

LFW parameters and materials being welded. The main parameters of LFW process are frequency and amplitude of reciprocal vibrations, pressure at heating and forging, heating and forging time, upsetting value at heating and total upsetting during welding (see Figure 2) [10]. Additional LFW parameters that can influence joint formation are time of acceleration and stopping of vibrations.

Works [11, 12] present results of LFW studies of Ti-6Al-4V titanium alloy (Ti-64). Frequency of reciprocal vibrations in welding reached 119 Hz for vibration amplitude of 0.92 to 3 mm. It is shown that to produce sound joints in LFW it is necessary to exceed a certain value of specific power of heat evolution that is determined as

$$\omega = \frac{\alpha f P}{2\pi A}, \quad (1)$$

where α , f is the amplitude and frequency of reciprocating displacement, respectively; P is the force; A is the blank cross-sectional area.



Producing sound joints (without pores or oxide inclusions) is possible in the case of simultaneous provision of certain critical conditions, namely, high enough values of vibration amplitude and frequency and welding pressure. By the data of [12] an important parameter for sound weld formation is total upsetting of blanks, its optimum value being different for different structural materials.

Work [13] gives the results of studies of LFW of aluminium, steel and high-temperature alloys, which were conducted on tee-joints of «pin-to-plate» type with pin rectangular cross-section of 12×4 and 20×4 mm, respectively. It is shown that three properties of metallic material, namely high-temperature strength, heat conductivity and friction coefficient, dependent on temperature, are important for LFW. Materials quickly losing their strength to great depth at heating, in particular, aluminium and aluminium alloy of AlMgSi1 system, are only partially suitable for LFW. Their stable heating requires ensuring considerable amplitudes and frequencies of reciprocating displacements at considerable welding force.

Study [14] gives a comparative characteristic of LFW and inertia FW. Investigations were conducted on samples from high-temperature aluminium alloy Al-11.7 % Fe-1.2 % V-2.4 % Si, produced by powder metallurgy techniques, as well as samples of this alloy with 2024-T351 aluminium alloy. It is shown that LFW allows reducing the intensity of thermodeformational welding cycle compared to inertia FW. Joint strength is about 81 % of that of joints produced by inertia FW that is related to large coarsening of the grain and lower hardness in the joint zone. LFW mode for rods of 25 mm diameter is as follows: 50 Hz frequency, 2 mm amplitude, 4 mm upsetting, 30 and 50 kN heating and forging forces, respectively.

In [6, 10, 13, 15] LFW capabilities at joining various steels (carbon, stainless, high-strength) were studied. Welding mode parameters were varied within the following ranges: 25–50 Hz vibration frequency, 1–3 mm amplitude, 40–240 MPa heating force, and 1–3 mm upsetting. Authors of [6, 13] note that LFW of carbon steel runs into the following problems: welded joints have undercuts on both sides of the joint zone. This is attributable to low linear speed (0.5 m/s), whereas it should be not less than 1 m/s for steels to ensure uniform heating and stable deformation of metal.

Tensile testing of welded samples from carbon steel [15] showed ultimate strength of 539–592 MPa with fracture through base metal (BM). Increase of metal microhardness in the

joint zone by more than 2 times compared to BM is observed. At deviation of LFW parameters from optimum values towards their lowering, welded joints fail through the butt with low strength values.

Sound joints from stainless steel AISI 3L61 [16] were produced at more than 160 MPa welding pressure and not less than 40 Hz vibration frequency. Mechanical testing showed ultimate strength of 549–610 MPa, relative elongation of 40–49 % with fracture running through BM. Failure of samples produced at less than 80 MPa welding pressures or at 25 Hz vibration frequency ran through the weld. It is established that maximum upsetting speed, which influences the amount of δ -ferrite in the joint zone, is achieved at high welding pressures and values of amplitude of 1.5 mm and frequency of 30 Hz.

The greatest number of publications is devoted to studying LFW of various titanium alloys [6, 17–22] that is due to LFW practical application in manufacture of welded rotors of aircraft GTE compressors («blisks»). Publication authors studied the following ranges of LFW parameters variation: 0.5–3.0 mm amplitude, 15–150 Hz frequency, 50–190 MPa pressure at heating and 320 MPa forging pressure.

In [6, 17] welded joints of Ti-6Al-4V titanium alloy produced by LFW were studied. At rupture testing of welded samples of 25×6 mm section [6] strength was 835 MPa with fracture running through BM. At bend testing fracture ran in the joint zone at bend angle of 50° . Mechanical testing of welded joints of $35 \times 26 \times 13$ mm model samples produced with upsetting limitation in welding of 1.75 mm, showed the following results [17]: ultimate strength of 916 to 1004 MPa, relative elongation of 13.7–15.2 %, yield point of 841–968 MPa. Microhardness increase in the joint zone up to *HV* 350 (compared to *HV* 300 in BM) was found at ± 0.6 –1.0 mm distance from weld axis, depending on welding pressure.

Work [18] is a study of the possibility of LFW application for new titanium pseudo- β -alloy Ti-5553 (Ti-5Al-5V-5Mo-3Cr), as well as for IMI-834 alloy (Ti-5.8Al-4Sn-3.5Zr-0.7Nb-0.5Mo-0.3Si). Mechanical testing of welded samples from Ti-5553 alloy showed that joint ultimate strength was equal to 94 % of BM strength (1042 MPa), yield point was 96 % (1005 MPa), relative elongation was 36 % of BM level. Lowering of microhardness in the joint zone by more than 17% compared to BM level at up to ± 1.6 mm distance from weld axis is found. Thermocouples were used to record the maximum temperature of friction surface at LFW of IMI-834 alloy in



the temperature range of 750–800 °C. It is shown that for IMI-834 alloy the nature of dependence of microhardness distribution on welding parameters, similar to that for Ti-64 alloy is preserved.

Work [19] is a study of LFW of titanium alloy Ti-6Al-2Sn-4Zr-6Mo (Ti-6246). Depending on heat treatment, this alloy can be regarded as β -alloy in one case, and as $\alpha + \beta$ alloy in another case. Investigations were performed on samples of 60 × 36 × 15 mm size. Welding of β -alloy and $\alpha + \beta$ -alloy Ti-6246 was performed. Postweld heat treatment included heating up to 620 °C and soaking for 4 h. At certain welding parameters welded joint ultimate strength (1078 MPa) on the level of 96 % of BM values of the less strong $\alpha + \beta$ Ti-6246 alloy, and yield point (1030 MPa) equal to 99 % of this value for $\alpha + \beta$ Ti-6246 alloy, are reached.

In [20, 21] formation of dissimilar joints at LFW of titanium alloys VT6 and VT8-1 was studied. Welding was performed on 35 × 26 × 13 mm samples with specifying 2 mm upsetting. Mechanical properties of the joints were as follows: 990–1020 MPa ultimate strength, 924–939 MPa yield point, 11.39–13.78 % relative elongation with fracture running through VT6 BM [21]. At testing of special samples with a recess along the joint line [20] for static tension, fracture ran through the thermomechanical impact zone (TMIZ) of VT8-1 alloy (ultimate strength of 1194 MPa). Here, the width of the joint TMIZ was not larger than 400 μm , its greater part being on VT8-1 alloy side.

Starting from the year 2000, the number of publications devoted to investigation of LFW of high-temperature nickel super alloys became much greater. Studied range of variation of super alloy LFW parameters was as follows: 2–3 mm amplitude, 40 to 100 Hz frequency, and 50–450 MPa pressure.

In [22] the process of LFW of Waspalloy nickel alloy on 18 × 13 × 11 mm samples was studied. It is established that producing sound joints is possible at a certain, high enough value of all LFW technological parameters (amplitude, frequency, pressure). It is shown that at 0.9 mm distance from the friction surface (dynamic recrystallization zone — DRZ), metal temperature was not higher than 1126 °C, that led to dissolution of strengthening γ' -phase and microhardness lowering. At 3.3 mm distance on both sides of the weld microhardness lowering by 40 % compared to BM values is observed. Producing sound joints (without pores or oxide inclusions) is achieved at more than 1.2 mm upsetting.

Work [23] is a microstructural study of joints of IN-738 nickel alloy. Samples of 12.8 × 11.1 × 17.7 mm size were used for LFW. Complete dissolution of strengthening γ' -phase to the depth of 600 μm on both sides of the weld is observed in the joint zone. It is established that peak temperature during welding was higher than 1230 °C.

In [24] optimization of LFW parameters for IN-718 nickel alloy was performed. Under certain conditions (for this alloy: 2 mm amplitude, 80 Hz frequency, 70 MPa pressure), a temperature of about 1200 °C is reached on the friction surface. TMIZ is characterized by microhardness lowering by 25 % compared to BM. Microscopic studies showed presence of dispersed oxides across the entire weld section, dimensions and amount of which depend on welding mode parameters.

Work [25] gives the results of studying LFW of CMSX-486 superalloy. Unlike titanium alloys, where flash has the form of «petals» common for both parts, for nickel alloys flash distribution into two individual «petals» is observed that is characteristic for joints at rotational FW. At tensile testing samples failed through BM. It should be also noted that conducted in [23, 25] microstructural analysis of welded samples of IN-738 nickel superalloy and CMSX-486 single-crystal superalloy showed that melt areas can form in the alloys during LFW process. It is established that application of compressive load at the forging stage leads to rapid solidification of the formed metastable liquid phase.

Authors of [26] studied the applicability of LFW for EP742 nickel alloy on samples of 35 × 26 × 13 mm size. Ultimate strength of welded joints was equal to 96–112 % of the value required by TU specification, and relative elongation was 98–132 %. Width of DRZ and TMIZ was equal to 0.6 and 0.8 mm, respectively. Microhardness drop in the joint zone is observed that is due to degradation of strengthening γ' -phase.

LFW can be used to produce sound CM joints. In [27] joints of CM based on aluminium alloy AA2124 (Cu – 3.8, Mn – 0.5, Mg – 1.4, Zn < 0.25) reinforced by 25 % of silicon carbide particles were studied. Sample size was 80 × 36 × 15 mm. Welding mode parameters were as follows: 50 Hz vibration frequency, 2 mm amplitude, 185 MPa heating and forging force, and 2 mm upsetting. Mechanical testing of samples showed that ultimate strength of welded joint is equal to 82 % of BM level, proof strength is 78 % and relative elongation is 60 % of BM value. Microhardness lowering in the welding zone by 10 % compared to BM of 2124Al/25 vol.% SiC composite is observed.

Thus, as shown by analysis of publications, LFW application for nickel and titanium alloys is cost-effective, as here the cost of development of specialized equipment for aircraft engine construction products is justified. Weldability of titanium alloys was studied in similar and dissimilar combinations, whereas LFW capabilities for superalloy welding are limited to investigation of joints in similar combinations.

Welded joint structure. On the whole, metal structure at LFW is similar to that at rotational FW [9]. Typical welded joint structure at LFW is given in Figure 4 for the case of AISI 316L steel [16].

At LFW metal in the joint zone is heated up to temperatures not exceeding the melting temperature. However, owing to heat conductivity and external pressure blank metal changes its properties and structure to a certain depth from the friction surface. As a rule, four zones differing by texture and microstructure, are distinguished in the welded joint [9, 16, 28] as follows:

1. DRZ, or fine-grain zone is the welded joint central part. Here, the metal undergoes phase transformations — an equiaxed fine-crystalline dynamically recrystallized structure forms;
2. TMIZ is characterized by metallographic texture. Grains and non-metallic inclusion stringers are elongated in the direction of deformation. In some materials phase transformations in this zone can also take place;
3. HAZ is the region between BM and TMIZ, where phase or structural transformations can proceed, unrelated to deformation process;
4. BM zone is the region where heating during welding did not have any noticeable influence on microstructure and mechanical properties.

Microstructural studies of samples of titanium alloys Ti-6Al-4V in [18] and Ti-6Al-2Sn-4Zr-6Mo in [19] welded by LFW showed that DRZ and TMIZ are directly proportional to welding time and inversely proportional to axial pressure, vibration frequency and amplitude. It is established that axial pressure is a determinant factor influencing DRZ and TMIZ dimensions.

For joints of similar materials structural changes are symmetrical relative to weld axis, unlike those for dissimilar material joints [20, 28].

LFW process modelling. In a number of studies an attempt has been made to apply calculation methods to describe energy characteristics of LFW process and determine the temperature mode of welding of various materials. In [29] it is proposed to determine the temperature in the butt at LFW at the moment before upsetting application from the following equation:

$$T = T_0 + \frac{1}{c\rho F_n \sqrt{4\pi a}} \int_0^t \frac{q(\tau)}{\sqrt{t_h - \tau}} \times \exp\left(-\frac{z^2}{4a(t-\tau)} - b(t_h - \tau)\right) d\tau, \quad (2)$$

where $q(\tau)$ is the law of variation of evolved power in time; t_h is the heating time; F_n is the rod cross-sectional area; a is the thermal diffusivity factor; b is the thermal efficiency factor; $c\rho$ is the volumetric heat capacity; T_0 is the initial temperature level.

Instant thermal power q [7, 10] evolved at friction can be determined from the following formula:

$$q = F_{fr}v, \quad (3)$$

where F_{fr} is the sliding friction force equal to

$$F_{fr} = Fk_{fr}; \quad (4)$$

where F is the welding force; k_{fr} is the friction coefficient; v is the sliding velocity (velocity of relative displacement of parts).

Sliding velocity [24, 27] depends on amplitude α and frequency f of reciprocal motion. For amplitude variable by sinusoidal law, average sliding velocity v_{sl} is equal to

$$v_{sl} = 4\alpha f. \quad (5)$$

For sinusoidal variation of amplitude, sliding velocity varies continuously from zero at peak amplitude up to maximum value at crossing a point, in which the blanks being welded are co-axial. Pressure in the contact zone also varies — at peak amplitude it has the maximum value,

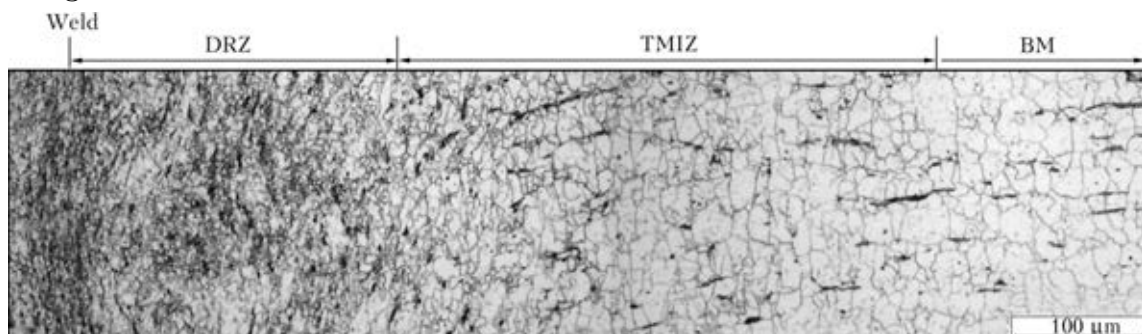


Figure 4. Microstructure of welded joint of AISI 316L steel

and at zero crossing it has minimum value (corresponds to welding force).

To determine the total energy [10], required for welded joint formation, the expression for instant thermal power is integrated over welding process time t :

$$E_x = \int_0^t q dt = \int_0^t F_{fr} v dt. \quad (6)$$

Friction force depends on a whole number of factors [1, 2]: velocity of relative motion of friction surfaces; material nature and presence of surface films; temperature mode; normal pressure value; friction assembly rigidity and elasticity; stationary contact duration; load application speed nature of body contact; surface size; relative overlap coefficient; surface quality and roughness.

It is established [1] that at friction of steel sliding over steel, friction coefficient can vary in broad ranges (0.1–1.0, depending on welding conditions). Work [30] gives the data on friction coefficient variation during LFW for titanium alloys in the range from 0.25 up to 0.55.

High intensity of physico-chemical processes proceeding in the joint zone at LFW makes mathematical modelling of this welding process a complex task, which is solved with application of computers and special software based on finite element method. Simplified models are used to reduce the time and computational power, for instance, calculation of temperature fields without allowing for material deformation, application of simplified 2D-models instead of 3D-modelling, consideration not

of the process as a whole, but of its individual stages; and prediction of the structure of individual welded joint zones [29–34].

Figure 5 gives the result of 2D-modelling of LFW process. Authors of [29–34] performed calculation of temperature fields at LFW of titanium alloys. It is established that for the studied parameters of welding VT6 alloy about 30 % of thermal energy, generated in the butt during the process, is removed into the flash together with plasticized metal. Calculations show that during welding temperature on friction surface reaches 1300 K, it, however, can go up even to 1500 K, depending on LFW parameters. Here, temperature increase up to 1000 °C lasts for less than 1 s [31]. In [33] temperature fields were calculated for welded joint of VT6 + VT8M-1 alloys; temperature field asymmetry relative to the joint line is noted.

In [31, 32] flash formation was modeled in addition to temperature fields. It is established that flash topology depends on welding mode parameters. Producing sound joints requires complete renewal of the friction surfaces and removal of contaminations into flash.

Upsetting speed depends on pressure, vibration amplitude and frequency. Their increase results in higher deformation and upsetting speeds, reduction of plasticized metal zone thickness and decrease of upsetting value required for surface cleaning. Increase of friction speed leads to higher maximum temperature in the butt, and with increase of welding pressure it decreases.

Authors of [31] suggested a model for prediction of HAZ structure in welded joint of Ti-64 alloy, as this zone is characterized by minimum strength and hardness. Size of β -phase grains is the main value of mechanical characteristics in this alloy HAZ. Therefore, this model is based on calculation of the size of β -phase grains after LFW, depending on welding mode and grain size before the process start.

In [30] modelling of LFW of links of round-link chains from 30CrNiMo8 steel was performed. Temperature variation during welding was considered in two points removed for 3.5 and 4.5 mm from the butt. Data obtained by calculations differ only slightly from experimental data. Difference between calculated and experimental data on sample upsetting was equal of 13 %.

LFW process modelling is limited to mostly titanium alloys that is due to the urgency of this welding process application for manufacture of components of aircraft GTE. Joint formation at LFW of nickel superalloys, Ni–Al, Ti–Al based intermetallics and CM in similar and dissimilar combinations is not well enough highlighted in

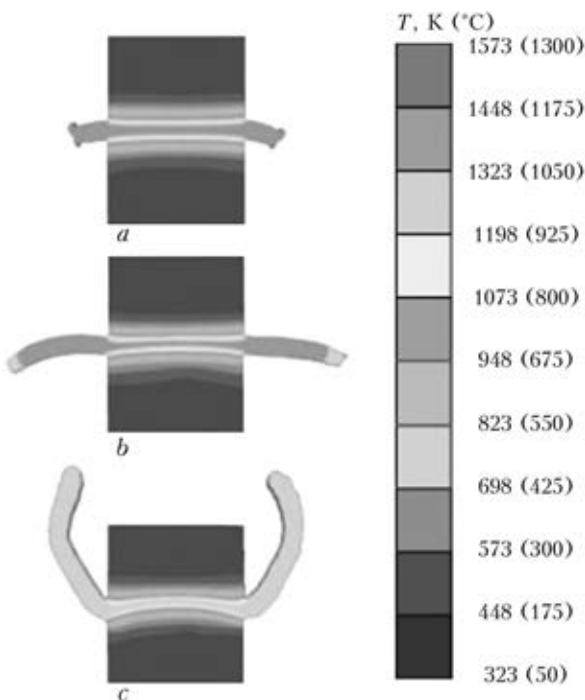


Figure 5. Results of 2D-modelling of Ti-64 alloy for low (a), medium (b) and high (c) welding pressures [34]

publications that necessitates performance of further research.

Conclusions

1. Requirements of leading enterprises in aircraft propulsion engineering determined the urgency of development of technologies and equipment for LFW of parts from high-strength and high-temperature alloys. LFW allows producing sound joints of titanium alloys, different steels, high-temperature nickel alloys and CM.

2. Structure of joints in LFW is similar to that for other FW variants. Width of characteristic sections of the joint (zones of dynamic recrystallization, thermomechanical and thermal impact) depends on LFW mode parameters, namely axial force, welding time, vibration amplitude and frequency.

3. Mathematical modelling of LFW process, based on finite element method, allows assessment of thermodeformational conditions of joint formation and prediction of structural changes in materials in the welding zone.

4. Lowering of the cost and improvement of reliability of equipment for realization of LFW of high-temperature and high-strength materials remains to be a problem, limiting the field of LFW application to predominantly aerospace industry enterprises.

5. Performance of further studies on LFW of nickel superalloys, Ni–Al, Ti–Al based intermetallics and CM in similar and dissimilar combination is urgent.

1. Lebedev, V.K., Chernenko, I.A., Vill, V.I. et al. (1987) *Friction welding*: Refer. Book. Leningrad: Mashinostroenie.
2. Vill, V.I. (1962) *Friction welding of metals*. New York: American Welding Soc.
3. Vavilov, A.F., Voinov, V.P. (1964) *Friction welding*. Moscow: Mashinostroenie.
4. Maurya, R., Kauzlarich, J. *Bonding apparatus – friction welding by reciprocal motion*. Pat. US 3420428-A. Publ. 1969.
5. Kulis, E.I., Lokishin, R.F. (1982) Friction welding of plastics. *Svarochn. Proizvodstvo*, **1**, 8–9.
6. Nicholas, E.D., Hone, P. (1989) *Developments in friction and MIAB welding*. Welding Institute Bull., R382/11/89.
7. Nicholas, E.D. (1991) *Linear friction welding*. Dueseldorf: DVS Verl., DVS Berichte, **139**, 18–24.
8. Nicholas, E.D. (1992) Friction surfacing and linear friction welding. In: *Proc. of Int. SAMPE and Metals Proc. Conf.* (Covina, CA, USA, 1992), 450–463.
9. Bhamji, I., Preuss, M., Threadgill, P.L. et al. (2010) Solid state joining of metals by linear friction welding: A literature review. *Mater. Sci. & Technol.*, **27**(1), 2–12.
10. Usani, U. Ofem, Colegrove, P.A., Addison, A. et al. (2010) Energy and force analysis of linear friction welds in a medium carbon steel. *Sci. and Technol. of Welding & Joining*, **15**(6), 479–485.
11. Vairis, A., Frost, M. (1998) High frequency linear friction welding of a titanium alloy. *Wear*, **217**, 117–131.
12. Wanjara, P., Jahazi, M. (2005) Linear friction welding of Ti–6Al–4V: Processing, microstructure and mechanical property interrelationships, metal. *Mater. Transact. A*, **36**, 2149–2164.
13. Netwig, A. (1993) Entwicklung und Trends beim Reibschweißen. *Der Praktiker*, **9**, 546–555.
14. Koo, H.H., Baeslack, W.A. (1992) Friction welding of rapidly solidified Al–Fe–V–Si alloy. *Welding J.*, **5**, 20–24.
15. Addison, A., Threadgill, P. (2010) Initial studies of linear friction welding of C–Mn steel. *Welding and Cutting*, **4**, 364–370.
16. Bhamji, I., Preuss, M., Threadgill, P.L. et al. (2010) Linear friction welding of AISI 316L stainless steel. *Mater. Sci. and Eng.*, **528**, 680–690.
17. Kallee, S.W., Nicholas, E.D., Russell, M.J. (2003) Friction welding of aeroengine components. In: *Proc. of 10th World Conf. on Titanium* (Hamburg, Germany, 2003), 2859–2867.
18. Evolution of microstructure, microtexture and mechanical properties in linear friction welded titanium alloys. digitool.library.mcgill.ca/thesisfile103485.pdf
19. Corzo, M., Torres, Y., Anglada, M. et al. (2007) Fracture behaviour of linear friction welds in titanium alloys. *Annales de la Mecanica de Fractura*, **1**, 75–80.
20. Diakonov, G.S., Izmajlova, N.F., Bychkov, V.M. et al. (2012) Examination of weld zone microstructure in linear friction welding of VT6 and VT8 titanium alloys. *Vestnik UGATU*, **16**(7), 48–52.
21. Medvedev, A.Yu., Bychkov, V.M., Selivanov, A.S. et al. (2012) Application of linear friction welding for joining of VT6 and VT8-1 alloys. *Ibid.*, **16**(7), 63–67.
22. Chamanfar, A., Jahazi, M., Gholipour, J. et al. (2011) Mechanical property and microstructure of linear friction welded WASPALLOY. *Metallurg. and Mater. Transact. A*, **42**(March), 729–744.
23. Ola, O.T., Ojo, O.A., Wanjara, P. et al. (2012) Analysis of microstructural changes induced by linear friction welding in a nickel-base superalloy. *Ibid.*, **42** (Dec.), 3761–3777.
24. Linear friction welding of IN-718: Process optimization and microstructure evolution <http://www.scientific.net/AMR.15-17.357>.
25. Ola, O.T., Ojo, O.A., Wanjara, P. et al. (2012) A study of linear friction weld microstructure in single crystal CMSX-486 superalloy. *Metallurg. and Mater. Transact. A*, **43**(March), 921–933.
26. Bychkov, V.M., Selivanov, A.S., Medvedev, A.Yu. et al. (2012) Study of weldability of heat-resistant nickel alloy EP742 by method of linear friction welding. *Vestnik UGATU*, **16**(7), 112–116.
27. Rotundo, F., Ceschini, L., Morri, A. et al. (2010) Mechanical and microstructural characterization of 2124Al/25 vol.% SiCp joints obtained by linear friction welding (LFWptA). *Composites*, **41**, 1028–1037.
28. Karavaeva, M.V., Kiselyova, S.K., Bychkov, V.M. et al. (2012) Influence of upset value on formation of welded joint in linear friction welding. *Pisma o Materialakh*, **2**, 40–44.
29. Medvedev, A.Yu., Pavlinich, S.P., Atroshchenko, V.V. et al. (2010) Modeling of temperature field in linear friction welding. *Vestnik UGATU*, **14**(2), 75–79.
30. Wen-Ya Li, Tiejun Ma, Jinglong Li. (2010) Numerical simulation of linear friction welding of titanium alloy: Effects of processing parameters. *Materials and Design*, **31**, 1497–1507.
31. Grujicic, M., Arakere, G., Pandurangan, B. et al. (2012) Process modeling of Ti–6Al–4V linear friction welding (LFW). *J. Mater. Eng. and Performance*, **21**(10), 2011–2023.
32. The importance of materials data and modeling parameters in an FE simulation of linear friction welding. <http://www.hindawi.com/journals>
33. Kiselyeva, S.K., Yamileva, A.M., Karavaeva, M.V. et al. (2012) Computer modeling of linear friction welding based on the joint microstructure. *J. Eng. Sci. and Technol. Rev.*, **5**, 44–47.
34. Turner, R., Gebelin, J.-C., Ward, R.M. et al. (2011) Linear friction welding of Ti–6Al–4V modeling and validation. *Acta Materialia*, **59**, 3792–3803.
35. Linear friction welding of high strength chains. http://www.raiser.de/download/innovationspreis/bewerber2013/Linear_Friction_Welding_of_High_Strength_Chains_Mucic-Fuchs-Enzinger.pdf

Received 09.10.2014

FLASH-BUTT WELDING OF THIN-WALLED PROFILES OF HEAT-HARDENED ALUMINIUM ALLOYS

P.N. CHVERTKO, L.A. SEMYONOV and K.V. GUSHCHIN
 E.O. Paton Electric Welding Institute, NASU
 11 Bozhenko Str., 03680, Kiev, Ukraine. E-mail: office@paton.kiev.ua

Thin-walled profiles of high-strength aluminium alloys have found application in longitudinal load-carrying elements of flying vehicles and other critical structures. In industry, the serial profiles, heat-treated for maximum strength, are used, that excludes the feasibility of their welding by fusion arc methods. The problem of producing the welded joints of the above-mentioned load-carrying elements in solid phase is urgent. The present work is aimed at the study of formation of thin-walled profile joints of dissimilar (AK6 + D16) and similar (V95) heat-hardened aluminium alloys in the flash-butt continuous welding. Peculiarities of the resistance flash-butt welding with formation of joints during upsetting with extrusion were investigated and basic technology was developed, which is used for producing joints of aluminium alloy parts. This technology allows increasing greatly the quality of welded joints of this group of alloys, and also widening the range of thicknesses of metal, being joined by the flash-butt welding. Given are the main parameters of the flash-butt continuous welding modes. Strength properties of welded joints are not less than 90 % of the base metal strength. 6 Ref., 8 Figures.

Keywords: flash-butt welding, continuous flashing, upsetting, formation of joints, aluminium alloys

Alloys V95, D16 and AK6 are widely used in manufacture of critical elements and structures in aircraft and rocket construction. Thus, at the present time the riveted joints of alloys V95,

AK6 + D16 are used for manufacture of a longitudinal load-carrying structure of casings of aerospace engineering equipment, because these alloys are referred to the hard-to-weld group. The important drawback of the riveted joint is the increase in mass of structure due to the appearance of auxiliary elements during riveting of elements being abutted (Figure 1, a). The riveting is a labor-consuming operation, connected with hard labor conditions. It is necessary to make a careful treatment of the hole surface for riveting to provide the reliable joining of the product. During long-term service the riveted joint is subjected to losing, having an influence on the product service life.

Application of welding instead of riveting (Figure 1, b) is one of the effective methods of solution of the problem of improving the strength, quality of the joint and increasing the tactical-technical characteristics of flying vehicles, in particular, the decrease in structure mass and, accordingly, the increase in payload of the flying vehicles [1].

One of the main load-carrying elements of the flying vehicle structure is the stringer-fitting joints. Stringers are manufactured in majority of cases from T-section of high-strength heat-hardened alloys D16, V95, etc. Fittings are manufactured by milling from different semi-products (for example, forgings of alloy AK6 or plates of the same alloy as the stringer panels).

In this connection the assessment of weldability of thin-walled profiles of different sections

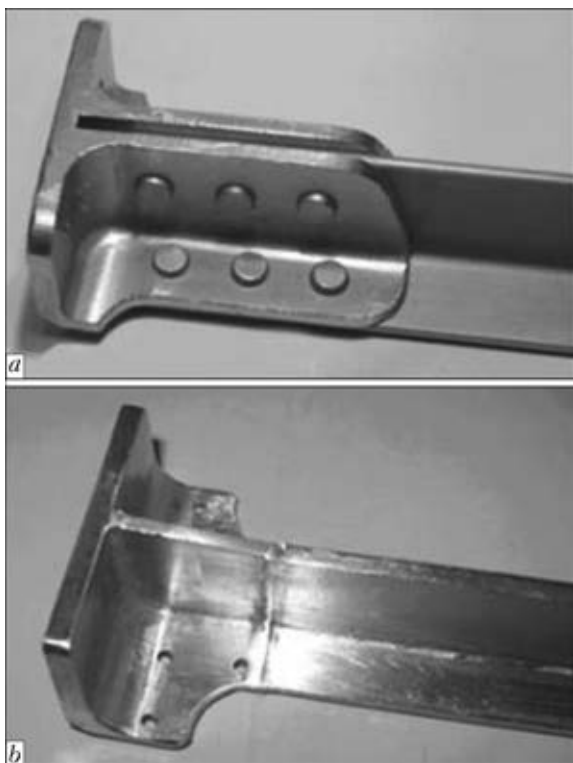


Figure 1. Joining of elements of fitting-stringer type of longitudinal load-carrying structure of flying vehicles by riveting (a) and flash-butt welding (b)

of alloy V95-T1 and plates of alloy D16-T + AK6-T1 was made during their welding.

Semi-products of alloy D16 and V95 have found a wide application in industry. These alloys are hardened by the heat treatment and, as a result, acquire the high mechanical properties and retain a sufficient technological ductility.

Among the high-strength alloys on aluminium base alloy V95, which is referred to Al-Zn-Mg-Cu (5.0–7.0 % Zn, 1.8–2.8 % Mg, 1.4–2.0 % Cu), found the largest application in rocket-space and aircraft structures. Zinc, magnesium and copper form solid solutions with aluminium and between themselves and different metallic compounds – phases M ($MgZn_2$), S (Al_2CuMg), T ($Al_2Mg_3Zn_3$), playing a large role in alloy hardening at its heat treatment.

D16 is the alloy of, at least, six components: aluminium, copper, magnesium, manganese, iron and silicon, though the main alloying elements are copper and magnesium (3.8–4.9 % Cu, 1.2–1.8 % Mg), therefore it refers to the alloys of Al-Cu-Mg system.

Alloy AK6 of Mg-Si-Cu alloying system is mainly used in the form of forgings, produced mainly from the pressed rods. Main alloying elements are magnesium, silicon and copper (0.6–1.0 % Mg, 0.9–1.0 % Si, 2.0 % Cu). The alloy is widely used in industry (construction, transport machine building, aviation) for manufacture of stamped and forged parts of intricate shape, as well as for loaded parts of the type of frames, fittings, etc. Microstructure of alloy AK6 consists after heat treatment of grains of aluminium solid solution and inclusions of metallic compounds $CuAl_2$ and Mg_2Si . Alloy AK6 is less sensitive to heating than alloys D16 and V95 [2, 3].

Thermomechanically strengthened alloys are very sensitive to heating. Degree of weakening depends on heating temperature and time of heating duration. During welding the highest mechanical properties can be obtained in that case when the duration of heating up to the temperatures above critical ones does not exceed the definite limits [4]. It is difficult to provide such temperature cycle in welding of aluminium alloys due to their heat conductivity. The intensive high-concentrated heat input to the heating zone is required.

One of the most challenging methods of producing the quality welded joints with high mechanical properties is the flash-butt welding (FBW) with a continuous flashing.

The present work is aimed at the study of peculiarities of formation of joints of thin-walled profiles of dissimilar (D16 + AK6) and similar

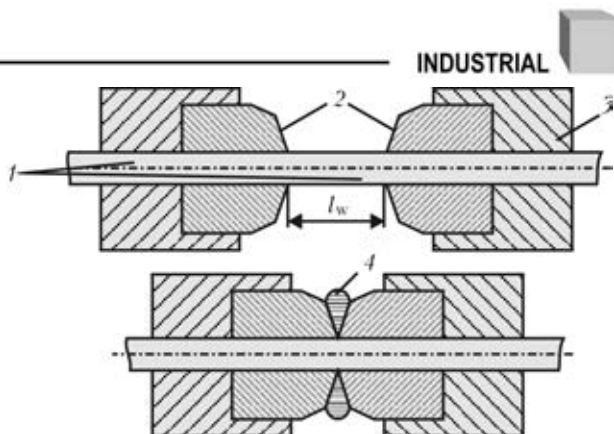


Figure 2. Scheme of FBW with formation of joint: 1 – parts; 2 – forming devices; 3 – current connector; 4 – extruded metal; l_w – tolerance for welding

(V95) heat-hardened aluminium alloys at the continuous FBW with extrusion.

The welding process is performed automatically, providing high stable quality of the joint. Design of welding equipment and technological rigs provide combining of assembly-welding works in a single cycle and high accuracy of the welded joint geometric sizes [5].

The obligatory condition of producing the quality welded joints of aluminium alloys is the formation of joint with metal extrusion during upsetting into gap between the forming devices. In this case, the degree of deformation is increased with knives approaching [6]. Scheme of FBW process with the joint formation is given in Figure 2. The forming devices are fulfilling two important functions: during upsetting they form the joint under conditions of volume-plastic deformation, and also fulfill the function of knives for the flash cutting. As a result the welded joint is formed, which does not need the next mechanical cleaning from the flash (Figure 3).

Welding of alloys of different systems of alloying (D16-T and AK6-T1) was carried out on plates of 2.5–5.0 thickness and 25–35 mm width.

To make prototyping of the welded joint of elements of the fitting-stringer type, the investigations were carried out on T-section of alloy



Figure 3. Welded joint of T-section profile of aluminium alloy V95-T1

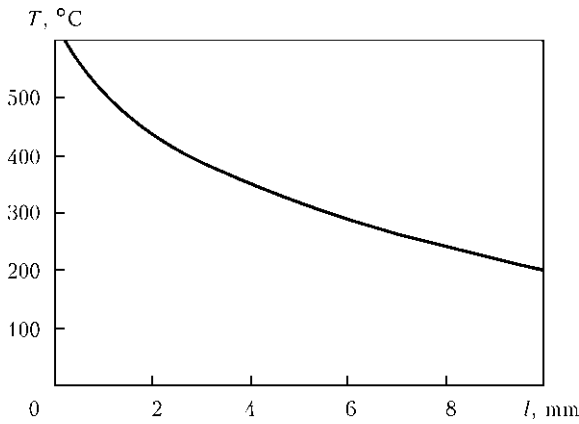


Figure 4. Distribution of temperature for depth l heated by flashing of near-contact zone 4.0 mm thick plate of alloy D16-T before upsetting

V95-T1 with thickness of flanges $\delta = 2.5$ and 4.0 mm. Welding fixture in the form of jigs was designed for the experiments on welding.

Welding of specimens was carried out in the universal laboratory machine for FBW with continuous flashing, which was equipped by a pneumo-hydraulic drive of upsetting at the force $F_{\text{ups}} = 130$ kN and welding transformer of 150 kV·A capacity.

Differences in physical properties of alloys (heat conductivity of alloy AK6 is by 30 % higher than that of alloy D16 [2, 3]) have a great influence on their heating during flashing, weld formation, character of deformation and structural transformations in the HAZ.

Selection and subsequent correction of welding modes were carried out experimentally with account for above-mentioned peculiarities of alloys. Express analysis of the welded joint quality, consisting in bending of notched specimens across weld up to fracture, was carried out in the process of run-out of the welding modes. The joint quality was evaluated by the presence or absence of defects in visual inspection of the specimen, fractured across weld (oxide films, etc.). Attempts were made to minimize the time of welding in welding modes to reduce the metal weakening

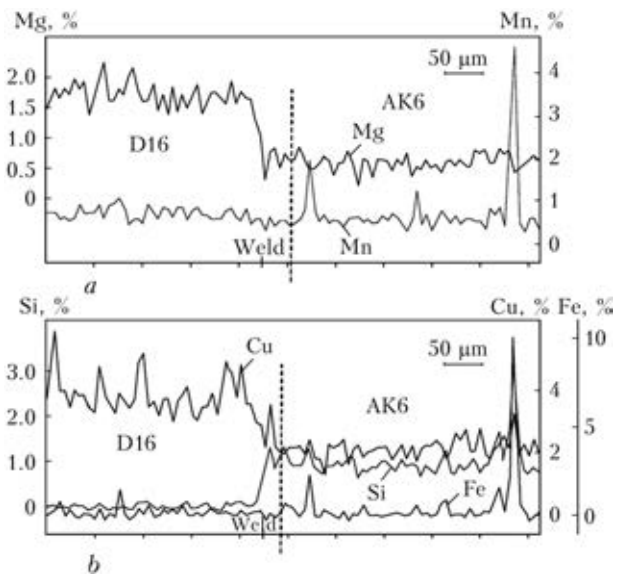


Figure 5. Distribution of elements in welded joint (a) and HAZ (b)

during heating. Using the described procedure, the optimum modes, which provide the absence of defects in fusion line, were determined.

Main parameters of welding: secondary voltage $U_{20.c} = 4$ V, rate of flashing is changed exponentially from 2 up to 25 mm/s, upsetting rate is not more than 5 s, time of welding is not more than 5 s.

The distribution of temperature in near-contact zone of edges heated by flashing directly before upsetting is given in Figure 4.

To determine the redistribution of alloying elements between alloys in weld, the X-ray spectral microanalysis of AK6-T1 + D16-T welded joints was made (Figure 5). Transition zone of redistribution of alloying elements in weld is approximately 300 μm . Beyond the transition zone the content of alloying elements in weld corresponds to the base metal composition.

In the process of upsetting the texture of welded joint with a typical turning of base metal fibers at 90° is formed as a result of extrusion of metal between the forming devices. Figure 6 gives

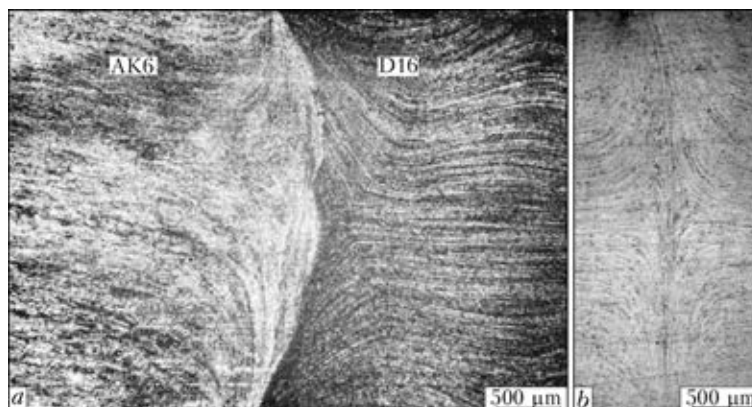


Figure 6. Macrostructure of welded joint butt: a – AK6 + D16; b – V95

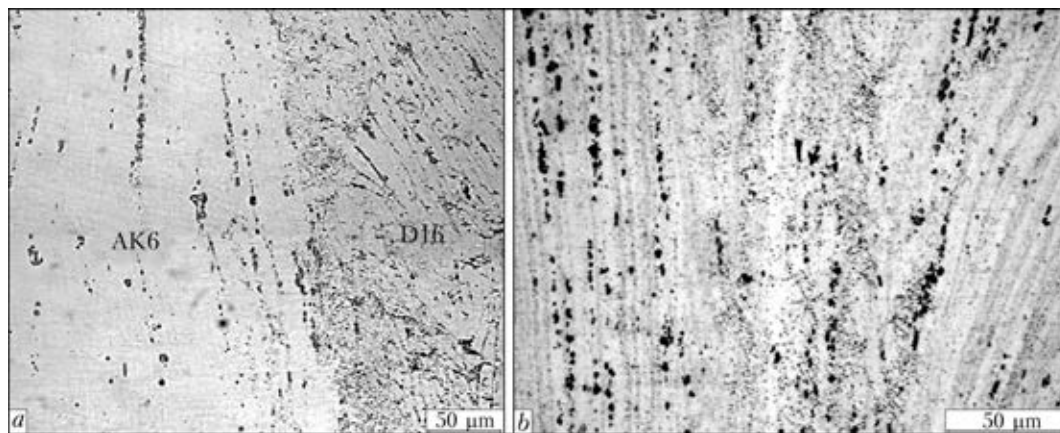


Figure 7. Microstructure of weld alloy AK6-T1 + D16-T (a) and V95-T1 (b) joints

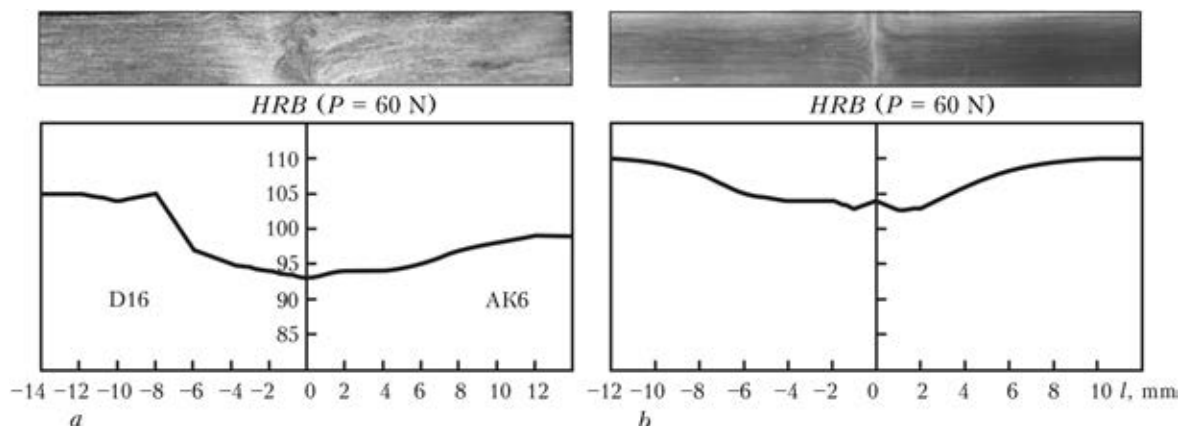


Figure 8. Distribution of hardness in welded joint of plates from alloys AK6-T1 + D16-T and profile of alloy V95-T1 (b)

the microstructures of welded joints. The microstructure of the joint zone is characterized by the deformed elongated grains of solid solution at a high density of intermetallic phases in the form of elongated chains (Figure 7). With weld approaching the intermetallic inclusions are refined. In the structure of welded joint profile of alloy V95-T1 the weld 6.0 μm thick is formed, which has a typical fine-grained structure of solid solution and refined intermetallic phases of 1.0–2.0 μm .

According to the results of carried out investigations of the distribution of metal hardness in welded joints (Figure 8) the total HAZ value is 15–20 mm, maximum weakening of weld does not exceed 6 %.

Results of mechanical tests of the base metal and welded specimens of AK6-T1 + D16-T alloys showed the strength of the welded joints at the level of base metal of the less strong alloy AK6-T1 ($\sigma_t^w = 386$ MPa, $\sigma_t^{BM\ AK6} = 387$ MPa, $\sigma_t^{BM\ D16} = 455$ MPa). Specimens were fractured in HAZ on the side of alloy AK6-T1.

The strength of welded joints of V95-T1 alloy profile is at the level higher than 90 % of the base metal strength ($\sigma_t^w = 521$ –542 MPa, $\sigma_t^{BM\ B95-T1} = 580$ MPa)

From the obtained results of investigations the positive conclusion can be made about the challenging application of FBW technology with continuous flashing for joining the elements of thin-walled profiles of high-strength aluminium alloys in critical structures. This technology makes it possible to weld elements of structures in heat-hardened state with a loss in strength of not more than 10 %.

1. Nikolaev, G.A., Fridlyander, I.N., Arbutov, Yu.P. (1990) *Aluminium alloys to be welded*. Moscow: Metallurgiya.
2. (1973) *Aluminium alloys. Application of aluminium alloys*: Manual. Ed. by A.T. Tumanov, I.N., Fridlyander. Moscow: Metallurgiya.
3. (1984) *Commercial aluminium alloys*: Refer. Book. Ed. by F.I. Kvasov, I.N. Fridlyander. Moscow: Metallurgiya.
4. Kuchuk-Yatsenko, S.I., Chvertko, P.N., Semyonov, L.A. et al. (2010) Peculiarities of flash butt welding of high-strength aluminium alloy 2219. *The Paton Welding J.*, **3**, 7–9.
5. Kuchuk-Yatsenko, S.I. (1992) *Flash-butt welding*. Kiev: Naukova Dumka.
6. Kuchuk-Yatsenko, S.I., Chvertko, P.N., Semyonov, L.A. et al. (2013) Flash butt welding of products of high-strength alloys based on aluminium. *The Paton Welding J.*, **7**, 2–6.

Received 19.05.2014

APPLICATION OF COMPLEX-ALLOYED POWDERS PRODUCED BY THERMOCENTRIFUGAL SPUTTERING IN FLUX-CORED WIRES

A.P. ZHUDRA, S.Yu. KRIVCHIKOV and V.I. DZYKOVICH

E.O. Paton Electric Welding Institute, NASU

11 Bozhenko Str., 03680, Kiev, Ukraine. E-mail: office@paton.kiev.ua

This paper presents the results of evaluation of the influence of complex-alloyed powders (CAP) on welding-technological properties of flux-cored wires and deposited metal performance. Possibility of ensuring a high degree of flux-cored wire alloying at reduction of its diameter is considered. Tribotechnical characteristics of metal deposited with flux-cored wires are determined at CAP application as a filler. The paper presents the results of metallographic investigations of deposited metal. It is established that CAP application as flux-cored wire core is favourable for the mode of electrode metal melting and transfer leading to improvement of their welding-technological characteristics. Wear resistance studies of deposited metal showed an improvement of wear resistance of deposited metal operating under the conditions of abrasive wear and metal-over-metal friction. 4 Ref.. 5 Tables. 3 Figures.

Keywords: *flux-cored wire, thermocentrifugal sputtering of ingots, complex-alloyed powders, welding-technological characteristics of flux-cored wire, tribotechnical characteristics of deposited metal*

Flux-cored wires produced to GOST 26101–84 have a core, in which the alloying part consists of crushed ferroalloys and metal powders. Ensuring a high degree of alloying, usually, necessitates application of high (40–50 %) values of the filling coefficient. This, in its turn, leads to increase of flux-cored wire diameter up to 3.2 mm and more. Stable process of surfacing with such flux-cored wire requires considerable current (400–500 A) and arc voltage (28–32 V), that is not rational or inadmissible for some types of parts being reconditioned, which are sensitive to high temperature impact, prone to thermal deformation, etc. (in such cases application of large-diameter flux-cored wires leads to considerable power consumption). Thus, solution of the problem of flux-cored wire diameter reduction at preservation of its required alloying level, is of considerable practical interest.

PWI developed the technology of producing complex-alloyed powders (CAP), which consists in melting out an ingot of cylindrical form of the required composition from a mixture of ferroalloys and other alloying materials, and its subsequent plasma-arc centrifugal sputtering in the modes, ensuring production of spherical powder particles of the required granulometric composition. The composition of each particle should correspond to calculated composition of surfacing

electrode materials, namely flux-cored wires, strips, filler rods, stick electrodes, etc.

In addition, spherical shape of CAP particles (Figure 1, *b*), unlike irregular-shaped particles (Figure 1, *a*), will ensure a more dense filling of the core and will enable reducing flux-cored wire diameter.

On the other hand, replacement of mechanical mixture of core materials of nonuniform structure, properties and chemical composition by CAP, will result in changes of core electric and thermophysical properties. This, in its turn, will influence the welding-technological properties of flux-cored wire and, possibly, deposited metal characteristics.

The objective of this work is experimental investigation of CAP influence on welding-technological characteristics of flux-cored wires and wear resistance of deposited metal. Earlier [1] PWI performed investigations on application of granulated alloy of the respective composition as the core of PP-Np-25Kh5FMS flux-cored wire. This study focused on improvement of deposited metal high-temperature resistance.

As objects of study, we selected two flux-cored wires of another type: PP-AN170 (PP-Np-80Kh20R3T), applied for hardfacing of parts operating under the conditions of intensive abrasive and hydroabrasive wear (teeth of excavator ladders, dredge noses, etc), and PP-AN160 (PP-Np-200KhGR) used for hardfacing of parts operating under the conditions of lubricated friction of metal over metal (cast iron crankshafts of car engines).

Two pairs of flux-cored wires were manufactured to perform comparative testing: first — PP-AN170 and PP-AN170SF, and the second — PP-AN160 and PP-AN160SF. In each pair the first flux-cored wire is manufactured in keeping with the requirements of GOST 26101–84, and the second — with application of CAP as the core.

Composition of CAP, produced by thermocentrifugal sputtering in OB-2327 unit [2], is given in Table 1.

Modes of test ingot sputtering

Welding current, A	350–500
Arc voltage, V	28–34
Rotation speed, rpm	3500–5000
Ingot feed rate, m/min	1.50–1.5

To assess CAP influence on welding-technological characteristics of test flux-cored wires, deposition of isolated beads was performed in the following mode: $I_d = 280\text{--}300$ A, $U_a = 26\text{--}28$ V, $v_d = 15$ m/h for flux-cored wires PP-AN170 and PP-AN170SF, and $I_d = 170\text{--}180$ A, $U_a = 20\text{--}26$ V, $v_d = 7.7$ m/h for flux-cored wires PP-AN160 and PP-AN160SF. Kind of current is direct, polarity is reverse.

Conducted testing (Table 2) revealed that CA application as flux-cored wire core improves arcing stability (determined by the value of arc voltage variation K_v : the smaller K_v value, the more stable the arcing process), reduces electrode metal losses for sputtering ψ_{sp} , and promotes improvement of the quality of deposited metal formation b/h (assessed by the value of the ratio of width b of deposited bead to its height h : the larger b/h value, the higher the formation quality). Spherical shape of CAP particles allowed reducing flux-cored diameter $d_{fl.w}$ and, thus, low-

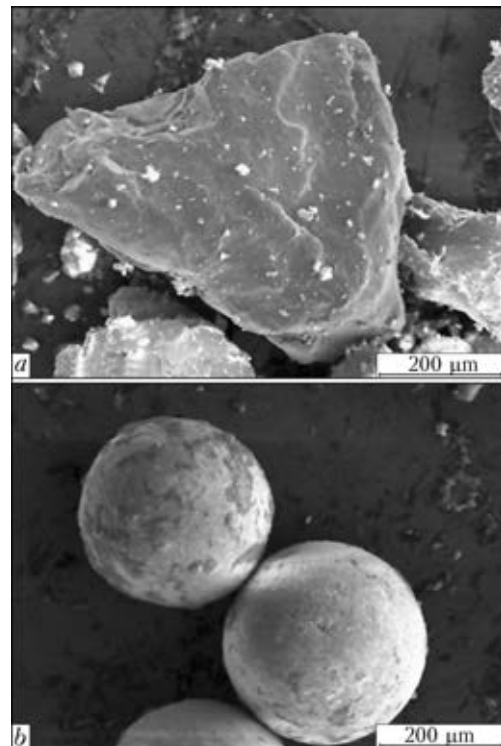


Figure 1. Appearance of fragmented particles of ferroalloys (a) and spherical granules produced by the method of thermocentrifugal sputtering (b)

ering minimum possible values of arc current and voltage, at which the surfacing process runs in a stable manner. CAP positive influence on K_v , b/h and ψ_{sp} is due to favourable nature of their melting and electrode metal transfer: more uniform melting of the core and sheath, reduction of the size of transferring electrode drops, quantity and duration of short-circuiting of the arc gap. The most significant changes of the above parameters are found at CAP application as the core of PP-AN170 flux-cored wire.

Table 1. Composition of CAP for flux-cored wire production

Flux-cored wire type	Element content, wt.%							
	C	Cr	Mn	Si	Ti	B	Al	Fe
PP-AN170	3	50	4	4	1.5	8	–	–
PP-AN160	19	5	9	13	5	1	2	Res.

Table 2. Welding-technological characteristics of test flux-cored wires

Flux-cored wire type	Welding-technological parameter values					
	ψ_{sp} , %	b/h	K_v , %	Surfacing modes and flux-cored wire diameters		
				I_d , A	U_a , V	$d_{fl.w}$, mm
PP-AN170	16.8	2.0	25.6	280–300	26–28	3.2
PP-AN170SF	9.2	4.3	18.5	220–240	22–24	2.6
PP-AN160	7.4	4.5	9.4	170–180	21–22	1.8
PP-AN160SF	6.2	5.0	7.2	140–150	18–20	1.6

Table 3. Chemical composition of deposited metal, wt.%

Flux-cored wire type	C	Cr	Si	Mn	Ti	Al	B
PP-AN160	2.2	0.3	1.2	0.8	0.3	0.2	0.08
PP-AN160SF	2.0	0.5	0.8	0.6	0.3	0.1	0.1
PP-AN170	1.1	18.5	0.7	0.8	0.3	–	2.6
PP-AN170SF	0.9	19.1	0.5	0.8	0.4	–	2.9

Abrasive wear-resistance testing of metal deposited with PP-AN170 and PP-AN170SF flux-cored wires was conducted in NKM friction machine by «stationary ring» schematic at friction against non-fixed abrasive [3]. Test samples of $16 \times 16 \times 6$ mm size were cut out of the third or fourth layer of multilayer deposit, produced in the above mode. Deposited metal composition is given in Table 3. Relative wear resistance was assessed as the ratio of the loss of reference-sample mass (metal deposited with flux-cored wire PP-AN170) to loss of mass of the sample, deposited with PP-AN170SF flux-cored wire. Derived results are given in Table 4.

Test results indicate that CAP application as the core of PP-AN170 flux-cored wire leads to increase of deposited metal abrasive wear resistance by 22–23 %. Comparative metallographic analysis of deposited metal structures (Figure 2) showed that CAP does not have any influence

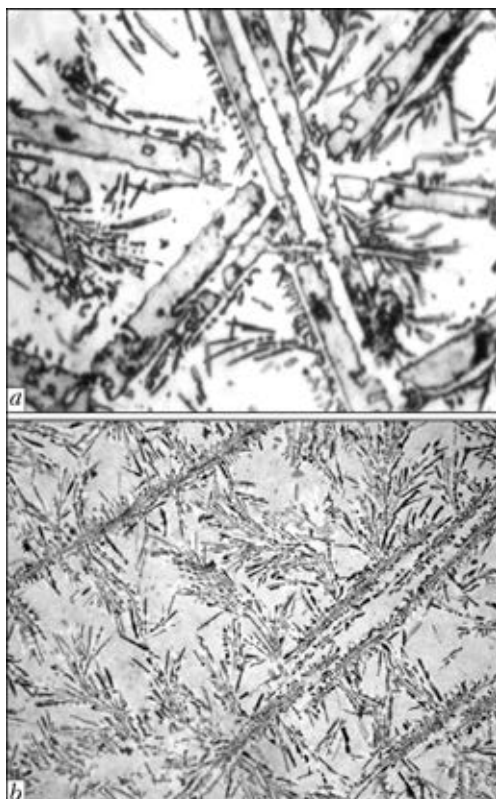

Figure 2. Structure ($\times 500$) of metal deposited with flux-cored wires PP-AN170 (a) and PP-AN170SF (b)

Table 4. Results of abrasive wear resistance testing of metal deposited with PP-AN170 and PP-AN170SF flux-cored wires

Sample grade	Sample mass, g		Wear, g	Relative wear resistance
	Before testing	After testing		
170-1	12.0436	11.9017	0.1419	1
170SF-1	12.0003	11.8888	0.1115	1.27
170-2	12.4266	12.2736	0.1530	1
170SF-2	11.6245	11.4991	0.1254	1.22
170-3	12.1111	11.9717	0.1394	1
170SF-3	12.2234	12.1176	0.1058	1.32

on composition, but changes the degree of dispersity and hardness of structural components.

So, metal deposited with PP-AN170SF flux-cored wire (Figure 2, b) is characterized by formation of carboborides and eutectic with higher degree of dispersity than for metal deposited with PP-AN170 flux-cored wire (Figure 2, a). Both in the first and in the second case hardness of carboborides and eutectic is practically the same, and is equal to $HV1-14000-17000$ and $HV1-9200-14500$, respectively. At the same time, hardness of the matrix of metal deposited with PP-AN170CF flux-cored wire is higher and is equal to $HV1-7200-8600$, whereas for metal deposited with AN170 flux-cored wire it is $HV1-6500-7400$. In all probability, higher hardness of deposited metal matrix is also responsible for its higher abrasive wear resistance.

Determination of tribotechnical parameters of metals deposited with PP-AN160 and PP-AN160SF flux-cored wires was conducted in friction machine SMT-1 by roller–block method to GOST 23224–86. Blocks were segments of standard car inserts AO 20-1. Blanks of VCh50-2 cast iron were used for roller production. Their cylindrical surface was surfaced with test flux-cored wires in the above modes, and then ground to nominal dimensions: 12 mm thickness and 50 mm diameter. Composition of tested deposited metals is given in Table 3.

Testing of friction-sliding pairs with lubrication was performed in two stages: in running-in mode and at working load. Value of optimum working load P_{op} was selected on the basis of preliminary experiments, which showed that its increase can lead to «seizure» on deposited metal–insert mating surface. Total wear rate I_{Σ} on the whole was determined as a sum of intensities of wearing of insert I_b and roller I_r . Procedure of determination of these values is given in GOST 23.224–86. In addition, during testing the change of the coefficient of mating surface friction f_{fr}

Table 5. Tribotechnical characteristics of friction-sliding pairs

Mating surface number	Type of mating surface and flux-cored wire	Performance characteristics		Wear rate, mm/m·10 ⁻⁴			$f_{fr} \cdot 10^{-2}$
		P_{op} , MPa	T_{fr} , °C	I_r	I_b	I_{Σ}	
1	Deposited metal–insert. PP-AN160 flux-cored wire	11	72	0.24	0.26	0.5	45
2	Deposited metal–insert. PP-AN160SF flux-cored wire	14	50	0.22	0.12	0.34	20

and temperature of frictional heating of oil T_{fr} was recorded.

Obtained data (Table 5) show that wear resistance of deposited metal of mating surfaces 1 and 2 is approximately the same. At the same time I_{Σ} of mating surface 2 is 1.5 times lower than that of mating surface 1, that is due to smaller I_b value of mating surface 2. Proceeding from that it can be stated that for the two compared mating surfaces application of PP-AN160SF flux-cored wire provides deposited metal with higher antifriction properties.

Metallographic examination of deposited metal of mating surfaces 1 and 2 was conducted to detect the causes affecting the derived results. It should be noted that detailed analysis of structural-phase state of the multicomponent alloy, which solidified under non-equilibrium conditions, is a rather labour-consuming task. However, it can be stated with sufficient degree of validity that the deposited metal structure (at application of both PP-AN160 and PP-AN160SF flux-cored wire) consists of two main phases: austenite decomposition products (pearlite + residual austenite) and carbide-cementite phase (Figure 3). The latter has the form of ramified reinforcing net with regions of different thickness in the section plane.

In the micrograph this phase is of white colour, and pearlite-austenite phase is black that allowed assessment of their quantitative ratio. As a result, it was established that deposited metal of mating surface 1 contains 40–46 % of «white» (carbide-cementite) phase of hardness $HV_{0.5}$ 8000–8200. Hardness of solid solution grains is $HV_{0.5}$ 5000–5200. In the deposited metal of mating surface 2 the fraction of carbide-cementite phase is 28–33 %, and its hardness remains to be the same as in the deposited metal of mating surface 1. At the same time, pearlite hardness in deposited metal of mating surface 2 ($HV_{0.5}$ 5800–6200) is significantly higher than that of deposited metal of mating surface 1.

Thus, it can be stated that reduction of the fraction of hard carbide phase in the deposited metal, which is also abrasive relative to the insert, promotes lowering of wear rate of the insert

and mating surface as a whole. At the same time, reduction of the quantity of wear-resistant structural component is compensated by increase of solid solution hardness and quantity. As a result, wear rates of deposited metal of mating surfaces 1 and 2 remain approximately the same. Metallographic analysis could not reveal the mechanism of CAP influence on quantitative ratio of phases in the deposited metal and their hardness. It can be assumed, however, that this is related to influence of boron as an active modifying and carbide-forming element.

In [4] it is shown that the form of boron-containing material (B_4C , B_2O_3 , BN, etc.) in the

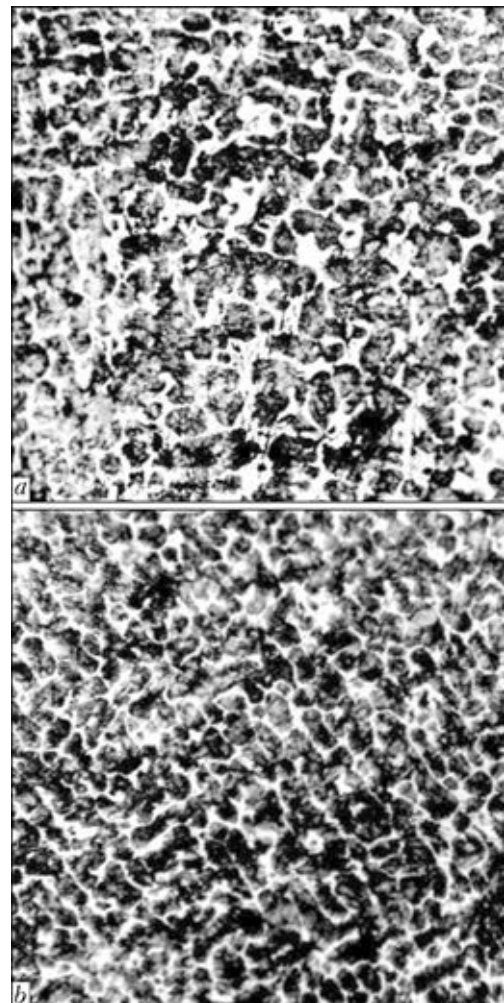


Figure 3. Structure ($\times 320$) of metal deposited with flux-cored wire PP-AN160 (a) and PP-AN160SF (b)



composition of flux-cored wire core has an essential influence on their quantitative ratio and morphology of deposited metal phase components. Even though boron was added to the composition of PP-AN160 and PP-AN160SF flux-cored wire cores in the same amounts, but different boron-containing materials were used: in the first case – iron-chromium-boron master alloy, and in the second case – CAP particles. It is also possible that different content of carbide-cementite phase in the studied samples of deposited metal is the result of varying carbide-forming activity of boron, depending on its compositional state.

Conclusions

1. Application of complex-alloyed powders as core of complex-alloyed flux-cored wires allows an essential reduction of its diameter without changing the alloying level, reduction of power consumption in surfacing processes and improvement of deposited metal performance. Replacement of core of PP-AN170 flux-cored wire by CAP core allowed improvement of its welding-technological characteristics, reducing its diameter from 3.2 to 2.6 mm and increasing abrasive wear resistance of deposited metal by 1.2–1.3 times.

2. Replacement of mechanical mixture of charge materials of non-uniform composition in flux-cored wire core by CAP influences the quantitative composition and hardness of deposited metal structural components. CAP application in PP-AN160 flux-cored wire reduces the fraction of abrasive carbide phase and increases the hardness of deposited metal pearlite base that increases by 1.3 times the wear resistance of mating surface exposed to metal-over-metal friction in service.

1. Kondratiev, I.A. (1980) Flux-cored wire filled by granular alloy. In: *Theoretical and technological principles of surfacing. Surfacing of metallurgical and power engineering parts*. Kiev: PWI.
2. Dzykovich, V.I. (2010) *Study and development of materials for wear-resistant surfacing based on spheroidized granules of tungsten carbides*: Syn. of Thesis for Cand. of Techn. Sci. Degree. Kiev.
3. Yuzvenko, Yu.A., Gavrish, V.A., Marienko, V.Yu. (1979) Laboratory units for evaluation of wear resistance of deposited metal. In: *Theoretical and technological principles of surfacing. Properties and tests of deposited metal*. Kiev: PWI.
4. Zhudra, A.P., Krivchikov, S.Yu., Petrov, V.V. (2004) Selection of boron-containing charge materials for the core of flux-cored wire. *The Paton Welding J.*, 4, 51–52.

Received 22.09.2014

MODERNIZATION OF CONTROL SYSTEM OF A1756 MACHINE FOR PLASMA-POWDER SURFACING

E.F. PEREPLYOTCHIKOV, I.A. RYABTSEV, Yu.N. LANKIN, V.F. SEMIKIN and P.P. OSECHKOV

E.O. Paton Electric Welding Institute, NASU

11 Bozhenko Str., 03680, Kiev, Ukraine. E-mail: office@paton.kiev.ua

Given are the results of modernization of control system of A1756 machine for plasma-powder surfacing. New control system allows for complete automating of surfacing process as well as optimizing consumption of filler powder and minimizing its loss. Control of surfacing process is carried out with the help of programmer, designed using PIC16F886 (Microchip) microcontroller and alphanumeric OLED indicator WEH1601A (Winstar). Microprocessor block of the programmer allows for setting the parameters of time characteristics for surfacing current and powder consumption and their processing in process of program control. Scheme of programmer connection to A1756 machine with capability of operation switching from programmer as well as in simple design mode was developed and built. The programmer allows for carrying out setting of modes, providing good bead formation during automatic plasma-powder surfacing, quality filling of crater and minimum loss of filler powder. 2 Ref., 7 Figures.

Keywords: *plasma-powder surfacing, surfacing machine, control system, powder consumption, surfacing mode, programmer*

Characteristics of transfer and melting of filler material in plasma-powder surfacing are not directly related with current and arc voltage and being mainly determined by mass feed rate and fractional composition of filler powder as well as its physical properties. An important problem, considering a fact of application of expensive powders from nickel- and cobalt-based alloys as well as special surfacing iron-based alloys as filler materials in plasma-powder surfacing, is optimizing of powder consumption and minimizing of its loss using this method of surfacing [1].

Powder consumption and its loss depend on design of some assemblies of surfacing equipment (powder feed, plasmatron), modes of surfacing and, to some extent, structure of part to be surfaced (geometry of surface). Loss of powder will rise, in particular, if plasmatron is located or periodically passes close to edge of part being surfaced as well as if width of substrate being surfaced is less than nozzle diameter.

Figure 1 shows a scheme of drum-type feeder, developed at the E.O. Paton Electric Welding Institute [2]. The feeder consists of sealed housing 1, hopper 6 with branch tube, drum 2 and setting mechanism, made in a form of spring loaded bush 4, being moved along the branch tube with the help of lever-screw regulator 3. Mechanism 5 allows for controlling a level of powder in the feeder. The drum is actuated by DC motor by means of worm gear (not indicated

in Figure 1). A gap between bush and drum is set in such a way that in the case of fixed drum the powder will remain in the hopper. Drum movement drags the powder and directs it in a receiving cone, from which powder is transported through tube 7 into plasmatron by transporting gas. Rate of filler powder feeding into plasmatron can be changed by means of regulation of drum rotation rate (Figure 2). Transporting gas feeds the filler powder in a gap between focusing 1 and plasma-forming 2 nozzles.

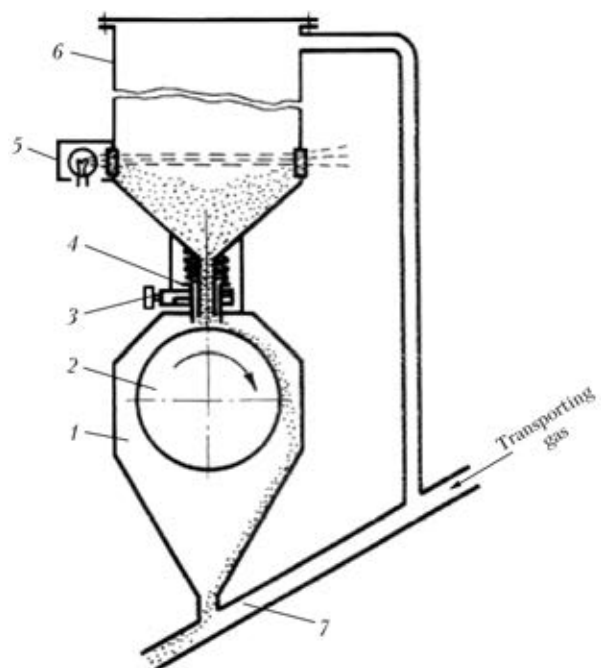


Figure 1. Scheme of drum feeder for filler powder feed (designations see in the text)

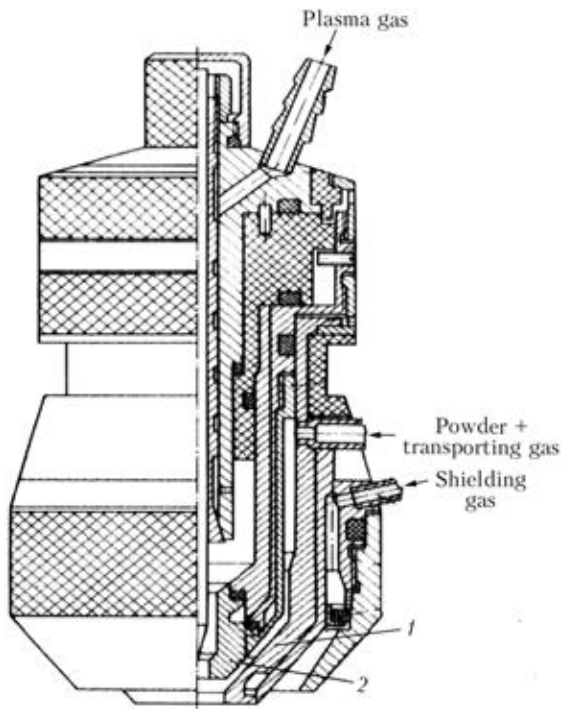


Figure 2. Plasmatron A1756.05 for plasma-powder surfacing: 1 – focusing; 2 – plasma-forming nozzle

The plasmatron has four variants of combination of plasma forming and focusing nozzles $d_{pl} + d_f$: 2 + 4; 3 + 6; 4 + 7.5; 5 + 9 mm, that also allows for regulating powder feed rate. Surfacing

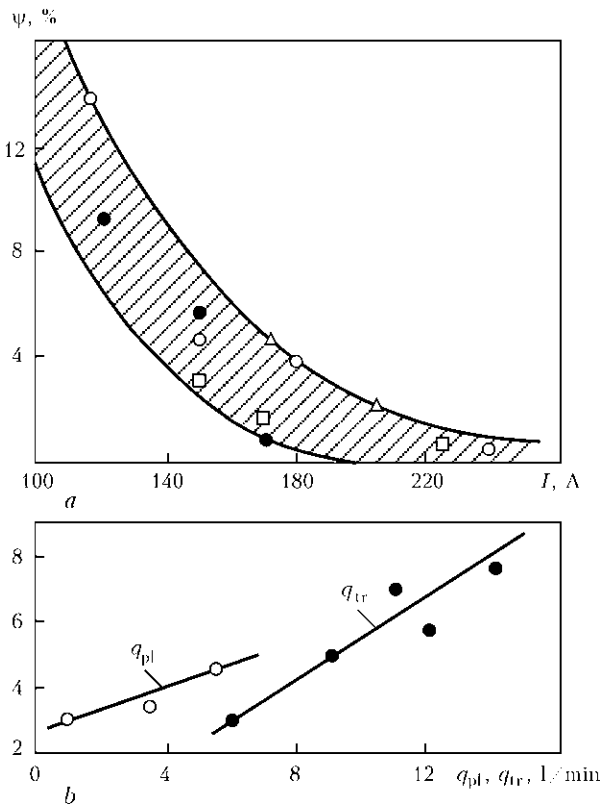


Figure 3. Dependence of coefficient of powder loss ψ on surfacing current I (a) and consumption of plasma q_{pl} and transporting q_{tr} gases [1] (b); a – powder feed: ● – 1.2; ○ – 2.0; □ – 3.5; Δ – 6 kg/h; b – 2 kg/h

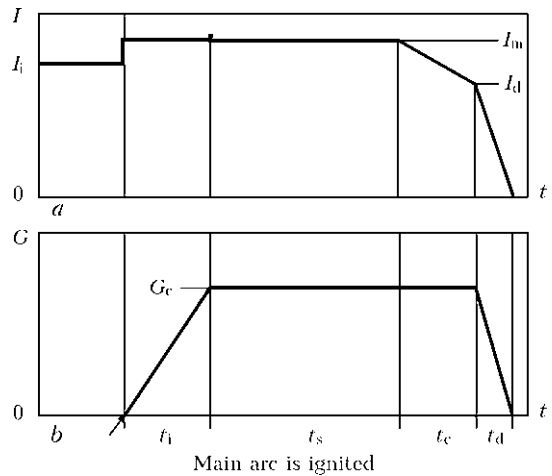


Figure 4. Cyclogram of process of plasma-powder surfacing: a – surfacing current; b – powder consumption; I_i – current of indirect arc; I_m – current of main arc; I_d – current at the moment of beginning of drop of powder feed rate; G_c – maximum level of powder consumption (feed rate); t_i – duration of increment; t_s – duration of soaking in steady process; t_c – duration of correction; t_d – duration of drop

technology [1] determines a variant of optimum combination of nozzle diameters.

Intensity of surfacing current and consumption of transporting gas (Figure 3) are the main parameters of surfacing mode effecting consumption and loss of filler powder. Increase of intensity of surfacing current reduces filler powder loss in whole range of rates of its feed (Figure 3, a), since larger amount of powder can be melted in arc as well as weld pool.

Small consumption of transporting gas (3–4 l/min) often disturbs surfacing process due to

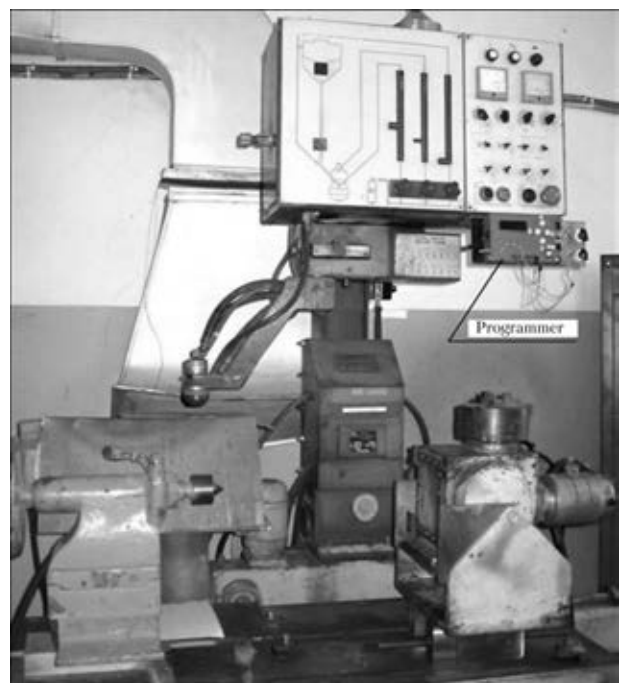


Figure 5. View of A1756 machine for plasma-powder surfacing with programmer for control of surfacing process

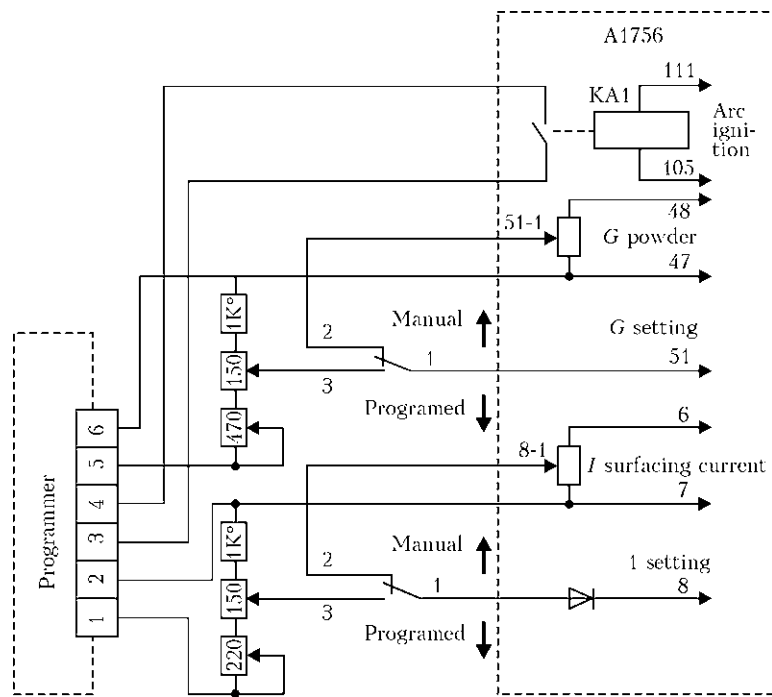


Figure 6. Principal diagram of programmer

blocking of plasmatron channels with powder. Loss of powder grows with increase of transporting gas consumption (Figure 3, *b*) as a result of rising of initial particle rate and deterioration of conditions of their heating in the arc.

At that, according to the experience, only part of powder particles, moving in a periphery of arc column, enters the weld pool. The particles, which fall on surface being surfaced in front of or from the side of weld pool, are irreversibly lost as a result of rebound resilience from this surface. Consumption of transporting gas in the

range of 6–9 l/min, at which powder loss does not exceed 5–8 %, is supposed to be the optimum one.

There is also loss of powder at the beginning and end of surfacing process, which is difficult to be optimized and controlled, in addition to the loss, determined by technological peculiarities of steady process of plasma-powder surfacing. In theory, a cyclogram of the whole process of plasma-powder surfacing can be represented in the following way (Figure 4).

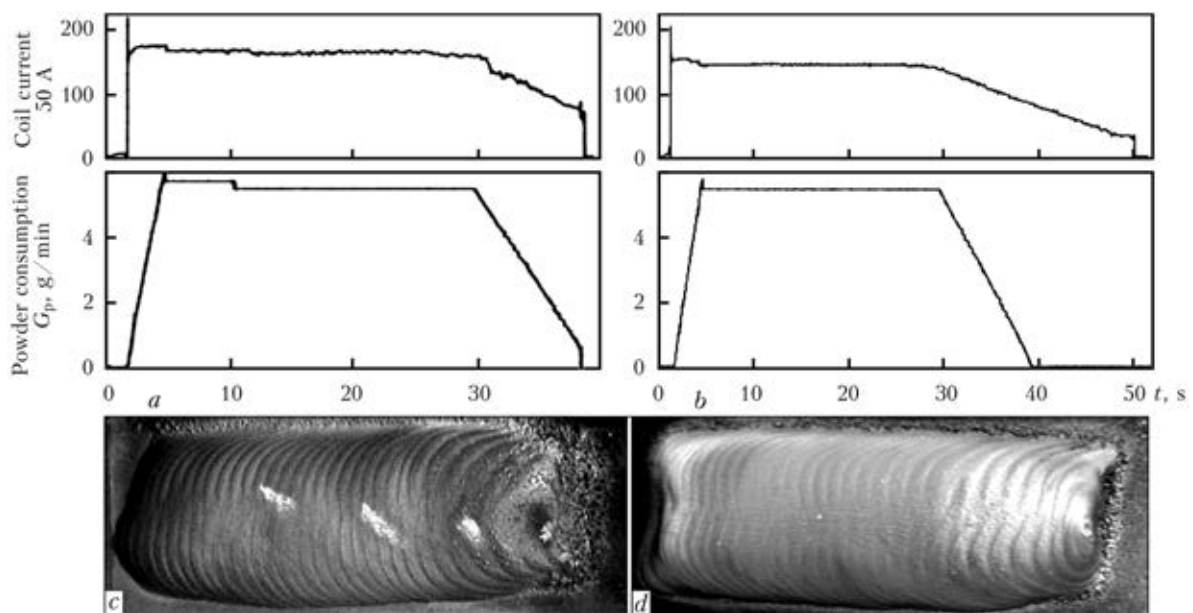


Figure 7. Time characteristics of technological parameters of surfacing (*a, b*) and beads surfaced by these modes (*c, d*): *a, c* – current and powder feed were switched-off simultaneously; *b, d* – powder feed was stopped before current switching-off



Feeding of filler powder should be started after main arc ignition (Figure 4, *b*). Powder feed is increased during time t_1 to value G_c determined by the technology. Crater filling is necessary to be carried out at the end of surfacing process with stepwise synchronous reduction of surfacing current and rate of powder feed.

The E.O. Paton Electric Welding Institute developed a programmer for control of plasma-powder surfacing process. It was designed with application of microcontroller PIC16F886 (Microchip) and alphanumeric OLED indicator WEH1601A (Winstar). Microprocessor block of the programmer allows for setting the parameters of time characteristics of surfacing current and powder consumption for plasma-powder surfacing machine A1756 (Figure 5) and their optimizing in the process of program control.

Principal diagrams, printed circuit boards, structure and software were developed for the programmer. Software was adjusted for technological conditions of A1756 machine:

- technological parameters are set in actual values (surfacing current in amperes, powder consumption in g/min);
- entered are the technological limits for setting the parameters of time characteristics 0–250 A and 0–120 g/min.

Scheme of programmer connection to A1756 machine with capability of switching of operation from programmer as well as in simple design mode was developed and built (Figure 6).

The programmer was technologically tested on A1756 machine by recording the main parameters of surfacing mode, i.e. current and powder feed. Stated problem lied in development of such modes of surfacing, which would provide for minimum powder loss and quality formation of surfaced beads, including quality crater filling.

If current is switched-off simultaneously or before stopping of powder feed, this will result in bad crater filling and excessive powder loss (Figure 7, *a, c*).

In the case, when powder feed is stopped before current switching-off, quality crater filling is provided and powder loss is reduced to the minimum (Figure 7, *b, d*). Beginning of drop of current and powder feed are matched in time, however, powder feed is stopped somewhat earlier (Figure 7, *b*).

Thus, developed programmer allows for setting the modes, providing good formation of surfaced beads, in automatic plasma-powder surfacing on A1756 machine, quality crater filling and minimum loss of filler powder.

1. Gladky, P.V., Pereplyotchikov, E.F., Ryabtsev, I.A. (2007) *Plasma surfacing*. Kiev: Ekotekhnologiya.
2. Gladky, P.V., Pereplyotchikov, E.F., Saprykin, Yu.I. et al. (1970) *Drum feeder*. USSR author's cert. 266111. Int. Cl. 21h 30/17. *Otkrytiya. Izobreteniya*, **11**, 76.

Received 22.09.2014



TRAINING OF SPECIALISTS-WELDERS OF KAZAKHSTAN IN UKRAINE

One of the tendencies of the modern industrial production is the transition to the International norms and standards. This widens greatly the opportunity of enterprises in cooperation with foreign partners in the scope of the products conformity to the established requirements. These tendencies are especially characteristic of the welding production, the efficiency of which is defined significantly by the quality of the personnel professional competence.

The professional training of the personnel, capable to realize the advantages of advanced welding technologies, has its peculiar features, connected with the specifics of the welding process and high requirements to the quality of the welded structures. These features have been realized in training programs of the International Institute of Welding, on the basis of which the international system of training and certification of the personnel is functioning, starting from the workers-welders and finishing by the diploma engineers on welding. Due to application of single training programs and standardized certification tests, the qualifications in the field of welding are recognized in different countries.

At the present time the training of the personnel of welding production within the frames of the International Certification System is carried out by the Authorized National Bodies (ANB), accredited by the IIW, one of which is the PWI Inter-Industry Training Certification Center (IITCC). Since 1998 the Center is an active participant of the international programs and showed itself as a reliable partner both in Ukraine and also abroad. The specialists, trained by it, are working successfully in many countries.

In April, 2014 a group of trainees of nine citizens of Kazakhstan came for training on program «International welder» in accordance with application of «Transcargo International Ltd.», participating in the State Program of accelerated



Teachers of IITCC: Drs G.E. Saksonov, E.P. Chvertko and P.P. Protsenko, Director of IITCC (*lower row*)

industrial-innovation development of Republic of Kazakhstan. During 16-week training they passed the full course of professional-theoretical and practical training, specified by the IIW program. They mastered the technique of manual arc coated electrode welding of different joints of flat parts and pipes of structural steels. From the results of the certification tests, including checking of theoretical knowledge and practical habits, the IITCC examination commission awarded five trainees the qualification of the International welder of pipes and four trainees the qualification of the International welder of plates.

Authority of «Transcargo International Ltd.» recognized the good level of organizing the theoretical and practical training, high skill of teachers and foremen of production training, quality of methodical provision of training process and expressed the readiness to continue cooperation in the field of professional training of personnel also in accordance with other international qualifications.

Dr. P.P. Protsenko, PWI IITCC

INDEX OF ARTICLES FOR TPWJ'2014, Nos. 1–12

Pilot Plant of Welding Equipment of the E.O. Paton Electric Welding Institute at the nowadays stage	4	Influence of active gas content and disperse filler continuity on the process of bead formation in microplasma powder surfacing of nickel superalloys (Yushchenko K.A. and Yarovitsyn A.V.)	6/7
The 80th Anniversary of the E.O. Paton Electric Welding Institute of the NAS of Ukraine	9	Investigation of influence of microalloying with titanium and boron of weld metal on its mechanical properties in underwater welding (Maksimov S.Yu., Machulyak V.V., Sheremeta A.V. and Goncharenko E.I.)	6/7
VIII INTERNATIONAL CONFERENCE ON WELDING CONSUMABLES			
CONSUMABLES FOR MANUAL ARC WELDING			
Electrodes for welding of dissimilar chromium martensitic and chromium-nickel austenitic steels (Zakharov L.S., Gavrik A.R. and Lipodaev V.N.)	6/7	Manufacturing defects in welding consumables influencing the quality of welded joints (Turyk E.V.)	6/7
Heating and melting of electrodes with exothermic mixture in coating (Vlasov A.F., Makarenko N.A. and Kushchy A.M.)	6/7	Materials for strengthening of gas turbine blades (Kostin A.M., Butenko A.Yu. and Kvasnitsky V.V.)	6/7
Investigation of composition and structure of weld metal of Kh20N9G2B type made in wet underwater welding (Yushchenko K.A., Bulat A.V., Kakhovsky N.Yu., Samoilenko V.I., Maksimov S.Yu. and Grigorenko S.G.)	6/7	New capabilities of the oldest enterprise on production of welding fluxes (Zalevsky A.V., Galinich V.I., Goncharov I.A., Osipov N.Ya., Netyaga V.I. and Kirichenko O.P.)	6/7
Investigation of transition zone of low-carbon steel joint with high-alloyed Cr-Ni deposited metal (Yushchenko K.A., Kakhovsky Yu.N., Bulat A.V., Morozova R.I., Zvyagintseva A.V., Samoilenko V.I. and Olejnik Yu.V.)	6/7	Physical-metallurgical and welding-technological properties of gas-shielded flux-cored wires for welding of structural steels (Shlepakov V.N.)	6/7
Status of normative base, certification and attestation of welding consumables in Ukraine (Protsenko N.A.)	6/7	Restoration and strengthening surfacing of parts of die equipment (Solomka E.A., Lobanov A.I., Orlov L.N., Golyakevich A.A. and Khilko A.V.)	6/7
Towards the problem of dispersity and morphology of particles in welding aerosols (Gubanya I.P., Yavdoshchin I.R., Stepanyuk S.N. and Demetskaya A.V.)	6–7	Role of welding flux in formation of weld metal during arc welding of high-strength low-alloy steels (Golovko V.V., Stepanyuk S.N. and Ermolenko D.Yu.)	6/7
Ultraviolet radiation in manual arc welding using covered electrodes (Levchenko O.G., Malakhov A.T. and Arlamov A.Yu.)	6/7	Selection of shielding gas for mechanized arc welding of dissimilar steels (Elagin V.P.)	6/7
CONSUMABLES FOR MECHANIZED METHODS OF WELDING			
Application of flux-cored wires for welding in industry (Rosert R.)	6/7	Tungsten carbide based cladding materials (Zhudra A.P.)	6/7
Application of pulse atomizing jet in electric arc metallizing (Royanov V.A. and Bobikov V.I.)	6/7	PROCESSES OF ARC WELDING. METALLURGY. MARKETS	
Development of high-vanadium alloy for plasma-powder surfacing of knives for cutting of non-metallic materials (Pereplyotchikov E.F.)	6/7	Application of shielding gases in welding production (Review) (Paton B.E., Rimsky S.T. and Galinich V.I.)	6/7
Discrete filler materials for surfacing in current-conducting mould (Kuskov Yu.M.)	6/7	Effect of scandium-containing wire on structure and properties of joints of aluminum-lithium alloys produced by argon-arc welding (Markashova L.I., Kushnaryova O.S. and Alekseenko I.I.)	6/7
Effectiveness of application of new consumables in welding and surfacing of copper and its alloys (Review) (Ilyushenko V.M., Anoshin V.A., Majdanchuk T.B. and Lukianchenko E.P.)	6–7	Effect of structural factors on mechanical properties and crack resistance of welded joints of metals, alloys and composite materials (Markashova L.I., Poznyakov V.D., Berdnikova E.N., Gajvoronsky A.A. and Alekseenko T.A.)	6/7
Evaluation of suitability of welding wire of Sv-10GN1MA type produced by ESAB for manufacturing NPP equipment (Livshits I.M.)	6/7	Ensuring integrity of welded structures and constructions at their long-term service with application of renovation technologies (Steklov O.I., Antonov A.A. and Sevostianov S.P.)	6/7
Flux-cored strips for wear-resistant surfacing (Voronchuk A.P.)	6/7	Interaction of hydrogen with deformed metal (Paltsevich A.P., Sinyuk V.S. and Ignatenko A.V.)	6/7
Flux-cored wires for surfacing of steel hot mill rolls (Konratiev I.A. and Ryabtsev I.A.)	6/7	Investigation of cracking susceptibility of austenitic material using PVR-test procedure (Yushchenko K.A., Savchenko V.S., Chervyakov N.O., Zvyagintseva A.V., Monko G.G. and Pestov V.A.)	6/7
Flux for electric arc surfacing providing high-temperature removal of slag coating (Strelenko N.M., Zhdanov L.A. and Goncharov I.A.)	6/7	Market of welding consumables in Ukraine (Mazur A.A., Pustovojt S.V., Petruk V.S. and Brovchenko N.S.)	6/7
		Peculiarities of degradation of metal of welded joints of steam pipelines of heat power plants (Dmitriuk V.V. and Bartash S.N.)	6/7

Underwater welding and cutting in CIS countries (Kononenko V.Ya.)	6/7	Electron beam welding of sheet commercial titanium VT1-0, hardened by nitrogen in the process of arc-slag remelting, and properties of produced joints (Saenko V.Ya., Polishko A.A., Ryabinin V.A. and Stepanyuk S.N.)	11
TECHNOLOGIES, EQUIPMENT AND CONTROL IN CONSUMABLES PRODUCTION			
Directions of improvement of equipment and technology for electrode manufacture (Gnatenko M.F., Voroshilo V.S. and Suchok A.D.)	6/7	Estimation of possibility for producing full-strength joint of large steel parts using the method of autovacuum brazing of threaded profile (Polshchuk M.A., Atroshenko M.G., Puzrin A.L. and Shevtsov V.L.)	10
Effect of charge grain composition on rheological characteristics on rheological characteristics of compounds for low-hydrogen electrodes (Marchenko A.E.)	6/7	Fatigue calculation for welded joints of bearing elements of freight car bogie (Lobanov L.M., Makhnenko O.V., Saprykina G.Yu. and Pustovoj A.D.)	10
Improvement of adaptability to fabrication and welding properties of electrodes for tin bronze welding and surfacing (Majdanchuk T.B. and Skorina N.V.)	6/7	Features of reconditioning steel drill bit watercourse (Stefaniv B.V., Khorunov V.F., Sabadash O.M., Maksymova S.V. and Voronov V.V.)	11
State of raw material base of electrode production (Palievska E.A. and Sidlin Z.A.)	6/7	Flash-butt welding of thin-walled profiles of heat-hardened aluminium alloys (Chvertko P.N., Semyonov L.A. and Gushchin K.V.)	12
Thickness difference of electrode coatings caused by elastic turbulence of electrode compounds under condition of non-isothermal pressure flow (Marchenko A.E.)	6/7	Hybrid laser-GMA girth welding technologies for transmission pipelines (Keitel S. and Neubert J.)	4
INDUSTRIAL			
Analysis of some physical and technical characteristics of ion-plasma coating (TiZr)N on rotor blades of compressor of gas-turbine engine TV3-117 (Korsunov K.A. and Ashikhmina E.A.)	2	Industrial electron beam installation L-8 for deposition of heat-protective coatings on turbine blades (Grechanyuk N.I., Kucherenko P.P., Melnik A.G., Kovalchuk D.V. and Grechanyuk I.N.)	10
Application of complex-alloyed powders produced by thermocentrifugal sputtering in flux-cored wires (Zhudra A.P., Krivchikov S.Yu. and Dzykovich V.I.)	12	Joining of thick metal by multipass electroslag welding (Yushchenko K.A., Kozulin S.M., Lychko I.I. and Kozulin M.G.)	9
Assessment of effectiveness of residual stress lowering in circumferential joints of pipes after postweld explosion treatment (Bryzgalin A.G.)	5	Linear friction welding of metallic materials (Review) (Zyakhov I.V., Zavertanny M.S. and Chernobaj S.V.)	12
Automatic machine for wet underwater welding in confined spaces (Lebedev V.A., Maksimov S.Yu., Pichak V.G. and Zajnuln D.I.)	9	Modernization of control system of A1756 machine for plasma-powder surfacing (Pereplyotchikov E.F., Ryabtsev I.A., Lankin Yu.N., Semikin V.F. and Osechkov P.P.)	12
Braze-welded tubular billets for pipelines and high-pressure vessels (Pismenny A.A., Gubatyuk R.S., Prokofiev A.S., Muzhichenko A.F. and Shinkarenko A.S.)	10	Peculiarities of application of supercapacitors in devices for pulse welding technologies (Korotynsky A.E., Drachenko N.P. and Shapka V.A.)	9
Calculation of upsetting force in flash butt welding of closed-shape products (Chvertko P.N., Moltasov A.V. and Samotryasov S.M.)	1	Percussion capacitor-discharge welding of wire of composite superconducting alloy (Kaleko D.M.)	4
Computer-based technologies and their influence on welding education (Keitel S., Ahrens C. and Moll H.)	10	Producing of bimetal joints by laser welding with full penetration (Schmidt M. and Kuryntsev S.V.)	4
Development of technologies of repair by arc welding of operating main pipelines in Ukraine (But V.S. and Olejnik O.I.)	5	Properties of fusion-welded joints on high-strength titanium alloy T110 (Akhonin S.V., Belous V.Yu., Antonyuk S.L., Petrichenko I.K. and Selin R.V.)	1
Dry ice — useful material in welding performance (Zhiznyakov S.N.)	4	Prospects for development of load-carrying elements of freight car bogie (Makhnenko O.V., Saprykina G.Yu., Mirzov I.V. and Pustovoj A.D.)	3
Effectiveness of natural gas transportation by sea at application of high pressure welded cylinders (Paton B.E., Savitsky M.M., Savitsky A.M. and Mazur A.A.)	8	Reasons of stress corrosion failure of erection girth joint of main gas pipeline (Rybakov A.A., Goncharenko L.V., Filipchuk T.N., Lohman I.V. and Burak I.Z.)	3
Effectiveness of strengthening butt welded joints after long-term service by high-frequency mechanical peening (Knysh V.V., Solovej S.A. and Kuzmenko A.Z.)	11	Resistance butt welding of concrete reinforcement in construction site (Chvertko P.N., Goronkov N.D., Vinogradov N.A., Samotryasov S.M. and Sysoev V.Yu.)	3
Electrode and filler materials for surfacing and welding of cast tin bronzes (Review) (Majdanchuk T.B.)	1	Sanitary-hygienic evaluation of noise in manual arc welding with covered electrodes (Levchenko O.G., Kuleshov V.A. and Arlamov A.Yu.)	9
Electron beam welding of large-size thick-wall structures of magnesium alloys (Nesterenkov V.M. and Bondarev A.A.)	2	State-of-the-art and prospects of world and regional markets of welding materials (Review) (Mazur A.A., Pustovojt S.V., Makovetskaya O.K., Brovchenko N.S. and Petruk V.S.)	11

Structure and properties of welded joints of 15Kh1M1FL steel at repair of casting defects by transverse hill method (Efimenko N.G., Atozhenko O.Yu., Vavilov A.V., Kantor A.G. and Udalova E.I.)

Technological peculiarities of laser microplasma and hybrid laser-microplasma welding of aluminium alloys (Shelyagin V.D., Orishich A.M., Khaskin V.Yu., Malikov A.G. and Chajka A.A.)

Technology for manufacture of gas-and-oil line pipes using high-frequency method of welding at Company «Interpipe NMPP» (Antipov Yu.N., Dmitrenko E.V., Kovalenko A.V., Goryanov S.A., Rybakov A.A., Semyonov S.E. and Filipchuk T.N.)

Wear-resistant arc surfacing over the layer of alloying charge (Peremitko V.V.)

Welded structure of Kiev TV-tower is 40 years old (Lobanov L.M., Garf E.F., Kopylov L.N. and Sineok A.G.)

55th ANNIVERSARY OF WELDING PRODUCTION CHAIR OF ADMIRAL MAKAROV NATIONAL SHIPBUILDING UNIVERSITY

Effect of stress-strain state on structure and properties of joints in diffusion welding of dissimilar metals (Kvasnitsky V.V., Kvasnitsky V.F., Markashova L.I. and Matvienko M.V.)

Effect of weld convexity sizes on stress state of butt joint during tension (Ermolaev G.V., Martynenko V.A. and Marunich I.V.)

Increase of service properties of electric-arc and plasma coatings by use of electric-pulse effect on double-phase high-temperature flow (Dubovoj A.N., Karpechenko A.A. and Bobrov M.N.)

Instability of mode in circuit with capacity and electric arc supplied by direct current source (Vereshchago E.N. and Kostyuchenko V.I.)

Regularities of creation of modified interlayers in using of highly-concentrated energy flows (Kvasnitsky V.F., Kvasnitsky V.V., Cherenda N.N., Koval N.N. and Levchenko I.L.)

Stress-strain state at force and temperature loading of assemblies from dissimilar steels with soft interlayer (Kolesar I.A. and Ermolaev G.V.)

Technological characteristics of automatic submerged arc surfacing with high-frequency oscillations of electrode end (Lebedev V.A., Dragan S.V., Goloborodko Zh.G., Simutenkov I.V. and Yaros Yu.A.)

INFORMATION

Paton Turbine Technologies — new name of a well-known company

The 55th Anniversary of the Experimental Design Technological Bureau of the E.O. Paton Electric Welding Institute

Today's Foreign Trade Company «INPAT» of the E.O. Paton Electric Welding Institute

Training of specialists-welders of Kazakhstan in Ukraine 20 years in the world of flux-cored wires

NEWS

International Conference «Welding Consumables»

International Conference «Welding and Related Technologies — Present and Future»

The Evgeny Paton Prize Winners of 2013

SCIENTIFIC AND TECHNICAL

Analysis and procedure of calculation of series connection electronic devices for contactless arc excitation (Makhlin N.M. and Korotynsky A.E.)

Cermet coatings of chromium carbide-nichrome system produced by supersonic plasma gas air spraying (Korzhih V.N., Borisova A.L., Popov V.V., Kolomytsev M.V., Chajka A.A., Tkachuk V.I. and Vigilyanskaya N.V.)

Cracking susceptibility of welded joints in repair structures on main gas pipelines (But V.S., Maksimov S.Yu. and Olejnik O.I.)

Deformation-free welding of stringer panels of titanium alloy VT20 (Paton B.E., Lobanov L.M., Lysak V.L., Knysh V.V., Pavlovsky V.I., Prilutsky V.P., Timoshenko A.N., Goncharov P.V. and Guan Qiao)

Determination of the causes for crack initiation in structural elements of the tower of new ventilation pipe at Chernobyl NPP (Torop V.M., Garf E.F., Yakimkin A.V. and Gopkalo E.E.)

Detonation coatings of composite powder of ferromolybdenum-silicon carbide produced using method of mechanical-and-chemical synthesis (Borisov Yu.S., Borisova A.L., Astakhov E.A., Burlachenko A.N., Ipatova Z.G. and Gorban V.F.)

Effect of cyclic load on microstructure and cold resistance of the 10G2FB steel HAZ metal (Poznyakov V.D., Markashova L.I., Maksimenko A.A., Berdnikova E.N., Alekseenko T.A. and Kasatkin S.B.)

Effect of electric parameters of arc surfacing using flux-cored wire on process stability and base metal penetration (Lankin Yu.N., Ryabtsev I.A., Soloviov V.G., Chernyak Ya.P. and Zhdanov V.A.)

Effect of nickel and manganese on structure of Ag-Cu-Zn-Sn system alloys and strength of brazed joints (Khorunov V.F., Stefaniv B.V. and Maksymova S.V.)

Effect of temperature of thermomechanical treatment on quality of dissimilar metal joints (Demidenko L.Yu., Onatskaya N.A. and Polovinka V.D.)

Elimination of local deformations of buckling type by means of electrodynamic treatment (Lobanov L.M., Pashchin N.A., Mikhoduj O.L. and Solomijchuk T.G.)

Fatigue life of deposited repair welds on single-crystal high-temperature nickel alloy under cyclic oxidation (Belyavin A.F., Kurenkova V.V. and Fedotov D.A.)

Features of melting, structure and properties of Ni-Mn-Cu system nickel alloys (Khorunov V.F. and Lototsky P.N.)

High-power laser welding of austenitic stainless steel with electromagnetic control of weld pool (Bachmann M., Avilov V., Gumenyuk A. and Rethmeier M.)

Improvement of power efficiency of machines for resistance spot welding by longitudinal compensation of reactive power (Pismenny A.A.)

Improvement of the procedure of mode parameter calculation for gas-shielded multipass welding (Buzorina D.S., Sholokhov M.A. and Shalimov M.P.)

Increase of fatigue resistance of sheet welded joints of aluminum alloys using high-frequency peening (Knysh V.V., Klochkov I.N., Pashulya M.P. and Motrunich S.I.)

Influence of heating rate on inflammation temperature of multilayer Ti/Al foil (Kuzmenko D.N., Ustinov A.I., Kotsintsev S.G. and Petrushinets L.V.)

Influence of non-metallic inclusions in pipe steels of strength class X65–X80 on values of impact toughness of flash-butt welded joints (Kuchuk-Yatsenko S.I., Shvets Yu.V. and Shvets V.I.)	12	Peculiarities of structure of coatings of Fe–Cr–Al system flux-cored wire produced under conditions of supersonic electric arc metallization (Korzhih V.N., Borisova A.L., Gordan G.N., Lyutik N.P., Chajka A.A. and Kajda T.V.)	2
Influence of non-uniformity of heating on upsetting force value and forging time in flash-butt welding of flat ring (Moltasov A.V., Samotryasov S.M., Knysh V.V., Chvertko P.N. and Gushchin K.V.)	10	Prediction of thermodynamical properties of melts of CaO–Al ₂ O ₃ system (Goncharov I.A., Galinich V.I., Mishchenko D.D. and Sudavtsova V.S.)	4
Integrated evaluation of effect of main impurities on weldability of copper (Anoshin V.A., Ilyushenko V.M., Bondarenko A.N., Lukianchenko E.P. and Nikolaev A.K.)	11	Quasi-crystalline alloys-fillers for composite layers produced using method of furnace surfacing (Sukhovaya E.V.)	1
Investigation of spraying spot and metallization pattern under conditions of microplasma spraying of coatings of titanium dioxide (Borisov Yu.S., Vojnarovich S.G., Kislitsa A.N. and Kalyuzhny S.N.)	12	Redistribution of residual welding stresses in in-vessel core barrel of WWER-1000 reactor during operation (Makhnenko O.V., Velikoivanenko E.A. and Mirzov I.V.)	11
Investigation of thermal resistance of deposited metal designed for restoration of mill rolls (Babinets A.A., Ryabtsev I.A., Kondratiev I.A., Ryabtsev I.I. and Gordan G.N.)	5	Resistance to cold crack formation of HAZ metal of welded joint on high-strength carbon steels (Gajvoronsky A.A.)	2
Investigation of wear resistance of composite alloys under the conditions of gas-abrasive wear at elevated temperatures (Zhudra A.P.)	11	Simulation of electric arc with refractory cathode and evaporating anode (Krikent I.V., Krivtsun I.V. and Demchenko V.F.)	9
Laser and laser-microplasma alloying of surface of 38KhN3MFA steel specimens (Shelyagin V.D., Markashova L.I., Khaskin V.Yu., Bernatsky A.V. and Kushnaryova O.S.)	2	Structural changes in overheating zone of HAZ metal of railway wheels in arc surfacing (Gajvoronsky A.A., Zhukov V.V., Vasiliev V.G., Zuber T.A. and Shishkevich A.S.)	1
Methods of mathematical modelling of the processes of electrode metal drop formation and transfer in consumable electrode welding (Review) (Semyonov A.P.)	10	Structural features of FSW joints of metals with different element solubility in the solid phase (Grigorenko G.M., Adeeva L.I., Tunik A.Yu., Stepanyuk S.N., Poleshchuk M.A. and Zelenin E.V.)	4
Microstructure of brazed joints of nickel aluminide (Maksymova S.V., Khorunov V.F., Myasoed V.V., Voronov V.V. and Kovalchuk P.V.)	10	Structure of surface-melted zone of cast high-nickel alloy KhN56MBYuDSH after laser surface treatment (Polishko A.A., Saenko V.Ya., Tunik A.Yu. and Stepanyuk S.N.)	3
Modeling of weld pool behaviour in spot welding by pulsed laser radiation (Semyonov A.P., Shuba I.V., Krivtsun I.V. and Demchenko V.F.)	4	System for measurement of temperature of biological tissues in bipolar high-frequency welding (Lankin Yu.N., Sushy L.F. and Bajshtruk E.N.)	11
Numerical modeling and prediction of weld microstructure in high-strength steel welding (Review) (Ermolenko D.Yu. and Golovko V.V.)	3	Technological peculiarities of welding of wrought magnesium alloys by electron beam in vacuum (Bondarev A.A. and Nesterenkov V.M.)	3
Peculiarities of alloying of weld metal of high-strength aluminium alloy welded joints with scandium (Fedorchuk V.E., Kushnaryova O.S., Alekseenko T.A. and Falchenko Yu.V.)	5	Tribotechnical properties of deposited metal of 50Kh9S3G type with increased sulphur content (Osin V.V.)	12
		Index of articles for TPWJ'2014, Nos. 1–12	12
		List of authors	12

LIST OF AUTHORS

- A**deeva L.I. No.4
Ahrens C. No.10
Akhonin S.V. No.1
Alekseenko I.I. Nos. 6/7
Alekseenko T.A. No.5(2), 6/7
Anoshin V.A. No.6/7, 11
Antipov Yu.N. No.3
Antonov A.A. Nos. 6/7
Antonyuk S.L. No.1
Arlamov A.Yu. No.6/7, 9
Ashikhmina E.A. No.2
Astakhov E.A. No.3
Atozhenko O.Yu. No.2
Atroschenko M.G. No.10
Avilov V. No.3
- B**abinets A.A. No.5
Bachmann M. No.3
Bajshtruk E.N. No.11
Bartash S.N. Nos. 6/7
Belous V.Yu. No.1
Belyavin A.F. No.2
Berdnikova E.N. No.5, 6/7
Bernatsky A.V. No.2
Bobikov V.I. Nos. 6/7
Bobrov M.N. No.8
Bondarenko A.N. No.11
Bondarev A.A. No.2, 3
Borisov Yu.S. No.3, 12
Borisova A.L. No.2, 3, 12
Brovchenko N.S. No.6/7, 11
Bryzgalin A.G. No.5
Bugaenko B.V. No.8
Bulat A.V. Nos. 6/7(2)
Burak I.Z. No.3
Burlachenko A.N. No.3
But V.S. No.5, 11
Butenko A.Yu. Nos. 6/7
Buzorina D.S. No.10
- C**hajka A.A. No.2, 5, 12
Cherenda N.N. No.8
Chernobaj S.V. No.12
Chernyak Ya.P. No.9
Chervyakov N.O. Nos. 6/7
Chvertko P.N. No.1, 3, 10, 12
- D**emchenko V.F. No.4, 9
Demetskaya A.V. Nos. 6/7
Demidenko L.Yu. No.12
Dmitrenko E.V. No.3
Dmitrik V.V. Nos. 6/7
Drachenko N.P. No.9
Dragan S.V. No.8
- Dubovoj A.N. No.8
Dzykovich V.I. No.12
- E**fimenko N.G. No.2
Elagin V.P. Nos. 6/7
Emelianov V.M. No.8
Ermolaev G.V. No.8(2)
Ermolenko D.Yu. No.3, 6/7
- F**alchenko Yu.V. No.5
Fedorchuk V.E. No.5
Fedotov D.A. No.2
Filipchuk T.N. No.3(2)
- G**ajvoronsky A.A. No.1, 2, 6/7
Galinich V.I. No.4, 6/7(2)
Garf E.F. No.1(2)
Gavrik A.R. Nos. 6/7
Gnatenko M.F. Nos. 6/7
Goloborodko Zh.G. No.8
Golovko V.V. No.3, 6/7
Golyakevich A.A. Nos. 6/7
Goncharenko E.I. Nos. 6/7
Goncharenko L.V. No.3
Goncharov I.A. No.4, 6/7(2)
Goncharov P.V. No.9
Gopkalo E.E. No.1
Gorban V.F. No.3
Gordan G.N. No.2, 5
Goronkov N.D. No.3
Goryanov S.A. No.3
Grechanyuk I.N. No.10
Grechanyuk N.I. No.10
Grigorenko G.M. No.4
Grigorenko S.G. Nos. 6/7
Guan Qiao No.9
Gubatyuk R.S. No.10
Gubenya I.P. Nos. 6/7
Gumenyuk A. No.3
Gushchin K.V. No.10, 12
- I**gnatenko A.V. No.6/7
Ilyushenko V.M. No. 6/7, 11
Ipatova Z.G. No.3
- K**ajda T.V. No.2
Kakhovsky N.Yu. Nos. 6/7
Kakhovsky Yu.N. Nos. 6/7
Kaleko D.M. No.4
Kalyuzhny S.N. No.12
Kantor A.G. No.2
Karpechenko A.A. No.8
Kasatkin S.B. No.5
Keitel S. No.4, 10
Khaskin V.Yu. No.2, 5

Khilko A.V. Nos. 6/7
Khorunov V.F. No.4, 5, 10, 11
Kirichenko O.P. Nos. 6/7
Kislitsa A.N. No.12
Klochkov I.N. No.5
Knysh V.V. No.5, 9, 10, 11
Kolesar I.A. No.8
Kolomytsev M.V. No.12
Kondratiev I.A. No.5, 6/7
Kononenko V.Ya. Nos. 6/7
Kopylov L.N. No.1
Koritsky V.A. No.4
Korotynsky A.E. No.1, 9
Korsunov K.A. No.2
Korzhih V.N. No.2, 12
Kosintsev S.G. No.10
Kostin A.M. No.6/7, 8
Kostyuchenko V.I. No.8
Koval N.N. No.8
Kovalchuk D.V. No.10
Kovalchuk P.V. No.10
Kovalenko A.V. No.3
Kozulin M.G. No.9
Kozulin S.M. No.9
Krikent I.V. No.9
Krivchikov S.Yu. No.12
Krivtsun I.V. No.4, 9
Kucherenko P.P. No.10
Kuchuk-Yatsenko S.I. No.12
Kuleshov V.A. No.9
Kurenkova V.V. No.2
Kuryntsev S.V. No.4
Kushchy A.M. Nos. 6/7
Kushnaryova O.S. No.2, 5, 6/7
Kuskov Yu.M. Nos. 6/7
Kuzmenko A.Z. No.11
Kuzmenko D.N. No.10
Kvasnitsky V.F. No.8(2)
Kvasnitsky V.V. No.6/7, 8(2)

Lankin Yu.N. No.9, 11, 12
Lebedev V.A. No.8, 9
Levchenko I.L. No.8
Levchenko O.G. No.6/7, 9
Lipodaev V.N. No.1, 6/7, 8
Livshits I.M. Nos. 6/7
Lobanov A.I. Nos. 6/7
Lobanov L.M. No.1, 9, 10, 11
Lokhman I.V. No.3
Lototsky P.N. No.5
Lukianchenko E.P. No.6/7, 11
Lychko I.I. No.9
Lysak V.L. No.9
Lyutik N.P. No.2

Machulyak V.V. Nos. 6/7
Majdanchuk T.B. No.1, 6/7(2)
Makarenko N.A. Nos. 6/7
Makhlin N.M. No.1

Makhnenko O.V. No.3, 10, 11
Makovetskaya O.K. No.11
Maksimenko A.A. No.5
Maksimov S.Yu. No.6/7(2), 9, 11
Maksymova S.V. No.4, 10, 11
Malakhov A.T. Nos. 6/7
Malikov A.G. No.5
Marchenko A.E. Nos. 6/7(2)
Marinsky G.S. No.9
Markashova L.I. No.2, 5, 6/7(2), 8
Martynenko V.A. No.8(2)
Marunich I.V. No.8
Matvienko M.V. No.8
Mazur A.A. No.6/7, 8, 11
Melnik A.G. No.10
Mikhoduj O.L. No.11
Mirzov I.V. No.3, 11
Mishchenko D.D. No.4
Moll H. No.10
Moltasov A.V. No.1, 10
Monko G.G. Nos. 6/7
Morozova R.I. Nos. 6/7
Motrunich S.I. No.5
Muzhichenko A.F. No.10
Myasoed V.V. No.10

Nesterenkov V.M. No.2, 3
Netyaga V.I. Nos. 6/7
Neubert J. No.4
Nikolaev A.K. No.11

Olejnik O.I. No.5, 11
Olejnik Yu.V. Nos. 6/7
Onatskaya N.A. No.12
Orishich A.M. No.5
Orlov L.N. Nos. 6/7
Osechko P.P. No.12
Osin V.V. No.12
Osipov N.Ya. Nos. 6/7

Palievskaya E.A. Nos. 6/7
Paltsevich A.P. Nos. 6/7
Pashchin N.A. No.11
Pashulya M.P. No.5
Paton B.E. No.6/7, 8, 9
Pavlovsky V.I. No.9
Peremitko V.V. No.8
Pereplyotchikov E.F. No.6/7, 12
Pestov V.A. Nos. 6/7
Petrichenko I.K. No.1
Petruk V.S. No.6/7, 11
Petrushinets L.V. No.10
Pichak V.G. No.9
Pismenny A.A. No.1, 10
Poleshchuk M.A. No.4, 10
Polishko A.A. No.3, 11
Polovinka V.D. No.12
Popov V.V. No.12
Poznyakov V.D. No.5, 6/7

Prilutsky V.P. No.9
Prokofiev A.S. No.10
Protsenko N.A. Nos. 6/7
Protsenko P.P. No.12
Pustovoj A.D. No.3, 10
Pustovojt S.V. No.6/7, 11
Puzrin A.L. No.10

Rethmeier M. No.3
Rimsky S.T. Nos. 6/7
Rosert R. Nos. 6/7
Royanov V.A. Nos. 6/7
Ryabinin V.A. No.11
Ryabtsev I.A. No.5, 6/7, 9, 12
Ryabtsev I.I. No.5
Rybakov A.A. No.3(2)

Sabadash O.M. No.11
Saenko V.Ya. No.3, 11
Samojlenko V.I. Nos. 6/7(2)
Samotryasov S.M. No.1, 3, 10
Saprykina G.Yu. No.3, 10
Savchenko V.S. Nos. 6/7
Savitsky A.M. No.8
Savitsky M.M. No.8
Schmidt M. No.4
Selin R.V. No.1
Semikin V.F. No.12
Semyonov A.P. No.4, 10
Semyonov L.A. No.12
Semyonov S.E. No.3
Sevostianov S.P. Nos. 6/7
Shalimov M.P. No.10
Shapka V.A. No.9
Shelyagin V.D. No.2, 5
Sheremeta A.V. Nos. 6/7
Shevtsov V.L. No.10
Shinkarenko A.S. No.10
Shishkevich A.S. No.1
Shlepakov V.N. Nos. 6/7
Sholokhov M.A. No.10
Shuba I.V. No.4
Shvets V.I. No.12
Shvets Yu.V. No.12
Sidlin Z.A. Nos. 6/7
Simutenkov I.V. No.8
Sineok A.G. No.1
Sinyuk V.S. Nos. 6/7
Skorina N.V. Nos. 6/7
Solomijchuk T.G. No.11
Solomka E.A. Nos. 6/7
Solovej S.A. No.11
Soloviov V.G. No.9

Stefaniv B.V. No.4, 11
Steklov O.I. Nos. 6/7
Stepakhno A.V. No.4(2)
Stepanyuk S.N. No.3, 4, 6/7(2), 11
Strelenko N.M. Nos. 6/7
Suchok A.D. Nos. 6/7
Sudavtsova V.S. No.4
Sukhovaya E.V. No.1
Sushy L.F. No.11
Sysoev V.Yu. No.3

Timoshenko A.N. No.9
Tkachuk V.I. No.12
Torop V.M. No.1
Tunik A.Yu. No.3, 4
Turyk E.V. Nos. 6/7

Udalova E.I. No.2
Ustinov A.I. No.10

Vasiliev V.G. No.1
Vavilov A.V. No.2
Velikoivanenko E.A. No.11
Vereshchago E.N. No.8
Vigilyanskaya N.V. No.12
Vinogradov N.A. No.3
Vlasov A.F. Nos. 6/7
Vojnarovich S.G. No.12
Voronchuk A.P. Nos. 6/7
Voronov V.V. No.10, 11
Voroshilo V.S. Nos. 6/7

Yakimkin A.V. No.1
Yaros Yu.A. No.8
Yarovitsyn A.V. Nos. 6/7
Yavdoshchin I.R. Nos. 6/7
Yushchenko K.A. No.6/7(4), 9

Zajnuln D.I. No.9
Zakharov L.S. Nos. 6/7
Zalevsky A.V. Nos. 6/7
Zavertanny M.S. No.12
Zelenin E.V. No.4
Zelnichenko A.T. No.1, 8
Zhdanov L.A. Nos. 6/7
Zhdanov V.A. No.9
Zhiznyakov S.N. No.4
Zhudra A.P. No.6/7, 11, 12
Zhuk G.V. No.9
Zhukov V.V. No.1
Zuber T.A. No.1
Zvyagintseva A.V. Nos. 6/7(2)
Zyakhov I.V. No.12